

# Abbreviations

---

AE	Autoestimator
AMV	Atmospheric Motion Vectors
ATSR	Along Track Scanning Radiometer
AVHRR	Advanced Very High Resolution Radiometer
Cb	Cumulonimbus
CDS	Climate Data Set
CGMS	Coordination Group for Meteorological Satellites
CI	Convection Initiation
CII	Combined Instability Index
CLA	Cloud Analysis
CSR	Clear Sky Radiances
CTH	Cloud Top Height
ECMWF	European Centre for Medium-Range Weather Forecasts
ERS	European Remote Sensing
EUMETSAT	European Organization for the Exploitation of Meteorological Satellites
FAR	False Alarm Ratio
GERB	Geostationary Earth Radiation Budget
GII	Global Instability Indices
GOES	Geostationary Operational Environmental Satellite
GPCP	Global Precipitation Climatology Project
GTS	Global Telecommunications System

HE	Hydroestimator
HIRS	High Resolution Infrared Radiation Sounder
HK	Hanssen-Kuipers discriminant
HPI	High Resolution Precipitation Index
HRV	High Resolution Visible
IDS	ISCCP Data Set
IPCC	Intergovernmental Panel on Climate Change
IPWG	International Precipitation Working Group
IR	Infrared
ISCCP	International Satellite Cloud Climatology Project
ITCZ	Inter-tropical Convergence Zone
LDN	Lightning Detection Network
MFG	Meteosat First Generation
MODIS	MODerate resolution Infrared Spectrometer
MPEF	Meteorological Products Extraction Facility
MSG	Meteosat Second Generation
MTG	Meteosat Third generation
NESDIS	National Environmental Satellite, Data and Information Service
NIR	Near Infrared
NOAA	National Oceanic and Atmospheric Administration
NMC	National Meteorological Centre
NMHS	National Meteorological and Hydrological Services
NWP	Numerical Weather Prediction
POD	Probability of Detection

POFD	Probability of False Detection
PW	Precipitable Water
PWS	Public Weather Service
QPE	Quantitative Precipitation Estimation
RGB	Red-Green-Blue
RH	Relative Humidity
RII	Regional Instability Indices
RMS	Root Mean Square
RSMC	Regional Specialized Meteorological Centre
SAB	Satellite Analysis Branch
SAF	Satellite Application Facilities
SAST	South African Standard Time
SAWS	South African Weather Service
SEVIRI	Spinning Enhanced Visible and InfraRed Imager
SPE	Satellite precipitation estimates
SWFDP	Severe Weather Forecast Demonstration Project
T	Temperature
Tsfc	Temperature at lowest model level
TD	Dew point temperature
TDsfc	Dew point temperature at lowest model level
TH	Tropospheric Humidity
TOZ	Total Ozone
TPW	Total Precipitable Water content
TRMM	Tropical Rainfall Measuring Mission

Tsfc	Lowest model level air temperature
UAH	University of Alabama in Huntsville
UTC	Coordinated Universal Time
UW-CIMSS	University of Wisconsin Cooperative Institute of Meteorological Satellite Studies
VAS	VISSR Atmospheric Sounder
VIS	Visible
WMO	World Meteorology Organization
WV	Water Vapour

# Table of Contents

---

Declaration.....	ii
Acknowledgements.....	iii
Abstract.....	iv
Abbreviations.....	v
List of Figures.....	xiii
List of Tables.....	xviii

## **CHAPTER 1: BACKGROUND AND ENABLING TECHNOLOGY**

<b>1.1 INTRODUCTION.....</b>	<b>1</b>
<b>1.2 SOUTH AFRICA’S CLIMATE AND CONVECTIVE ACTIVITY.....</b>	<b>3</b>
<b>1.3 ENABLING TECHNOLOGY IN SOUTH AFRICA.....</b>	<b>6</b>
1.3.1 Meteosat Second Generation satellite data.....	6
1.3.2 Radar .....	8
1.3.3 Lightning.....	8
1.3.4 Unified Model .....	9
<b>1.4 RESEARCH PROBLEM .....</b>	<b>10</b>
<b>1.5 HYPOTHESIS .....</b>	<b>10</b>
<b>1.6 AIMS AND OBJECTIVES.....</b>	<b>11</b>
<b>1.7 LAYOUT OF THE THESIS .....</b>	<b>11</b>

## **CHAPTER 2: MSG APPLICATIONS FOR FORECASTING CONVECTION**

<b>2.1 BACKGROUND.....</b>	<b>12</b>
----------------------------	-----------

<b>2.2 METEOROLOGICAL PRODUCTS EXTRACTION FACILITY (MPEF)</b> .....	<b>12</b>
<b>2.3 THE GLOBAL INSTABILITY INDEX (GII)</b> .....	<b>13</b>
2.3.1 Theoretical background .....	14
<b>2.4 THE INITIAL EVALUATION OF GII IN SOUTH AFRICA</b> .....	<b>18</b>
2.4.1 Visual verification .....	18
<b>2.5 THE REGIONAL INSTABILITY INDICES (RII)</b> .....	<b>20</b>
2.5.1 Changes to the suite of instability indices .....	20
<b>2.6 SUMMARY</b> .....	<b>23</b>
<b>CHAPTER 3: EVALUATION OF GLOBAL AND REGIONAL INSTABILITY INDICES OVER SOUTH AFRICA</b>	
<b>3.1 BACKGROUND</b> .....	<b>24</b>
<b>3.2 DATA</b> .....	<b>24</b>
3.2.1 Case studies .....	24
3.2.2 Lightning data .....	28
3.2.3 RII data .....	30
<b>3.3 COMPARISON OF RII K INDEX AND LIFTED INDEX FIELDS AGAINST THE UNIFIED MODEL K INDEX AND LIFTED INDEX FIELDS</b> .....	<b>31</b>
<b>3.4 EVALUATION OF RII AGAINST OCCURRENCE OF LIGHTNING</b> .....	<b>35</b>
3.4.1 Initial evaluation with GII .....	35
3.4.2 Evaluation of individual RII against lightning .....	39
3.4.3 Comparison with similar work done in Poland .....	44
<b>3.5 SUMMARY</b> .....	<b>45</b>

## **CHAPTER 4: PRINCIPLES OF A NEW COMBINED INSTABILITY INDEX**

<b>4.1 BACKGROUND</b> .....	<b>46</b>
<b>4.2 USING THE FOUR REGIONAL INSTABILITY INDICES IN THE DEVELOPMENT OF A NEW INDEX</b> .....	<b>46</b>
4.2.1 Cumulative frequency graphs for Mixed KIndex and lightning .....	47
4.2.2 Cumulative frequency graphs for Mixed Total Totals and lightning .....	48
4.2.3 Cumulative frequency graphs for Lifted Index and lightning .....	49
4.2.4 Cumulative frequency graphs for Precipitable Water and lightning .....	50
<b>4.3 CUMULATIVE FREQUENCY GRAPHS FOR TOPOGRAPHY AND LIGHTNING</b> .....	<b>51</b>
<b>4.4 COMBINING THE FOUR RII AND TOPOGRAPHY FOR A NEW INDEX</b> .....	<b>53</b>
<b>4.5 EXAMPLES OF THE NEW COMBINED INSTABILITY INDEX (CII) WITH VISUAL VERIFICATION</b> .....	<b>60</b>
<b>4.6 SUMMARY</b> .....	<b>63</b>

## **CHAPTER 5: EVALUATION OF THE CII AGAINST THE OCCURRENCE OF LIGHTNING OVER SOUTH AFRICA**

<b>5.1 BACKGROUND</b> .....	<b>64</b>
<b>5.2 EVALUATION OF THE CII</b> .....	<b>64</b>
<b>5.3 CII STATISTICS FOR ALL FIFTY CASES</b> .....	<b>83</b>
<b>5.4 CII PERFORMANCE COMPARED TO THE PERFORMANCE OF THE INDIVIDUAL RII</b> .....	<b>85</b>
<b>5.5 SUMMARY</b> .....	<b>89</b>

## **CHAPTER 6: EVALUATION OF THE CII AGAINST PRECIPITATION ESTIMATES**

<b>6.1 BACKGROUND</b> .....	<b>91</b>
<b>6.2 SOUTH AFRICAN RAIN GAUGE NETWORK</b> .....	<b>92</b>
<b>6.3 HYDRO ESTIMATOR (HE)</b> .....	<b>93</b>

6.3.1 HE evaluated as part of the IPWG programme .....	95
6.3.2 Examples of 24 hour rain gauge totals versus 24 hour HE totals.....	97
<b>6.4 COMPARING THE CII WITH THE HYDROESTIMATOR RAINFALL .....</b>	<b>98</b>
<b>6.5 STATISTICS FOR CII VERSUS HE FOR ALL FIFTY CASES.....</b>	<b>103</b>
<b>6.6 VISUAL COMPARISONS OF THE OPERATIONAL CII, LIGHTNING OCCURENCE AND THE HE RAINFALL OVER SOUTHERN AFRICA.....</b>	<b>104</b>
<b>6.7 SUMMARY.....</b>	<b>107</b>
<b>CHAPTER 7 SUMMARY, RECOMMENDATIONS AND CONCLUSION</b>	
<b>7.1 BACKGROUND.....</b>	<b>109</b>
<b>7.2 SUMMARY AND DISCUSSION OF RESULTS .....</b>	<b>110</b>
7.2.1 Advantages of CII.....	111
7.2.2 Limitations of CII .....	113
<b>7.3 RECOMMENDATIONS.....</b>	<b>113</b>
<b>7.4 CONCLUSION .....</b>	<b>114</b>
<b>REFERENCES .....</b>	<b>116</b>

# List of Figures

---

Figure 1.1 Schematic of the role players in South Africa's summer circulation (after Hurry and Van Heerden, 1982) .....	3
Figure 1.2 Normal annual rainfall over South Africa (after Kruger, 2007) .....	4
Figure 1.3 Normal summer rainfall over South Africa (after Kruger, 2007) .....	5
Figure 1.4 Lightning flash density for 2006 to 2009 (left) and South Africa's topography (right).....	5
Figure 1.5 Location of lightning detection network sensors (after Gill, 2008b).....	9
Figure 2.1 Provinces of South Africa (left) and location of a few cities in Limpopo Province, amongst others, Polokwane (right) .....	19
Figure 2.2 ECMWF 24 hour forecast for the K Index at 0600 UTC on 6 November 2005 (left) and GII K Index over South Africa at 0645 UTC (right) .....	19
Figure 2.3 GII K Index (left) with a 15X15 pixel resolution and RII K Index (right) with a 3X3 pixel resolution.....	20
Figure 2.4 High terrain (left) and K Index (right) over South Africa, indicating areas above 850 hPa where K Index could not be computed.....	22
Figure 2.5 Normal K Index (left) and Mixed K Index (right), indicating areas where normal K Index are missing due to higher terrain, but Mixed K Index could be computed. ....	23
Figure 3.1 Projected detection efficiency in percentages (left) and projected location accuracy (km) of cloud to ground lightning flash data for the SAWS LDN from the VAISALA Network Performance Evaluation Program model (right) (from Gill, 2008b) .....	29
Figure 3.2 Relationship between convection and lightning (after Price, 2008).....	30
Figure 3.3 Mask used for the evaluation of lightning data .....	30
Figure 3.4 RII K Index in hourly averages (first four panes) and the time average over the period 0600 to 0900 UTC in the last pane .....	32

Figure 3.5 RII Total Totals (top left), Unified Model Total Totals (top right), difference field (bottom left) and the total number of lightning strokes which occurred later in the day (bottom right) for 4 January 2008.....	33
Figure 3.6 RII K Index (top left), Unified Model K Index (top right), difference field (bottom left) and the total number of lightning strokes which occurred later in the day (bottom right) for 1 February 2008 .....	34
Figure 3.7 K Index at 0400 UTC (top left), 0500 UTC (top right), 0600 UTC (middle left), 0700 UTC (middle right) and 0800 UTC (bottom) for 15 January 2007 .....	37
Figure 3.8 K Index at 0400 UTC (top left), 0500 UTC (top right), 0600 UTC (middle left), 0700 UTC (middle right) and 0800 UTC (bottom) for 16 January 2007 .....	38
Figure 3.9 Statistical scores for Mixed K Index for all fifty cases .....	41
Figure 3.10 Statistical scores for Mixed Total Totals for all fifty cases .....	42
Figure 3.11 Statistical scores for Lifted Index for all fifty cases .....	43
Figure 3.12 Statistical scores for Precipitable Water for all fifty cases .....	44
Figure 4.1 Cumulative frequency graph for Mixed K Index values (°C) for 2007/8 and 2008/9 seasons .....	47
Figure 4.2 Cumulative frequency graph for Mixed Total Totals values (°C) for 2007/8 and 2008/9 seasons .....	48
Figure 4.3 Cumulative frequency graph for Lifted Index values (°C) for 2007/8 and 2008/9 seasons .....	49
Figure 4.4 Cumulative frequency graph for Precipitable Water values (mm) for 2007/8 and 2008/9 seasons .....	50
Figure 4.5 Average amount of lightning for 2008 (left) and topography of South Africa (right) .....	51
Figure 4.6 Frequency histogram of lightning for 2008 (red) and cumulative frequency graph (blue) related to topography of South Africa, indicated in intervals of 125 m.....	52
Figure 4.7 CII time average between 0600 and 0900 UTC (top left), occurrence of lightning between 1200 and 2100 UTC (top right), Convection RGB product (bottom left) at 1400 UTC and the High Resolution Visible RGB product (bottom right) at 1400 UTC for 2 November 2008.....	61

Figure 4.8 CII time average between 0600 and 0900 UTC (top left), occurrence of lightning between 1200 and 2100 UTC (top right), Convection RGB product (bottom left) at 1300 UTC and the High Resolution Visible RGB product (bottom right) at 1300 UTC for 3 March 2009 .....	62
Figure 5.1 CII (left) and occurrence of lightning (right) for 29 November 2007 .....	65
Figure 5.2 CII statistical scores against the occurrence of lightning for 29 November 2007 .....	65
Figure 5.3 CII (top left) and occurrence of lightning (top right). Areas covered by cloud so that CII values are not available are shown in the 0600 UTC IR108 image below and also indicated by the grey areas in the CII graphic for 14 December 2007 .....	66
Figure 5.4 CII statistical scores against the occurrence of lightning for 14 December 2007 .....	67
Figure 5.5 CII (top left) and occurrence of lightning (top right). Areas covered by cloud so that CII values are not available are shown in the 0600 UTC IR108 image below and also indicated by the grey areas in the CII graphic for 6 January 2008.....	68
Figure 5.6 CII statistical scores against the occurrence of lightning for 6 January 2008.....	69
Figure 5.7 CII (top left) and occurrence of lightning (top right). Areas covered by cloud so that CII values are not available are shown in the 0600 UTC IR108 image below and also indicated by the grey areas in the CII graphic for 7 February 2008 .....	70
Figure 5.8 CII statistical scores against the occurrence of lightning for 7 February 2008 .....	70
Figure 5.9 CII (top left) and occurrence of lightning (top right). Areas covered by cloud so that CII values are not available are shown in the 0600 UTC IR108 image below and also indicated by the grey areas in the CII graphic for 5 March 2008.....	72
Figure 5.10 CII statistical scores against the occurrence of lightning for 5 March 2008 .....	73
Figure 5.11 CII (top left) and occurrence of lightning (top right). Areas covered by cloud so that CII values are not available are shown in the 0600 UTC IR108 image below and also indicated by the grey areas in the CII graphic for 9 November 2008.....	74
Figure 5.12 CII statistical scores against the occurrence of lightning for 9 November 2008.....	75
Figure 5.13 CII (top left) and occurrence of lightning (top right). Areas covered by cloud so that CII values are not available are shown in the 0600 UTC IR108 image below and also indicated by the grey areas in the CII graphic for 23 December 2008.....	76
Figure 5.14 CII statistical scores against the occurrence of lightning for 23 December 2008.....	77

Figure 5.15 CII (top left) and occurrence of lightning (top right). Areas covered by cloud so that CII values are not available are shown in the 0600 UTC IR108 image below and also indicated by the grey areas in the CII graphic for 13 January 2009.....	78
Figure 5.16 CII statistical scores against the occurrence of lightning for 13 January 2009 .....	79
Figure 5.17 CII (top left) and occurrence of lightning (top right). Areas covered by cloud so that CII values are not available are shown in the 0600 UTC IR108 image below and also indicated by the grey areas in the CII graphic for 20 February 2009 .....	80
Figure 5.18 CII statistical scores against the occurrence of lightning for 20 February 2009 .....	81
Figure 5.19 CII (top left) and occurrence of lightning (top right). Areas covered by cloud so that CII values are not available are shown in the 0600 UTC IR108 image below and also indicated by the grey areas in the CII graphic for 13 March 2009 .....	82
Figure 5.20 CII statistical scores against the occurrence of lightning for 13 March 2009 .....	83
Figure 5.21 Statistical scores for CII for fifty case studies .....	84
Figure 5.22 POD for the RII and CII.....	87
Figure 5.23 POFD for the RII and CII .....	88
Figure 5.24 FAR for the RII and CII .....	88
Figure 5.25 Hanssen-Kuipers discriminant for the RII and CII .....	89
Figure 6.1 Climatological observation stations in South Africa.....	92
Figure 6.2 Rainfall stations in South Africa .....	93
Figure 6.3 Example of IPWG evaluation of the Hydroestimator used in Northern America, from <a href="http://cics.umd.edu/~johnj/us/gifs/hydroe+radar.20100115.gif">http://cics.umd.edu/~johnj/us/gifs/hydroe+radar.20100115.gif</a> .....	96
Figure 6.4 Rainfall totals over 24 hours from rain gauges (left) and HE (right) for 18 October 2008 .....	97
Figure 6.5 Rainfall totals over 24 hours from rain gauges (left) and HE (right) for 12 November 2008.....	98
Figure 6.6 CII (top left), HE nine hour total (top right), sum of lightning strokes for nine hours (bottom) for 18 October 2008 .....	99

Figure 6.7 Statistical scores of CII versus HE for 18 October 2008 .....	100
Figure 6.8 Statistical scores of CII versus lightning for 18 October 2008 .....	100
Figure 6.9 CII (top left), HE nine hour total (top right), sum of lightning strokes for nine hours (bottom) for 12 November 2008 .....	101
Figure 6.10 Statistical scores of CII versus HE for 12 November 2008 .....	102
Figure 6.11 Statistical scores of CII versus lightning for 12 November 2008 .....	102
Figure 6.12 CII versus HE for all fifty cases from the two summer seasons .....	103
Figure 6.13 CII time average (top left), HE nine hour total (top right), HE together with IR108 and lightning occurrence (indicated by red, green and blue crosses) at 1600 UTC (bottom left) and MSG Day Natural RGB at 1500 UTC (bottom right) for 1 February 2010 .....	104
Figure 6.14 CII time average (top left), HE nine hour total (top right), HE together with IR108 and lightning occurrence (indicated by red, blue and green crosses) at 1600 UTC (bottom left) and MSG Day Natural RGB at 1500 UTC (bottom right) for 10 February 2010 .....	106
Figure 6.15 CII time average (top left), HE nine hour total (top right), HE together with IR108 and lightning occurrence (indicated by red, blue and green crosses) at 1500 UTC (bottom left) and MSG Day Natural RGB at 1500 UTC (bottom right) for 18 January 2010 .....	107
Figure 7.1 CII three hourly time averages: 0400 to 0700 UTC (top left), 0500 to 0800 UTC (top right), 0600 to 0900 UTC (bottom left) and 0700 to 1000 UTC (bottom right) for 31 January 2010 .....	112

# List of Tables

---

Table 1.1 SEVIRI Imaging Channels (adapted from Morgan, 2002, MSG Brochure: Applications of MSG) .....	7
Table 2.1 List of MPEF products supplied by EUMETSAT adapted from <a href="http://www.eumetsat.int/Home/Main/Access_to_Data/Meteosat_Meteorological_Products/Product_List/index.htm?l=en">http://www.eumetsat.int/Home/Main/Access_to_Data/Meteosat_Meteorological_Products/Product_List/index.htm?l=en</a> .....	13
Table 2.2 Possible threshold values for Lifted Index, adapted from: Severe weather indices page <a href="http://www.theweatherprediction.com/severe/indices">http://www.theweatherprediction.com/severe/indices</a> .....	15
Table 2.3 Possible threshold values for K Index, adapted from: Severe weather indices page <a href="http://www.theweatherprediction.com/severe/indices">http://www.theweatherprediction.com/severe/indices</a> .....	15
Table 2.4 Possible threshold values for Precipitable Water adapted from: Severe weather indices page <a href="http://www.theweatherprediction.com/severe/indices">http://www.theweatherprediction.com/severe/indices</a> .....	16
Table 2.5 Possible threshold values for Total Totals adapted from: Severe weather indices page <a href="http://www.theweatherprediction.com/severe/indices">http://www.theweatherprediction.com/severe/indices</a> .....	21
Table 3.1 List of cases used in this study with the effects and location of the event (SAWS, Climate data base) .....	25
Table 3.2 Statistical scores calculated for evaluation purposes adapted from <a href="http://www.cawcr.gov.au/projects/verification/">http://www.cawcr.gov.au/projects/verification/</a> .....	36
Table 3.3 Evaluation results for K Index for five cases .....	36
Table 3.4 Additional statistical scores calculated for evaluation purposes adapted from <a href="http://www.cawcr.gov.au/projects/verification/">http://www.cawcr.gov.au/projects/verification/</a> .....	40
Table 3.5 Comparison between evaluation scores for K Index and Lifted Index in Poland and South Africa .....	45
Table 4.1 Look up table for Mixed K Index .....	53

Table 4.2 Look up table for Mixed Total Totals.....	54
Table 4.3 Look up table for Lifted Index.....	55
Table 4.4 Look up table for Precipitable Water.....	56
Table 4.5 Look up table for topography .....	58
Table 5.1 Threshold values for each RII corresponding to more than 80% of lightning (from Chapter 4) .....	86
Table 5.2 Lower and upper threshold values for each RII on the normalized scale.....	86

# Chapter 1

## BACKGROUND AND ENABLING TECHNOLOGY

---

### 1.1 INTRODUCTION

Global climate change is a reality of life in the 21<sup>st</sup> Century. There is mounting evidence that changes in the earth's climate system will result in more frequent extreme events. According to the Intergovernmental Panel on Climate Change (IPCC), the frequency of heavy precipitation events has increased over most land areas, consistent with warming and increases of atmospheric water vapour. The possibility exists that the likelihood of temperature extremes, heat waves, and heavy precipitation events will continue to increase (IPCC, 2007). Extreme weather events need to be anticipated not only in the time scale of months or seasons, but also on a day to day basis. The importance of early warning systems to warn the public of these types of weather events therefore becomes more and more critical.

According to the World Meteorological Organization (WMO) Public Weather Service (PWS) programme, nowcasting "comprises the detailed description of the current weather along with forecasts obtained by extrapolation for a period of 0 to 6 hours ahead" (<http://www.wmo.int/pages/prog/amp/pwsp/Nowcasting.htm>). In this time range forecasters use the latest data from remote sensing tools such as radar and satellite, as well as observational data, to analyze and forecast smaller scale weather features for the following few hours. Nowcasting is thus an important tool to issue warnings to the general public of hazardous weather including tropical cyclones, thunderstorms and tornados which is accompanied by flash floods, lightning and destructive wind. For the aviation industry nowcasting is useful for take-off and landing situations as well as in the en-route environment. Nowcasting also serves a purpose for the off-shore oil drilling community, the construction industry and the leisure industry.

While nowcasting is a description of current weather parameters and forecasts for the next six hours, very short range weather forecasting implies forecasts for up to twelve hours. The Hyogo Framework for Action 2005-2010 (<http://www.unisdr.org/wcdr/intergover/official-doc/L-docs/Hyogo-framework-for-action-english.pdf>) which was adopted by 168 governments in January 2005, conducted a survey amongst WMO members in 2006. Poolman *et al.* (2008) listed the objectives of this survey as:

1. “To compile information on severe weather warning systems operated by members with a view to publishing a reference on such systems;
2. To assess the vulnerability of various members to weather related disasters with a view to develop workshops to address the gaps and weaknesses identified, and
3. To assess the PWS needs of National Meteorological and Hydrological Services (NMHS) with a focus on identifying opportunities to improve products and services, in particular, severe weather warning services”.

Results of this survey indicated that rain was the hazard of most concern and forecasting accuracy of rain events was the main challenge. The WMO thus recommended that the focus should be on the enhancement of the predictability of rain (as defined in the survey). It was also recommended that the vulnerability of member countries should be reduced by improving the early warning of short term severe weather phenomena, especially rainstorms.

The WMO organized a series of sub-regional demonstration projects to improve severe weather forecast services in countries where sophisticated forecast systems are not currently used (mostly developing countries). Such a project is currently running from South Africa and is called the Severe Weather Forecast Demonstration Project (SWFDP). The goals of this project include:

1. “To improve the technical ability of weather services,
2. To improve the lead time of warnings,
3. To improve communication between global, regional and National Meteorological Centres (NMCs),
4. To improve interaction of NMCs with disaster management authorities before and during severe weather events and
5. To identify other gaps for improvement” (Poolman *et al.*, 2008).

The need to improve very short range and nowcasting services thus applies to the whole southern African region, specifically with regard to convective storm development and evolution. However, there are marked differences between the technologies available to support such services in the various countries of southern Africa. Most southern African countries are heavily reliant on satellite technology due to the limited number of surface and upper-air observations and the limited availability of numerical model output. They do not have access to weather radar or lightning information, nor the systems to integrate the data and products from various sources. South Africa, on the other hand, has a radar network and a lightning detection network, as well as the means to integrate, display and manipulate these various data sets.

In developing tools for the first twelve forecast hours, the South African Weather Service (SAWS) needs to keep in mind the national as well as the regional capacities. Although the approach to be followed for the southern African region outside of South Africa has to be distinctly different from the

possibilities for South Africa itself, some of the techniques developed for South Africa might also be useful within the region.

According to the Very Short Range Forecasting and Nowcasting business plan of the SAWS, the national requirements for the SAWS to improve its capabilities for warnings and forecasts for up to twelve hours have increased considerably in the past few years and these requirements are expected to grow even more as society becomes more susceptible to the effects of high-impact weather events. The SAWS has to render services to the public and private sectors including the issuing of advisories on the areas in which severe weather will develop and of severe storm warnings and flash flood guidance. The blending of a range of techniques in an optimal manner will be essential in achieving this.

## 1.2 SOUTH AFRICA'S CLIMATE AND CONVECTIVE ACTIVITY

In order to understand South Africa's climate and weather patterns better, a few comments on the general summer weather patterns, hazardous weather, seasonal rainfall patterns, thunderstorm occurrence as well as severe thunderstorm characteristics are given here. This will set the background for thunderstorm discussions, which will follow in the next chapters.

*General summer weather patterns:* South Africa's climate scene limits the occurrence of convective thundershowers to the summer season, starting in October and ending in March. The wind that originates from the Indian Ocean high pressure system, southeast of the country, travels across the warm Indian Ocean, picking up moisture, thus bringing moist air to the eastern parts of southern Africa. The Atlantic Ocean High pressure system, southwest of the country, is a source of dry subsiding air (Figure 1.1).

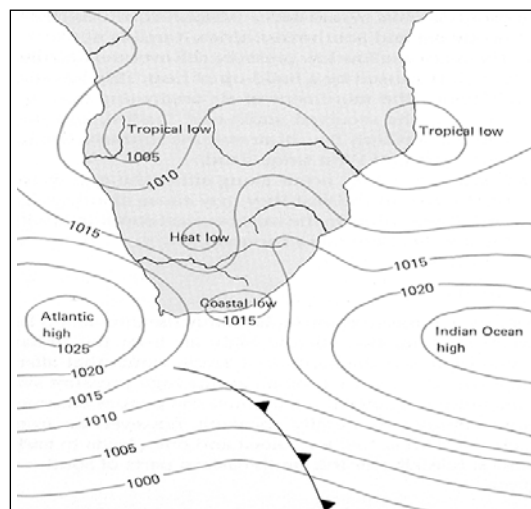


Figure 1.1 Schematic of the role players in South Africa's summer circulation (after Hurry and Van Heerden, 1982)

Where the air masses from the Atlantic Ocean High and the Indian Ocean High meet, a moisture boundary is formed. The position of this boundary affects the distribution of rainfall: when it lies to the north, dry conditions prevail and when it lies to the south, widespread rain is possible. Northeasterly monsoon winds occur over the eastern coast of southern Africa. They are closely linked to the great monsoon system over India and Asia. The northeast monsoon winds cross the equator and meet the southeast trade winds, forming another convergence zone, called the Inter-tropical Convergence Zone (ITCZ) (Hurry and van Heerden, 1982).

*Hazardous weather:* A large percentage of disasters across the world and in southern Africa are weather related. The fact that South Africa is influenced by both tropical and mid-latitude air masses and the interaction between them sets the scene for various types of severe weather events that are often difficult to predict with long lead times. A hazard analysis of South African data of extreme events shows that during the period 1961 to 2005, 39% of the events were related to flooding, 22% to severe storms and 15% to wind damage (Poolman, 2007).

*Rainfall:* The highest rainfall occurs along the eastern escarpment, in particular, along the mountain ranges in the South East. Rainfall generally decreases from east to west; the highest amounts in the east have an average of 800 mm per year, while amounts of less than 200 mm per year occur in the west (Figure 1.2, Kruger, 2007). Summer rainfall occurs over the northeastern half of the country (Figure 1.3, Kruger, 2007), with mainly winter rainfall in the southwestern parts.

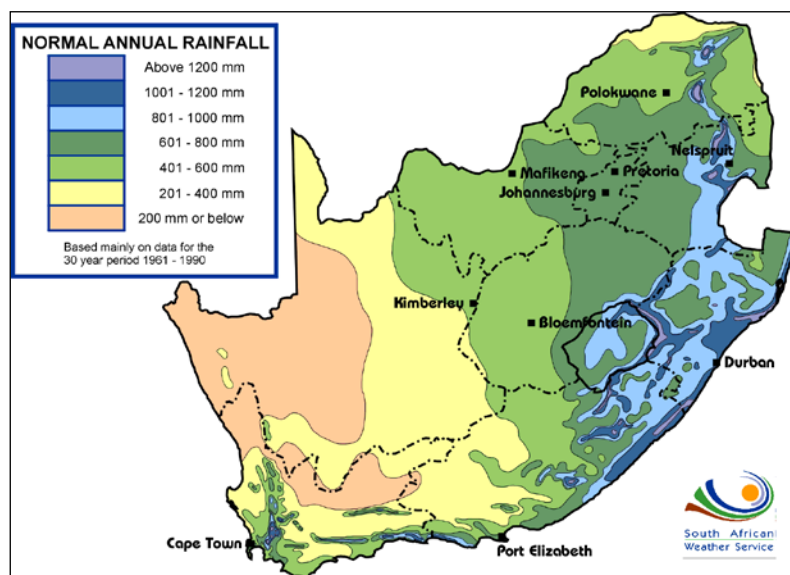


Figure 1.2 Normal annual rainfall over South Africa (after Kruger, 2007)

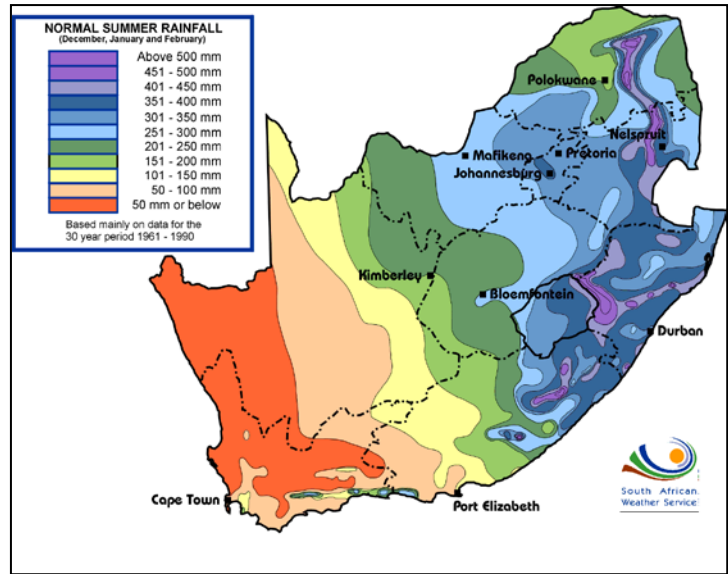


Figure 1.3 Normal summer rainfall over South Africa (after Kruger, 2007)

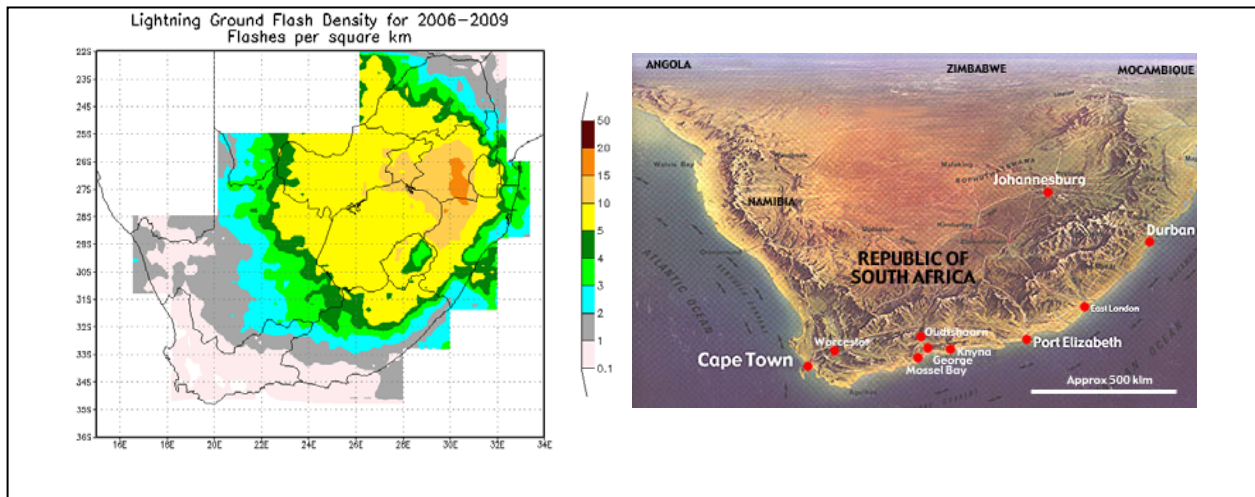


Figure 1.4 Lightning flash density for 2006 to 2009 (left) and South Africa's topography (right)

Thunderstorms, due to their high frequency of occurrence over South Africa and the high impact weather they produce, are the primary focus of very short range forecasting and nowcasting efforts in South Africa. Convective storms are a major producer of rainfall over the summer rainfall areas of South Africa. Kruger (2006) indicated that in the summer rainfall regions of South Africa the rainfall events are becoming more intense and produce larger extreme rainfall values. Most of these high rainfall events occur in conjunction with convection and lightning. Gill (2008a) analyzed the lightning data from the SAWS Lightning Detection Network (LDN) for 2006 and 2007 and found the lightning density to be more than six flashes per square kilometre over the northeastern half of the country (Figure 1.4).

*Severe thunderstorms:* Supercells, which are usually associated with severe weather such as tornadoes and hail, are relatively rare judging by the work done on the nature of hail producing storms

by Held (1978; 1982) and Carte and Held (1978). They studied 361 storm days on the plateau of South Africa and of those 39% of the days had isolated thunderstorms, 54% had scattered storms and squall lines only occurred on 7% of the days. De Coning et al. (2000) documented an example of a recent supercell event. Although tornadic events are less frequent than in the United States, an annual average of four tornadoes occur in South Africa (Goliger *et al.*, 1997). The 1998/9 summer season had an unusually high occurrence of tornadic events, although damage surveys are not officially done in South Africa to validate all of them (De Coning and Adam, 2000).

## **1.3 ENABLING TECHNOLOGY IN SOUTH AFRICA**

### **1.3.1 Meteosat Second Generation satellite data**

Both South Africa and Africa as a whole have had access to the European Geostationary Meteosat Second Generation (MSG) satellite image data and derived products since 2005. The first satellite of the series, then known as MSG, was launched on 28 August 2002 after a development phase conducted by the European Space Agency on behalf of EUMETSAT (European Organization for the Exploitation of Meteorological Satellites). An intensive commissioning phase then followed and by 29 January 2004 the satellite, now known as Meteosat-8, was in full operation, allowing access to its data on a routine basis throughout its wide field of view, encompassing Europe, Africa and the Middle East (Morgan, 2002). MSG-2 (Meteosat Second Generation-2) is the follow-on to MSG-1 and was launched on 21 December 2005. The two ton, spin stabilized craft carries the same instruments as MSG-1 (Spinning Enhanced Visible and InfraRed Imager or SEVIRI and Geostationary Earth Radiation Budget or GERB) and provides the same products. The satellite was renamed Meteosat-9 when it became operational in June 2006 (MSG-2 successfully launched, 2005).

This satellite offers a choice of twelve channels to use individually or in combination for various purposes, including nowcasting of convection (Table 1.1). For eleven of the twelve channels, image pixels are sampled every 15 minutes at intervals of 3 km over the entire area. The High Resolution Visible (HRV) channel has a sampling distance of just 1 km, with the east-west scan limited to half of the full earth disc.

**Table 1.1 SEVIRI Imaging Channels (adapted from Morgan, 2002, MSG Brochure: Applications of MSG)**

Channel name	Nominal central wavelength ( $\mu\text{m}$ )	Application and history
VIS 0.6	0.635	History: Similar channels of the Advanced Very High Resolution Radiometer (AVHRR) on National Oceanic and Atmospheric Administration (NOAA) satellites. Applications: cloud detection, cloud tracking, scene identification, monitoring of land surfaces and aerosols and in combination to generate vegetation indices.
VIS 0.8	0.81	
NIR 1.6	1.64	History: Along Track Scanning Radiometer (ATSR) on European Remote Sensing (ERS) satellites. Applications: discriminate between snow and cloud, as well as between ice and water clouds, aerosol information.
IR 3.9	3.92	History: AVHRR. Applications: detection of low cloud and fog at night, measurement of land and sea temperatures at night, the detection of forest fires.
WV 6.2	6.26	Applications: measurements of mid-atmosphere water vapour, tracers for atmospheric winds, height assignment for semi-transparent clouds.
WV 7.3	7.35	
IR 8.7	8.7	History: High Resolution Infrared Radiation Sounder (HIRS) on NOAA satellites. Applications: provide quantitative information on thin cirrus clouds, discrimination between ice and water clouds.
IR 9.7	9.66	Applications: ozone concentration in the lower stratosphere, to monitor total ozone, assess diurnal variability, tracking ozone patterns as an indicator of wind fields at that level.
IR 10.8	10.8	Applications: temperature of clouds and the surface, help to reduce atmospheric effects when measuring surface and cloud top temperatures, cloud tracking for atmospheric wind and for estimates of atmospheric instability.
IR 12.0	12.0	
IR 13.4	13.4	History: Geostationary Operational Environmental Satellite (GOES)-VISSR Atmospheric Sounder (VAS). Applications: estimation of atmospheric instability, temperature information on the lower troposphere.

With MSG it is possible to provide images, day and night, of clouds and cloud systems at nearly every scale. It is also possible to look at the clouds and learn about their internal processes and states, e.g. cloud droplet size can be inferred, surface fog may be detected even at night, vegetation growth monitored and many more. A number of applications have also been developed to make use of these new capabilities for nowcasting, especially for the detection and prediction of severe weather (Morgan, 2002). Chapter 2 will discuss these products in more detail.

#### *Hydroestimator*

Satellite precipitation estimates (SPE) offer an excellent way to compensate for some of the limitations of other sources of quantitative precipitation information. However, the relationship between satellite-measured radiances and rainfall rates is less robust than that between radar

reflectivities and rainfall rates. SPE should thus not be considered as a replacement for radar estimates and gauges but as a complement (Scofield and Kuligowski, 2003).

Scofield (2001) described the status and outlook of operational satellite precipitation algorithms for extreme precipitation events. Since 1978, SPE for flash floods have been produced using data from the GOES. They combine manual effort and computer algorithms with the main application to alert forecasters and hydrologists of the potential for heavy precipitation and flash floods. Due to the interactive nature of this method, these SPE cover limited areas over limited periods of time and take a significant amount of time to produce. To address these problems, the National Environmental Satellite, Data and Information Service (NESDIS) developed an automated SPE algorithm for high-intensity rainfall called the Autoestimator (AE). The original AE, developed by Vicente *et al.* (1998), computes rain rates from 10.7  $\mu\text{m}$  brightness temperatures based on a curve that was derived from more than 6000 collocated radar and satellite pixels.

The dependence of the initial AE on radar was a significant problem, because one of the advertised strengths of satellite QPE (Quantitative Precipitation Estimation) is its usefulness in regions for which radar and/or rain gauge coverage is unavailable. Another version of the AE, called the Hydroestimator (HE) has been developed which can be used outside of regions of radar coverage without compromising too much accuracy. In southern Africa a precipitation estimator independent of radars was required and thus the HE suited the need. During September 2007 a local version of the Hydroestimator was installed and tested at the South African Weather Service and has been running operationally ever since. More detail will follow in Chapter 6.

### **1.3.2 Radar**

The SAWS owns ten C-band and two S-band radar systems of various ages and manufacturers. These systems are equipped with a common receiver processor and a control system, which allow the data to be collected in continuous volume scan mode and to be transformed into a common format (Dixon and Wiener, 1993). Data are collected within a range of 200 km to 300 km. The spacing of these radars is not ideal for observing stratiform rain because such systems are relatively shallow, resulting in the radar beam overshooting the echo tops at long ranges. Convective storms, however, have relatively deep vertical dimensions allowing them to be observed, at least partially, at longer ranges. Calibration checks are routinely performed and the systems are stable. Comparisons between different radars in the overlap areas provide further confidence in the system performance (Terblanche *et al.*, 2001). Radar data will not be used in this study, but it forms part of the suite of nowcasting and very short range forecasting tools.

### **1.3.3 Lightning**

A Lightning Detection Network (LDN) consisting of 19 VAISALA LS7000 sensors was installed across South Africa by the beginning of 2006 (Figure 1.5). This network in South Africa is one of only three

ground-based lightning detection networks in the southern hemisphere. Data from this network provides only cloud-to-ground recordings, but constitutes a sufficient basis to start developing a lightning climatology for the country (Gill, 2008b).

Outside the boundaries of South Africa incorrect values of lightning occurrence are sometimes recorded by the LDN. According to Zajac and Rutledge (2001) lightning detected at a distance of more than 100 km from the outer ring of lightning sensors is very often a false recording. Data usage should thus be limited to continental South Africa and the ocean regions within 100 km of the coastline.

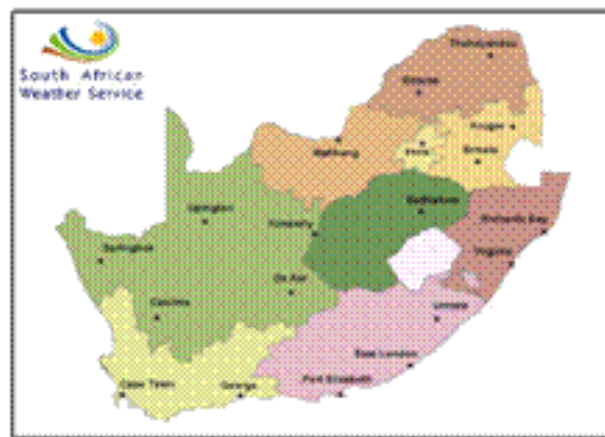


Figure 1.5 Location of lightning detection network sensors (after Gill, 2008b)

“One of the primary determinants of ground flash density in South Africa is topography. The major mountain ranges act to enhance convection on their windward slopes” (Gill, 2008a). Most of the lightning along the escarpment and into the interior is associated with deep convection. Gill (2008a) found that the areas at highest risk from both intense lightning and mainly lightning of positive polarity are found along the escarpment. This confirms findings of Cecil (2008) using Tropical Rainfall Measuring Mission (TRMM) that the areas where most thunderstorms occur are linked to orographic features, which enhance the forcing. Gill (2008b) developed a method to determine the lightning risk for different areas of the country.

### 1.3.4 Unified Model

The Unified Model is the suite of atmospheric and oceanic numerical modelling software, developed and used at the UK Meteorological Office since 1991. The Met Office maintains a suite of versions at particular resolutions that it encourages collaborating partner institutions to use. These include a regional 12 km, a mesoscale 4 km and a high-resolution 1.5 km model. In practice, the resolution and domain size of the limited area model chosen is constrained by the available computing power. At the SAWS, the Unified Model runs operationally at a horizontal resolution of 12 km and is scheduled to run twice daily to provide hourly numerical forecasts of atmospheric conditions for up to 48 hours ahead.

## 1.4 RESEARCH PROBLEM

Forecasting for the first twelve hours requires extensive use of remote sensing tools including radar, lightning networks and satellite. Various research programmes make use of satellite data since this type of data has become increasingly useful as a result of spatial and temporal resolution increases. Work done by researchers at the University of Alabama in Huntsville (UAH) and the University of Wisconsin Cooperative Institute of Meteorological Satellite Studies (UW-CIMSS) is focussed on enhancing GOES-based data with lightning information, as well as with data from the MODerate resolution Infrared Spectrometer (MODIS) to predict the onset of convection (Mecikalski *et al.*, 2007). Their Convection Initiation (CI) nowcasting method relies on the use of infrared and visible satellite data from GOES, and cloud-motion winds for tracking cumulus clouds (Bedka and Mecikalski, 2005; Mecikalski *et al.*, 2007; Mecikalski *et al.*, 2008). Recently this technique was also expanded to be used with MSG data over Europe and Africa (Mecikalski, 2007) and in the future with Meteosat Third Generation (MTG).

Convective cloud top temperatures and signatures, and cloud microphysics have been thoroughly described by, Setvak and Doswell (1990), Caruso *et al.* (2000), Setvak *et al.* (2003), Setvak and Rabin (2005), Rosenfeld and Lensky (2006) and many others. Signals of severe convection including the V-shaped cloud formation and the cold U-shape clouds have been analyzed together with radar data and in-cloud measurements, where possible.

Forecasting convection is one of the most difficult challenges facing forecasters in southern Africa. Now that South Africa is receiving MSG data, there is an opportunity to join the world of satellite researchers in a region where it is very much needed. Operational forecasters have a lot of data to analyze and combine into a forecast. One of their biggest needs is easy, simple ways to integrate all relevant data to make very short-range forecasts and nowcasts of convective activity. Despite the role that numerical weather prediction models play to give general guidance on where convection might be favourable, more detailed information is needed closer to time. If model data and satellite data can be combined, it will offer greater spatial as well as temporal guidance closer to the time of convective activity. The purpose of this study is to provide this much needed guidance in the form of a probability map for convection.

## 1.5 HYPOTHESIS

The hypothesis of this study is that remote sensing data from the geostationary MSG satellite and the lightning detection network can be integrated with numerical model data into a product, which will give forecasters guidance on where convection is more likely to occur, with at least a three to six hour lead time.

## **1.6 AIMS AND OBJECTIVES**

Aims of the study are twofold:

1. To provide operational forecasters in South Africa as well as the rest of southern Africa with a satellite derived product that will indicate the areas where convection is most likely to occur. This newly developed product will combine and modify existing products in order to provide a single map, which will indicate the probability of convective development over land with a three to nine hour lead time.
2. To test and verify the new combined product against observed lightning data and satellite based rainfall estimations using case studies from two summer seasons to prove its usefulness.

The ultimate goal of the research is to provide an operational probability map for the occurrence of convection over land with a three to nine hour lead time.

## **1.7 LAYOUT OF THE THESIS**

In Chapter 2 the role of satellite and model combination fields and how these combinations have been adjusted for South African circumstances are explained. In Chapter 3, the satellite based instability indices are compared to the Unified Model instability fields to determine whether the use of satellite fields adds value to the product derived solely from the model fields. Chapter 4 deals with the construction of the new, combined index to give a single probability map indicating where convection is likely. In Chapter 5 the new index is evaluated against the occurrence of lightning in 50 case studies over the 2007/8 and 2008/9 summer seasons in order to show the extent of the correlation between the two fields. Finally, in Chapter 6 the new index is compared to the local version of the Hydroestimator to show possible value for regions in southern Africa where lightning detection networks do not exist.

# CHAPTER 2

## MSG APPLICATIONS FOR FORECASTING OF CONVECTION

---

### 2.1 BACKGROUND

This chapter starts with a brief discussion of the visual by-products of MSG, which can be used for various purposes, including convection forecasting. A summarized description of the theory for the Global Instability Indices (GII) product follows, defining the relevant indices as well as the theory behind their calculations for the satellite and model combined fields. Initial evaluation of the GII in South Africa will be addressed subsequently, starting with a simple visual verification method. The final section deals with the local implementation of the GII in South Africa based on the 12 km version of the Unified Model. Changes were made to suit South African circumstances and these will be listed and discussed at the end of the chapter.

### 2.2 METEOROLOGICAL PRODUCTS EXTRACTION FACILITY (MPEF)

In addition to the purely visual interpretation of the MSG channels, the ultimate usefulness comes from digital products extracted from the data. The Satellite Application Facilities (SAF) in Europe have developed products for very specific applications, e.g. climate and land or ocean surface related products, but a comprehensive range of products has also been derived centrally within the MSG Meteorological Products Extraction Facility (MPEF) located at the EUMETSAT Headquarters in Darmstadt, Germany (Morgan, 2002). Many of the products were also available for the Meteosat First Generation (MFG) satellite data, but they are now improved because of the characteristics of the MSG SEVIRI instrument.

The first step in the MPEF processing is an automatic scene analysis of each image in near real time, using multispectral thresholding techniques to decide into which class each pixel of the image falls, e.g. sea, land type, low cloud, high cloud etc. This comprehensive analysis of each image forms the basis for further processing to calculate other MPEF products. All of this processing is done in near real time, every 15 minutes, and 24 hours a day. Resulting data are distributed on the Global Telecommunications System (GTS) of the WMO, as well as via the EUMETSAT dissemination service, called EUMETCast (Morgan, 2002). A list of the MPEF is shown in Table 2.1.

**Table 2.1 List of MPEF products supplied by EUMETSAT adapted from [http://www.eumetsat.int/Home/Main/Access to Data/Meteosat Meteorological Products/Product List/index.htm?l=en](http://www.eumetsat.int/Home/Main/Access%20to%20Data/Meteosat%20Meteorological%20Products/Product%20List/index.htm?l=en)**

PRODUCT	PURPOSE
AMV (Atmospheric Motion Vectors)	Most important product for Numerical Weather Prediction (NWP). Applications: information on atmospheric dynamics not available from other sources.
CSR (Clear Sky Radiances)	CSR are the mean radiances for cloud free pixels. Applications: useful for operational NWP.
GII (Global Instability Indices)	GII are airmass parameters which act as stability indicators of the atmosphere. Applications: used to complement upper-air sounding data on a real time basis.
TH (Tropospheric Humidity)	TH indicates the layer mean humidities between 500 and 200 hPa and between 850 and 300 hPa, respectively.
CLA (Cloud Analysis)	CLA is based directly on the scene analysis. Applications: information on cloud cover, cloud top temperature / pressure / height, cloud type and phase.
CTH (Cloud Top Height)	CTH provides the height of the highest cloud. Applications: aviation meteorology.
CDS (Climate Data Set)	CDS provides information on the scene classes in each segment. Applications: climate studies.
TOZ (Total Ozone)	The TOZ product provides information on ozone. Applications: information on high level wind, can also be assimilated directly into NWP models.
IDS (ISCCP Data Set)	The IDS is the EUMETSAT/MSG contribution to the International Satellite Cloud Climatology Project (ISCCP).
HPI (High Resolution Precipitation Index)	The HPI is the EUMETSAT/MSG contribution to the Global Precipitation Climatology Project (GPCP). Applications: tropical convective rainfall.

## 2.3 THE GLOBAL INSTABILITY INDICES (GII)

Since accuracy and timeliness of prediction of convective processes are so crucially important, many MSG based observations of clouds and their temporal evolution have been used in both their qualitative and quantitative aspects to identify the most severe parts of a convective cloud system (Setvák and Rabin, 2005; Rosenfeld and Lensky, 2006; Setvak *et al.*, 2007, Setvak *et al.*, 2008). Using the MSG infrared channels it is also possible to assess the air stability in pre-convective, i.e. still cloud free conditions. Air instability indices have been used for many years in evaluating the

convective potential of the atmosphere (Peppler, 1988). Values of convective indices can vary greatly with time and space because of frequent changes in wind and low-level moisture in storm environments. When these indices are calculated from radiosonde profiles, they are highly dependent on time and place and might not represent the environmental conditions accurately. Observations that are more frequent are needed to capture the degree of instability of the atmosphere properly (Wagner *et al.*, 2008).

Satellite based temperature and moisture retrievals are now being used for the derivation of instability indices. These types of retrievals of instability and air mass parameters are nothing new, having been made operationally since 1988 using first the GOES VISSR Atmospheric Sounder instrument and later the GOES Sounder (Hayden, 1988; Huang *et al.* 1992; Rao and Fuelberg, 1997; Menzel *et al.*, 1998; Dostalek and Schmit, 2001; Schmit *et al.*, 2002). Kitzmiller and McGovern (1989) have shown that the good spatial and temporal resolution of the VAS instrument and of the derived parameters does in fact add value when the potential of pre-convective conditions have to be determined.

The greatest advantage of these fields is the added capability of the nearly continuous monitoring of the instability fields guaranteed by the MSG 15 minute repeat cycle. This provides forecasters with new information much more frequently than the twice-daily soundings at only a limited number of radiosonde stations. This instability product is aimed at helping forecasters to focus their attention on a particular region, which can then be monitored more closely by other means such as satellite imagery and/or radar data. The indices can only assess the likelihood of convection within the next few hours and should be seen in combination with other triggering and/or lifting mechanisms (Koenig and de Coning, 2009).

## 2.3.1 Theoretical background

### 2.3.1.1 The parameters

The GII parameters are provided for the entire MSG field of view and the current operational setup is such that the product is derived as 15X15 pixel averages, i.e. over an area of approximately 50X50 km. The MPEF GII product includes two instability indices, the Lifted Index and the K Index, as well as Total Precipitable Water content (TPW) as an air mass analysis parameter.

The Lifted Index (Galway, 1956) is similar to the Showalter Index, except for the level from which the parcel is lifted. In addition, the Lifted Index is a forecast index whereas the Showalter Index is a static index (Peppler, 1988). It is defined as:

$$\text{Lifted Index} = T_{500} - T \text{ (surface skin temperature, lifted to 500hPa).} \quad (1a)$$



Meaningful values of the Lifted Index as used in the United States for the occurrence of convection are shown in Table 2.2. The value of -2°C was used as the threshold for severe storm formation in the Miller forecasting scheme (Miller, 1967, 1972 and 1975).

**Table 2.2 Possible threshold values for Lifted Index, adapted from: Severe weather indices page <http://www.theweatherprediction.com/severe/indices>**

Lifted Index	
-1 to -4°C	Marginal instability
-4 to -7°C	Large instability
Less than -8°C	Extreme instability

The K Index (George, 1960) combines the 850 and 500 hPa temperature difference, the 850 hPa dew point and the 700 hPa dew point depression to aid thunderstorm prediction in summer and is defined as:

$$K \text{ Index} = ( T_{850} - T_{500} ) + TD_{850} - ( T_{700} - TD_{700} )$$

where

T is the air temperature at the indicated levels and

TD is the observed dew point temperature at the indicated levels. (1b)

Meaningful values for the K Index as used in the United States are shown in Table 2.3. These values agree with Hambridge (1967) who found that, for the western United States, K Index values of between 15°C and 20°C indicate a less than 20% chance of thunderstorms, while for K Index values of above 40°C indicate that there is a 100% chance of seeing thunderstorms.

**Table 2.3 Possible threshold values for K Index, adapted from: Severe weather indices page <http://www.theweatherprediction.com/severe/indices>**

K Index	
15 to 25°C	Small convective potential
26 to 39°C	Moderate convective potential
More than 40°C	High convective potential

Total Precipitable Water is defined as:

$$\text{TPW} = \text{Vertically integrated water vapour content from the bottom to the top of the atmosphere} \quad (1c)$$

Meaningful values for TPW are shown in Table 2.4.

**Table 2.4 Possible threshold values for Precipitable Water adapted from: Severe weather indices page <http://www.theweatherprediction.com/severe/indices>**

Total Column Precipitable Water	
Less than 12.5 mm	Very low moisture content
13 to 31 mm	Low moisture content
32 to 44 mm	Moderate moisture content
More than 44 mm	High moisture content

Such indices are of course of empirical nature and are dependent on geographic regions and seasonal variation, but they can assess the likelihood of convection within the next few hours, thus providing a warning at short lead-time. Although these values can be used as an initial guide, they are highly dependent on the geography of the local environment and could need adjustment for another region. Human interpretation is still necessary for a correct usage of the provided indices and their threshold values (Koenig and de Coning, 2009).

### 2.3.1.2 The theory

For a thorough exposition of the GII concept, the reader is referred to Koenig (2002 and 2007) and Koenig and de Coning (2009). The most important features can be summarized as follows:

The GII retrieval algorithm is in theory very similar to the physical retrievals developed for the GOES Sounder instrument. Due to a number of differences in channels and the details of the applied radiative transfer model, the retrieval had to be adjusted accordingly. The algorithm works only for clear sky conditions, i.e. no instability information is available for cloudy pixels.

The GII retrieval attempts to construct an actual temperature and humidity profile from the satellite-observed radiances within a given set of channels and the air mass parameters are then derived from this profile. It is a “physical” method, as opposed to a statistical method. An inversion algorithm is

applied (Rodgers, 1976; Hayden, 1988; Ma *et al.*, 1999) that produces a retrieval, which is as close as possible to the observations. Generally speaking, this is a multi-solution problem and thus a suitable “background” or “first guess” profile is used as a constraint to the solution. The first guess is fed to the iteration scheme as an initial proposal for a solution and then modified in a controlled manner until its radiative properties (the simulated radiances at the top of the atmosphere for the MSG channels) fit the satellite observations.

The standard retrieval equation (Rodgers, 1976; Ma *et al.*, 1999) is used:

$$x_{n+1} = x_0 + (\mathbf{S}_x^{-1} + \mathbf{K}_n^T \mathbf{S}_\varepsilon \mathbf{K}_n)^{-1} \times \mathbf{K}_n^T \mathbf{S}_\varepsilon^{-1} [T_B - T_{B,n} + \mathbf{K}_n (x_n - x_0)] \quad (2)$$

with

$x$ : observation vector (temperature and humidity profile)

$n$ : iteration step,  $n=0$  denotes the first guess or background profile

$T_B$ : observed brightness temperature

$T_{B,n}$ : simulated brightness temperature for the profile of iteration step  $n$

$\mathbf{S}_x$ : covariance matrix of first guess errors

$\mathbf{K}_n$ : weighting function matrix (Jacobians)

$\mathbf{S}_\varepsilon$ : error covariance matrix of observed brightness temperatures and of the radiation.

The physical retrieval uses six channels: the three long wave window channels IR8.7, IR10.8 and IR12.0, the two water vapour channels WV6.2 and WV7.3, and the CO<sub>2</sub> channel IR13.4. The matrix  $\mathbf{S}_\varepsilon$  contains the temperature noise of the instrument in these six channels with the uncertainty of the radiation model added. The covariance matrix  $\mathbf{S}_x$  was produced from a near global (60°S to 60°N) set of atmospheric profiles (Chevallier, 2002) to cover a wide range of natural variability.

The background profile used for the GII is the 6-hour forecast from the ECMWF (European Centre for Medium-Range Weather Forecasts) global model on a 1° latitude/longitude grid, interpolated in time to the actual image time.

The observation vector  $x$  contains the full vertical temperature and humidity profile and the surface skin temperature as the important lower boundary condition for the IR window channels.

The radiation model RTTOV (Eyre, 1991; Saunders *et al.*, 1999) is used to derive the Jacobians,  $K_n$ , in a fast and effective manner. In addition, the forward model of RTTOV (version 8.7) is used to derive the simulated MSG temperatures for a given observation profile  $x$ . The iteration is terminated when the root mean square (RMS) difference between the observed and simulated brightness temperatures in the six channels becomes less than a given threshold (1.5 K).

A value is only assigned to a processing box if 50 percent or more of the box is cloud free, where the cloud information is taken from the MSG Cloud Mask product (Lutz, 2007). The brightness temperatures are averaged over these cloud free pixels only.

A last input parameter for the retrieval scheme which needs to be mentioned, is the spectral surface emissivity, which is important for the SEVIRI IR8.7 channel. Non-vegetated, desert type surfaces have a rather low surface emissivity of 0.75 to 0.80 in this channel, and this needs to be accounted for within the radiation model of the retrieval. The spectral emissivities from the IREMIS database (<http://cimss.ssec.wisc.edu/iremisp/>, Seemann *et al.*, 2008) are remapped to the MSG pixel locations. The inversion scheme depends on the first guess field. In many cases the first guess already matches the observations so closely that no changes are needed, but there are also cases where the first guess field is quite significantly changed within the retrieval. This added satellite information often modifies extreme values and local gradients.

## **2.4 THE INITIAL EVALUATION OF THE GII IN SOUTH AFRICA**

### **2.4.1 Visual verification**

A number of studies have been done since 2005 to show the value of the GII product for South African cases. Initially, the verification was of the simple visual variety. A good example of one such case is 6 November 2005 (Koenig and de Coning, 2006). During the weekend of 4 to 6 November 2005 heavy rainfall across South Africa brought welcome relief after very hot (heat wave) conditions over most of the country. Over the northern parts of the country large amounts of rain fell in short periods of time. This led to local flooding and considerable damage was caused by strong wind around 1530 UTC. Electricity cables were damaged which led to power outages, roofs were blown off and informal settlements were destroyed in some villages east of Polokwane, Limpopo Province (Figure 2.1).

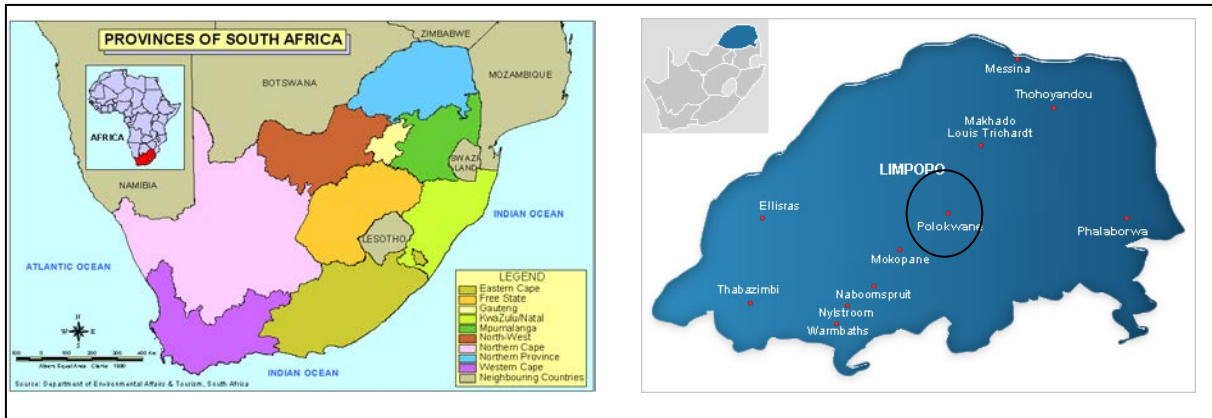


Figure 2.1 Provinces of South Africa (left) and location of a few cities in Limpopo Province, amongst others, Polokwane (right)

According to newspaper reports (Sowetan, 2005) a 10-year-old boy drowned when the shack where he lived washed away and three women were injured when their houses collapsed. On the 4<sup>th</sup> rainfall amounts over the northern most province of South Africa were less than 10 mm, but on the 5<sup>th</sup> rainfall totals were between 20 and 50 mm. Convection started to the west-northwest of the province on the surface dry line and migrated towards the east-northeast (along with the upper air flow) and entered the area of interest during the early afternoon.

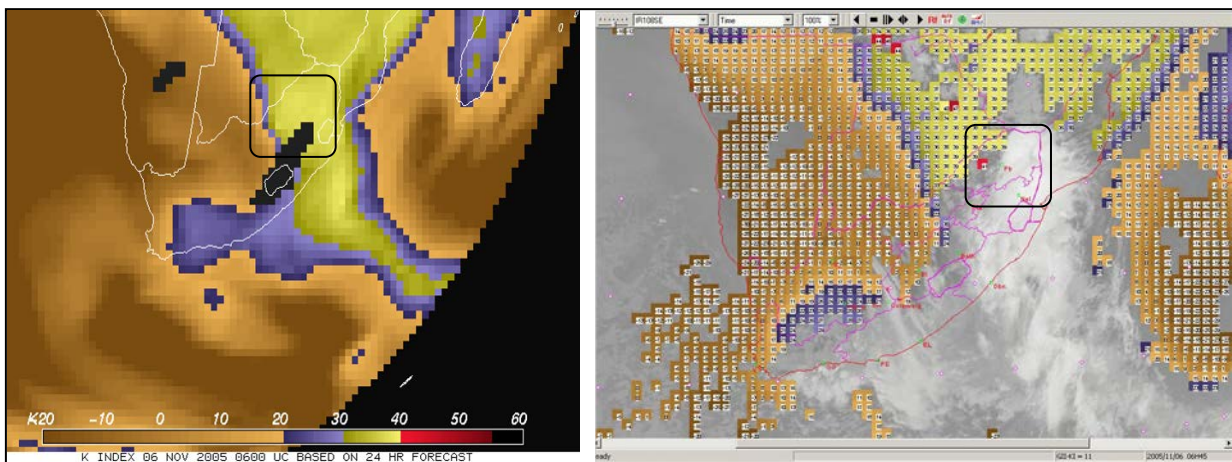


Figure 2.2 ECMWF 24 hour forecast for the K Index at 0600 UTC on 6 November 2005 (left) and GII K Index over South Africa at 0645 UTC (right)

The K Index, derived from the upper air sounding at Polokwane (circled in Figure 2.1, right) at midday, was more than 32°C, but the Lifted Index only -0.5°C. Using a 24-hour forecast for 0600 UTC from the ECMWF numerical weather prediction model, the K Index showed values greater than 30°C, which is a good indicator for instability and thus thunderstorm development (Figure 2.2, left).

Using the GII K Index at a resolution of 15X15 pixels at 0645 UTC, values of more than 40°C could be seen in the area where the severe weather occurred later in the day (Figure 2.2, right). The K Index

as calculated by the GII would have made it possible to see signs of the probability and severity of these thunderstorms already early in the morning (more than 9 hours in advance). These signs also persisted to later in the day. Adding the information of the six MSG channels to the model field thus adds value in computing the instability indices. The GII appeared to be successful as a very short term and/or nowcasting tool when used in combination with real time data.

## 2.5 THE REGIONAL INSTABILITY INDICES (RII)

The MPEF operational GII product uses the forecast fields from the ECMWF model with a 1° latitude/longitude horizontal resolution. A local version of the GII code installed at SAWS in September 2007 uses a local mesoscale model (a version of the Met Office Unified Model) with a 0.1° latitude/longitude resolution. It is now possible to calculate the values for a 3X3 MSG pixel block, replacing the coarser 15X15 pixel processing areas of the MPEF product. This local version of the GII is called the Regional Instability Indices (RII). The RII product does not cover the entire MSG footprint, but only the domain of the Unified Model run on South African computers, i.e. between 0.48° N and 44°S, and 10°W and 56°E, with an East/West resolution of 0.11° and a North/South resolution of 0.1112°. Typical output comparing the GII K Index to the RII K Index is given in Figure 2.3.

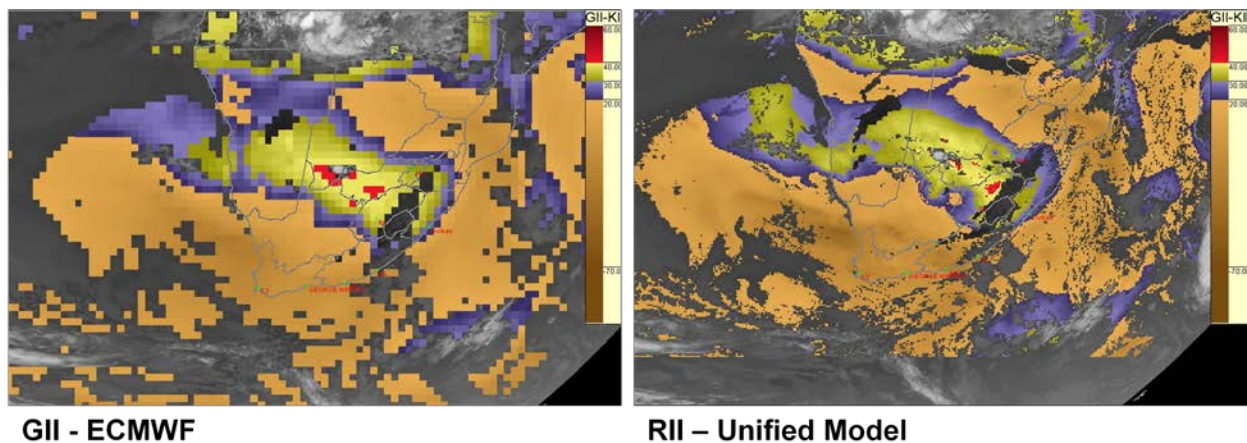


Figure 2.3 GII K Index (left) with a 15X15 pixel resolution and RII K Index (right) with a 3X3 pixel resolution

The output from the RII is available on local servers and could easily be manipulated to add and adjust indices. Consequently, Total Totals was added to the existing three indices and Lifted Index was adjusted.

### 2.5.1 Changes to the suite of instability indices

The GII Lifted Index was observed to be too negative. Values of less than -15°C were often seen in the GII field and do not occur in reality in South Africa. The calculation of the Lifted Index was

subsequently adjusted by changing the weight of the surface skin temperature and since then values have been much closer to the observed.

In an effort to include a parameter, which could add information on the severity of thunderstorms, Total Totals (Miller, 1967) was added to the list. Total Totals is defined as:

$$\text{Total Totals} = T(850) + TD(850) - 2T(500) \quad (4)$$

where

T is temperature at the indicated levels and

TD is dew point temperature at the indicated levels.

Meaningful values as used in the United States are listed in Table 2.5. This agrees with Miller (1967, 1972 and 1975) where a value of 44°C is a lower threshold for thunderstorm activity and more than 60°C indicates scattered severe thunderstorms with tornadoes.

**Table 2.5 Possible threshold values for Total Totals adapted from: Severe weather indices page <http://www.theweatherprediction.com/severe/indices>**

Total Totals	
Less than 44°C	Convection not likely
44 to 50°C	Likely thunderstorms
51 to 52°C	Isolated severe thunderstorms
53 to 56°C	Widely scattered severe thunderstorms

Another change was needed as a result of the topography of South Africa. The eastern part of the country is known as the escarpment or plateau due to its high elevation. In fact, a substantial part is higher than 850 hPa, which makes the calculation of K Index and Total Totals impossible. This is illustrated in Figure 2.4.

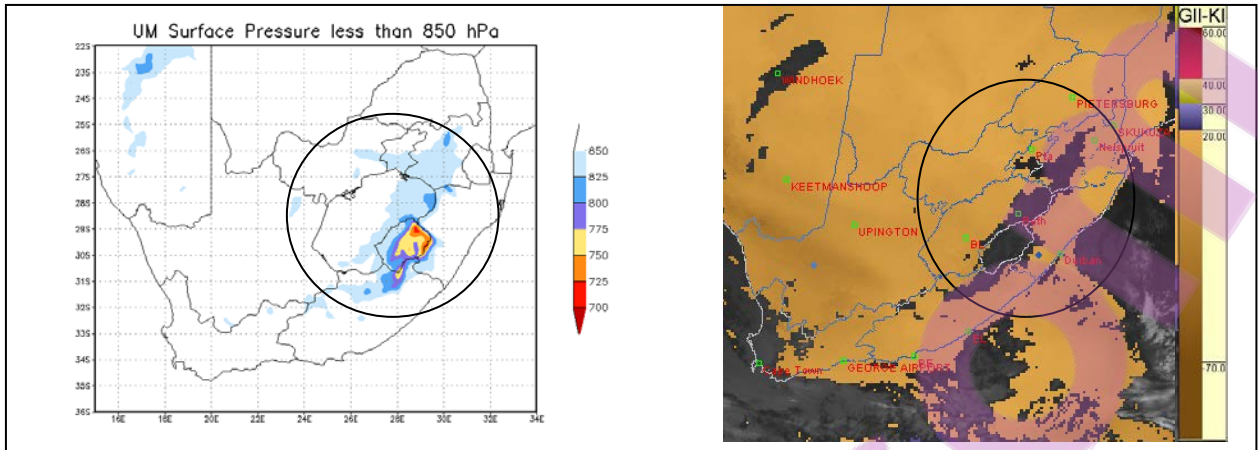


Figure 2.4 High terrain (left) and K Index (right) over South Africa, indicating areas above 850 hPa where K Index could not be computed.

It is clear that in the same area where the terrain is higher than the 850 hPa surface, a gap occurs in the K Index, which does not relate to cloud cover. To address this issue, the calculation of K Index and Total Totals (both using 850 hPa) was adjusted such that T850 and TD850 are replaced with:

$$T=(T_{sfc} + T_{825})/2 \text{ and}$$

$$TD=(TD_{sfc} + TD_{825})/2$$

with

T<sub>sfc</sub> and TD<sub>sfc</sub>: lowest model level air temperature and dewpoint temperature, respectively.

This definition is commonly referred to as a Modified K Index and Modified Total Totals (Charba, 1977), which is originally defined such that T<sub>850</sub> and TD<sub>850</sub> are replaced with

$$T= (T_{sfc}+T_{850})/2 \text{ and}$$

$$TD= (TD_{sfc} + TD_{850})/2.$$

The Modified K Index used in this study uses the 825 hPa level in order to better cover the high terrain areas of South Africa, while the original definition of the K Index (Equation 1b) is used for areas of surface pressure exceeding 850 hPa. There would thus not be any values for areas higher than 825 hPa since then it becomes too different from the original definition of K Index. Values of the Modified K Index should be somewhat larger than those of the K Index. The Modified K Index was found to be the best single predictor for thunderstorms among more than 40 other variables over the eastern United States in spring and summer (Charba, 1977 and 1984).

Total Totals was adjusted in exactly the same manner. Values indicating thunderstorm and severe thunderstorm probabilities would again be slightly higher than for the normal Total Totals. Modified

Total Totals was found to be one of the best predictors of spring and summer thunderstorms and the best single predictor of severe local storms in the United States (Charba, 1979 and 1984). An example of the K Index versus MIXED K Index is given in Figure 2.5.

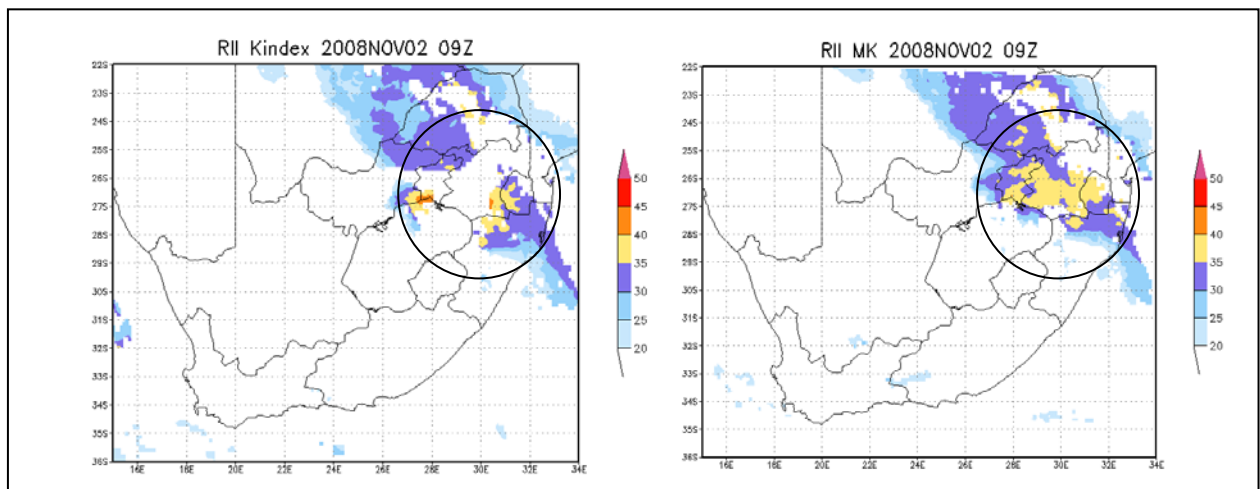


Figure 2.5 Normal K Index (left) and Mixed K Index (right), indicating areas where normal K Index are missing due to higher terrain, but Mixed K Index could be computed.

Although the picture could not be totally complete due to cloud cover at 0900 UTC, much more of the higher terrain could be covered. One should bear in mind that the terrain higher than 825 hPa would never have either K Index or Modified K Index values as a result of their definitions.

Another possibility to accommodate for the higher terrain would be to use terrain following (sigma) levels, instead of isobaric levels. Preliminary tests in this regard were done, but it was found that this change would result in a new definition of the thresholds needed for convection. For the sake of a more familiar feel for the traditional K Index values, it was decided to stay with isobaric levels.

## 2.6 SUMMARY

In this chapter the MSG applications for nowcasting and very short range forecasting were described. A basic theoretical background was supplied for the GII and how it is used, displayed and evaluated in South Africa. A description was given of how the GII was adapted for South African circumstances using the local version of the Unified Model at a higher resolution than the ECMWF model input thereby creating the RII. The various indices constituting the GII and the RII were defined as well as the way in which these were adjusted to suit the topographical needs of the country. Techniques to evaluate the individual indices against the relevant fields of the Unified Model, as well as against the occurrence of lightning in South Africa, will be discussed in Chapter 3.

# CHAPTER 3

## EVALUATION OF GLOBAL AND REGIONAL INSTABILITY INDICES OVER SOUTH AFRICA

---

### 3.1 BACKGROUND

In this chapter the accuracy of the GII and RII is assessed for South African circumstances. Since convection is mostly a summer phenomenon in South Africa, fifty cases from the summer seasons of 2007 to 2008 and 2008 to 2009 were selected. The first part of this chapter lists the cases and data used for the case studies, which are used in the following chapters.

The most obvious way of comparing the RII to another field, is to use the Unified Model fields for the same indices. Although the model fields are not seen as the ultimate truth, the differences between the RII and model fields provide a useful indication of the benefit of the satellite based fields. As mentioned in Chapter 2, it does happen that the model fields are already very good and the fields do not differ greatly, but on occasion the RII provide more detail in areas where convection occurs. Some examples of this principle will be shown in this chapter. Finally the RII are compared to the occurrence of lightning. The methodology for this is discussed in detail, as this forms the basis for the development of the new index, which will be described in Chapter 4.

### 3.2 DATA

#### 3.2.1 Case studies

For the purposes of this study, 24 cases were selected from the 2007/8 summer season when convection occurred from November 2007 to March 2008. A further 26 cases were selected from October 2008 to March 2009. Although thundershowers occurred on all of these days, not all of the cases were associated with structural or other damage or loss of life. Table 3.1 lists the events with their dates and location, together with possible information of injury, loss of life or damage to property according to the SAWS Climate Data Base.

**Table 3.1 List of cases used in this study with the effects and location of the event (SAWS, Climate data base)**

Case	Year	Month	Day	Event	Province	Comments
1	2007	11	6	Lightning and strong wind	Mpumalanga	4 people killed
2	2007	11	16	Hail	Gauteng	
3	2007	11	21	Strong wind	Free State	1 person killed
4	2007	11	22	Thunderstorms, heavy rain and lightning	Gauteng	1 person killed
4	2007	11	22	Thunderstorms	KwaZulu-Natal	
5	2007	11	28	Heavy rain, hail and strong wind	North West	
6	2007	11	29	Thunderstorms	Northern Cape	
7	2007	12	2	Thunderstorms	North West, Northern Cape	
8	2007	12	6	Thunderstorms	Limpopo, Northern Cape	
9	2007	12	7	Thunderstorms	Northern Cape, Free State	
10	2007	12	8	Heavy rain and floods	Gauteng	4 people drowned
11	2007	12	14	Hail and strong wind	North West	
12	2008	1	3	Strong wind	Free State	
13	2008	1	4	Heavy rain and floods	Gauteng	
13	2008	1	4	Hail and strong wind	Free State	
14	2008	1	6	Heavy rain	Gauteng	

Case	Year	Month	Day	Event	Province	Comments
15	2008	1	17	Heavy rain, floods and strong wind	North West	
16	2008	2	1	Thunderstorms	North West	
17	2008	2	4	Heavy rain, floods and lightning	Gauteng	1 person injured
17	2008	2	4	Lightning	North West	1 person injured
18	2008	2	7	Strong wind	North West	
19	2008	2	8	Thunderstorms	Northern Cape, Free State, KwaZulu-Natal	
20	2008	2	19	Thunderstorms	KwaZulu-Natal	
21	2008	2	20	Heavy rain and floods	KwaZulu-Natal	
22	2008	3	4	Thunderstorms	Free State, Eastern Cape	
23	2008	3	5	Heavy rain	Free State	
24	2008	3	10	Thunderstorms	Eastern Cape, KwaZulu-Natal	
25	2008	10	18	Hail	Mpumalanga	
26	2008	10	20	Lightning	Gauteng	
27	2008	11	2	Thunderstorms	Gauteng	Cars damaged by uprooted tree
28	2008	11	5	Strong wind and hail	North West	Damage to property, 38 people injured, 350 low cost houses destroyed
29	2008	11	9	Heavy rain, floods, hail and strong wind	Free State	
30	2008	11	11	Heavy rain	Gauteng	

Case	Year	Month	Day	Event	Province	Comments
31	2008	11	12	Heavy rain	Eastern Cape	25 people killed
31	2008	11	12	Strong wind	Western Cape	
31	2008	11	12	Tornado	Free State	
32	2008	12	23	Thunderstorms	Limpopo, Gauteng, Mpumalanga	
33	2008	12	27	Lightning, strong wind and floods	KwaZulu-Natal	
34	2008	12	28	Strong wind, hail	Eastern Cape	
35	2009	01	1	Thunderstorms	North West, Gauteng, Free State, KwaZulu-Natal	
36	2009	01	2	Storm and strong wind	Free State	
37	2009	01	3	Strong wind	Free State	
37	2009	01	3	Strong wind, floods and lightning	KwaZulu-Natal	7 people killed
38	2009	01	12	Floods	Gauteng	
39	2009	01	13	Strong wind and floods	Gauteng	
40	2009	01	28	Heavy rain	North West	1 person killed
41	2009	02	3	Heavy rain	Gauteng	
42	2009	02	10	Heavy rain, floods and lightning	Gauteng	7 people killed, 200 families left homeless, damage to property
43	2009	02	17	Heavy rain	North West	1 person killed
44	2009	02	20	Heavy rain	North West	1 person killed
45	2009	02	26	Heavy rain and floods	Gauteng	2 people killed
46	2009	02	28	Heavy rain and floods	KwaZulu-Natal	5 people killed, damage to property
47	2009	03	3	Thunderstorms	Free State, KwaZulu-Natal	

Case	Year	Month	Day	Event	Province	Comments
48	2009	03	7	Heavy rain and floods	KwaZulu-Natal	5 people killed, damage to property
49	2009	03	12	Thunderstorms	North West, Limpopo, Northern Cape	
50	2009	03	13	Thunderstorms	KwaZulu-Natal, Free State, North West	

### 3.2.2 Lightning data

Lightning data based on the 19 sensors installed over South Africa (see Chapter 1) was used for the 50 cases. An in depth study on the accuracy of the lightning data falls outside the scope of this study and the reader is referred to Gill (2008b) for more detail. Suffice it to say that the projected detection efficiency for the SAWS LDN is 90% over most of the country while the projected location accuracy is 0.5 – 1 km (Figure 3.1).

In order to evaluate the RII, one would need to confirm that convection did in fact take place when the indicators exceeded specific thresholds. The question could be asked: what would be confirmation of convection? Of course, the occurrence of a thunderstorm means that there is convection, but what would be a quantifiable measure of this? Using precipitation measurements is the first option. However, considering their spatial distribution, it is evident that rain gauges can provide only a limited picture of the precipitation. Radar measurements of precipitation can be considered, but the South African radars do not cover the entire country, so there would be no observations over some parts.

Satellite estimates of precipitation are another option and will be discussed in Chapter 6. A useful alternative is to use lightning detection as a confirmation of convective activity since most lightning is produced by convective clouds (Krider, 1986). Levin and Tzur (1986) reported on models of the development of the electrical structure in clouds and mention that lightning activity follows strong vertical air currents and precipitation. They state that the consequence of this correlation is that lightning is most frequently observed in cumulus clouds, rarely in stratus clouds and never in isolated cirrus clouds. Piepgrass *et al.* (1982) said, “when the meteorological conditions are favourable for the production of lightning, there is almost a direct proportionality between the total rainfall volume and the total number of flashes”. Since the lightning sensors in South Africa measure only cloud-to-ground lightning, it can be assumed that by the time we observe lightning on the ground, the thunderstorms are already in a mature phase (Figure 3.2, from Price, 2008). Acknowledging the fact that not all convection leads to lightning (Mecikalski, 2009) and that cloud-to-ground lightning by no means accounts for all the lightning, in this study the presence of lightning will be regarded as a confirmation of convective activity.

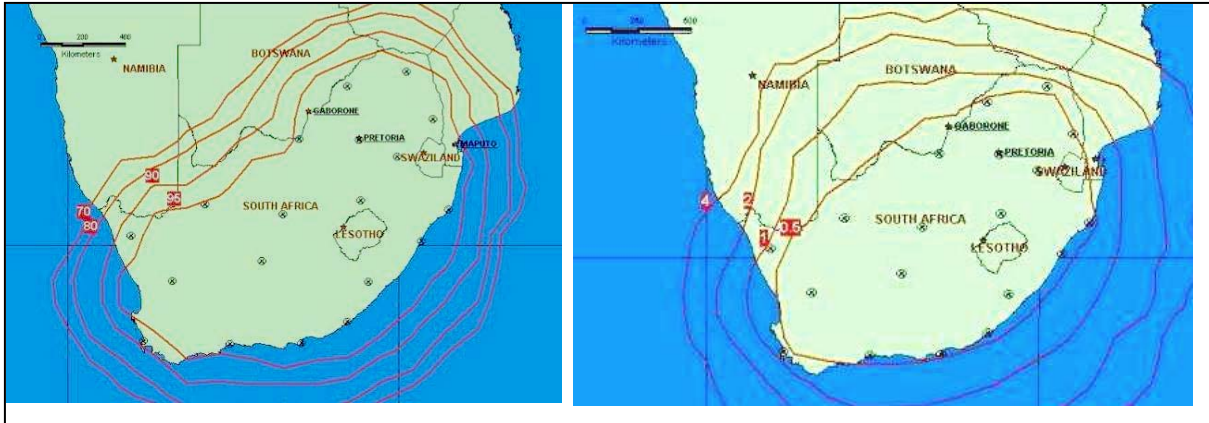


Figure 3.1 Projected detection efficiency in percentages (left) and projected location accuracy (km) of cloud to ground lightning flash data for the SAWS LDN from the VAISALA Network Performance Evaluation Program model (right) (from Gill, 2008b)

Convection is often heat driven in South Africa and thus usually occurs from the early afternoon to late evening. According to analysis of the 2007 and 2008 lightning data set the occurrence of lightning starts at around 1200 UTC (2 pm SAST) and continues until late at night, with a peak occurrence in the late afternoon (around 4 pm SAST). For the purposes of this study observations of lightning occurring between 1200 and 2100 UTC were used. For each of the case study days the total number of lightning strokes which occurred within this time interval was calculated and plots showing the spatial distribution of lightning for each day were produced. A mask was also used to restrict the use of the data to within the borders of South Africa to ensure maximum detection efficiency and accuracy (Figure 3.3). As a consequence of the use of this mask, distinct lines will be seen in lightning occurrence maps later in this study.

### 3.2.3 RII data

The coverage of the RII is restricted to the area 22°S to 36°S and 15°E to 34°E with a 0.1° resolution. Matrices with 174X128 grid points hold MSG data with a 3X3 pixel resolution and model data with a 0.1° (or 12 km) resolution. The RII are available every 15 minutes. The variables used in the study are as described in Chapter 2.

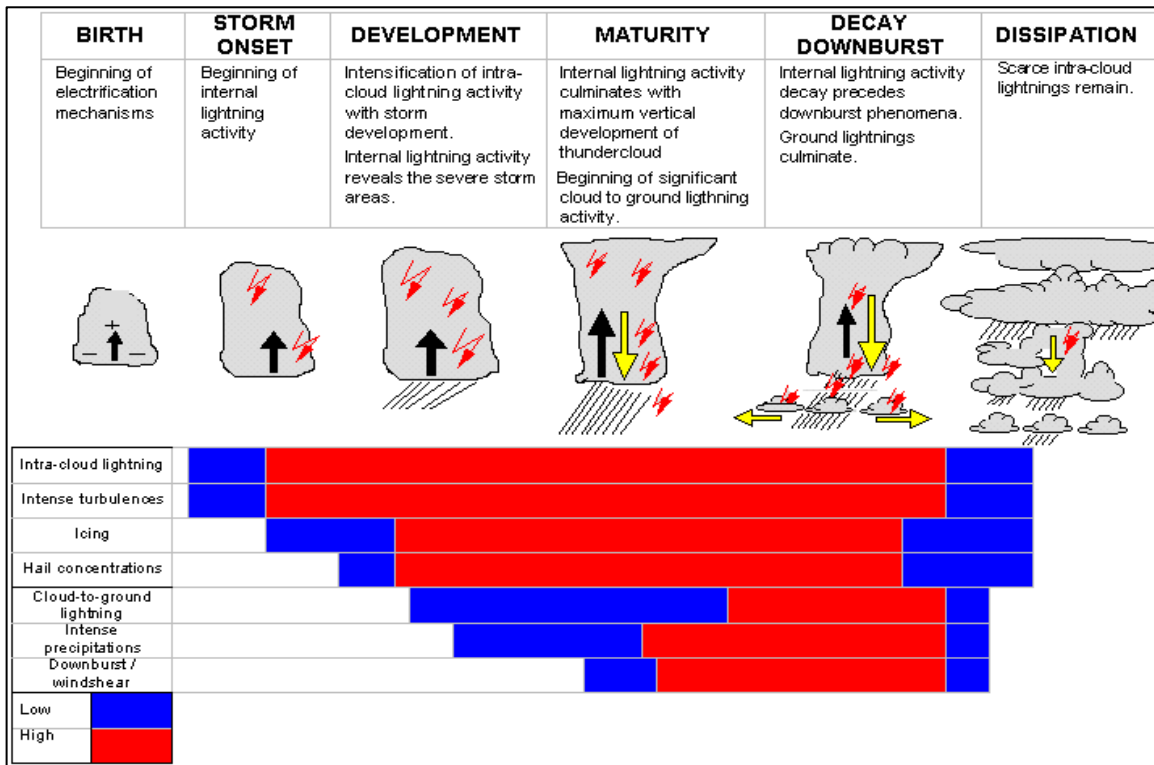


Figure 3.2 Relationship between convection and lightning (from Price, 2008) used with permission of the author

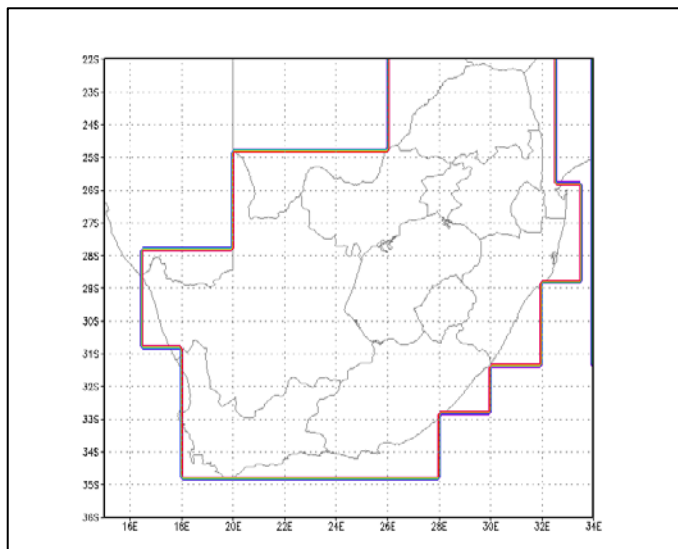


Figure 3.3 Mask used for the evaluation of lightning data

### **3.3 COMPARISON OF RII K INDEX AND LIFTED INDEX FIELDS AGAINST THE UNIFIED MODEL K INDEX AND LIFTED INDEX FIELDS**

The RII are the product of both model and satellite data, as explained in the previous chapters. The limitation of the RII is that they cannot be calculated where there are clouds. Unless there are clear skies, the field display of the RII will thus always include pixels with no value. One way of addressing this problem (to some extent) is to use a time averaged field. In this way, pixels which are covered at least some of the time will have a value. In South Africa summer days often start off fairly cloud free over the interior and then convection develops later in the day. It can, of course, happen that the instability changes with time as part of the diurnal cycle, but if there is a constant increase then this will also be reflected in the time average. If there were, however, a temporary change of short duration, it would weigh less in the averaging process. It was decided to use the RII values between 0600 and 0900 UTC to calculate a time averaged field. This should be the most cloud free time of the day and subsequently the RII fields should be filled in a meaningful manner. Not only does this lead to a more complete picture, it also provides more certainty that a positive indication for the development of convection provided by the RII, is consistent with time and not just an outlier. Use of time averages over the period 0600 to 0900 UTC then provides operational forecasters with useful information late in the morning (just after 11 am SAST) to be able to forecast convection for the afternoon. An example of such a time average is shown in Figure 3.4.

Instability fields from the Unified Model and RII may be expected to be rather similar, since model fields form a part of the input to the calculation of the RII (Chapter 2). However, one would hope for sufficient difference to show that adding information from the six MSG channels (Chapter 2) to the model information, does indeed add value. In such cases additional information is provided to the forecaster.

Both model and RII based K Index and Total Totals were averaged over these three hours for all 50 cases. To show all fifty examples here would not serve a useful purpose. In several cases the fields differed very little and emphasized similar areas for possible convective instability. Two examples of where the RII K Index and Total Totals did in fact add value to the model fields will be shown.

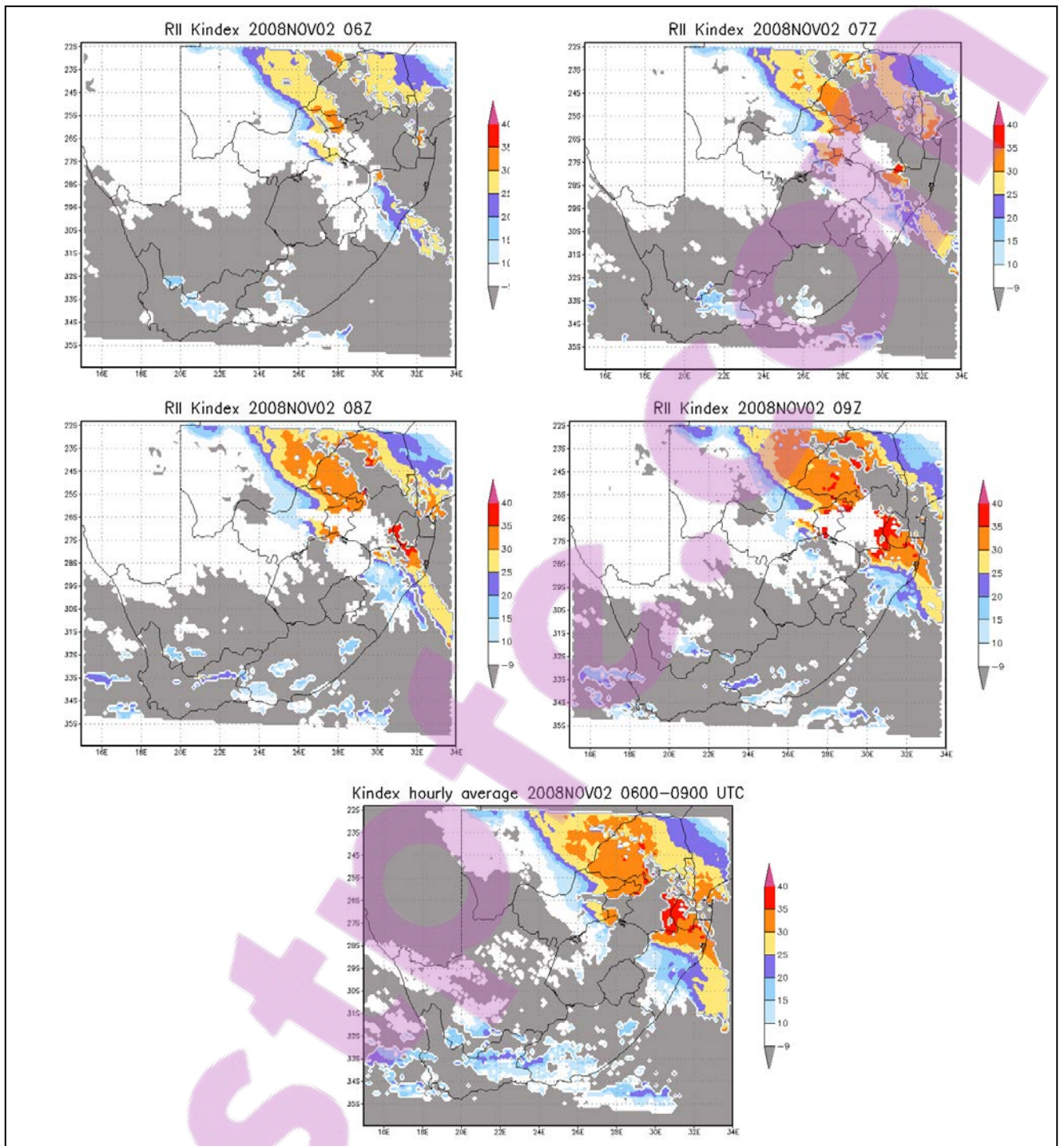


Figure 3.4 RII K Index in hourly averages (first four panes) and the time average over the period 0600 to 0900 UTC in the last pane

EXAMPLE 1: 4 January 2008

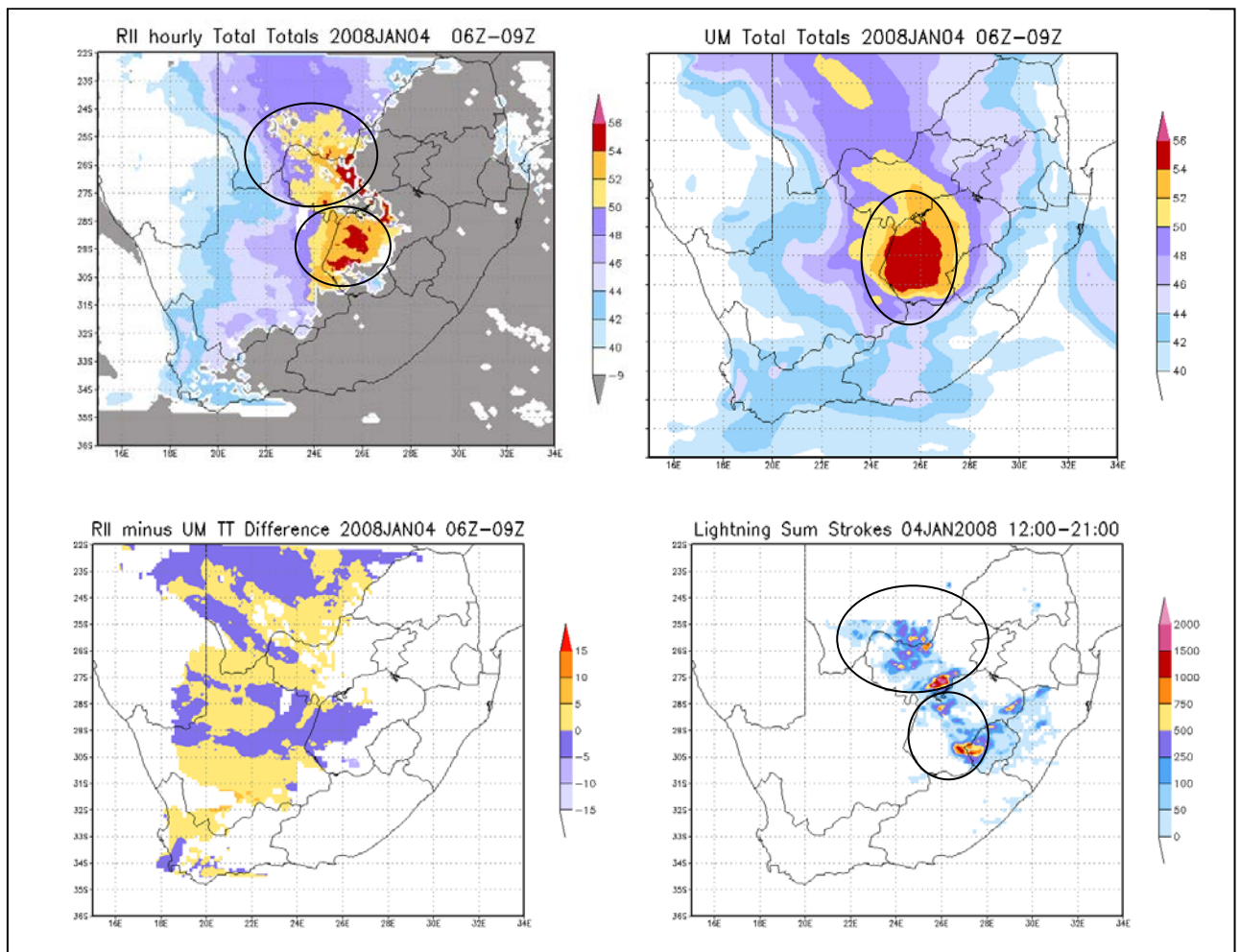


Figure 3.5 RII Total Totals (top left), Unified Model Total Totals (top right), difference field (bottom left) and the total number of lightning strokes which occurred later in the day (bottom right) for 4 January 2008

In the RII Total Totals graphic (Figure 3.5, top left) cloudy areas are indicated by the grey shade. Although at first glance the Total Totals fields from RII and the Unified Model look rather similar (Figure 3.5 top left and right), some differences are noticeable:

1. Figure 3.5 (bottom left) shows the RII Total Totals minus Model Total Totals. Differences are mostly between +5 to -5°C, which shows that there are differences but that they are small.
2. The Model Total Totals field has its highest values (>54°C) over the western Free State, while for the RII Total Totals there are two areas of high values (>54°C) – one over the western Free State but also one further north over the Northwest Province.
3. Looking at the spatial coverage of lightning (Figure 3.5, bottom right), lightning occurred over the southern Free State, as well as in the Northwest Province. The lightning maxima are

slightly more eastwards than the areas of more than 54°C for the Total Totals products of both the Unified Model and the RII. The lightning over the Northwest Province coincides well with the RII Total Totals maxima, which was not evident in the Unified Model Total Totals.

**EXAMPLE 2: 1 February 2008**

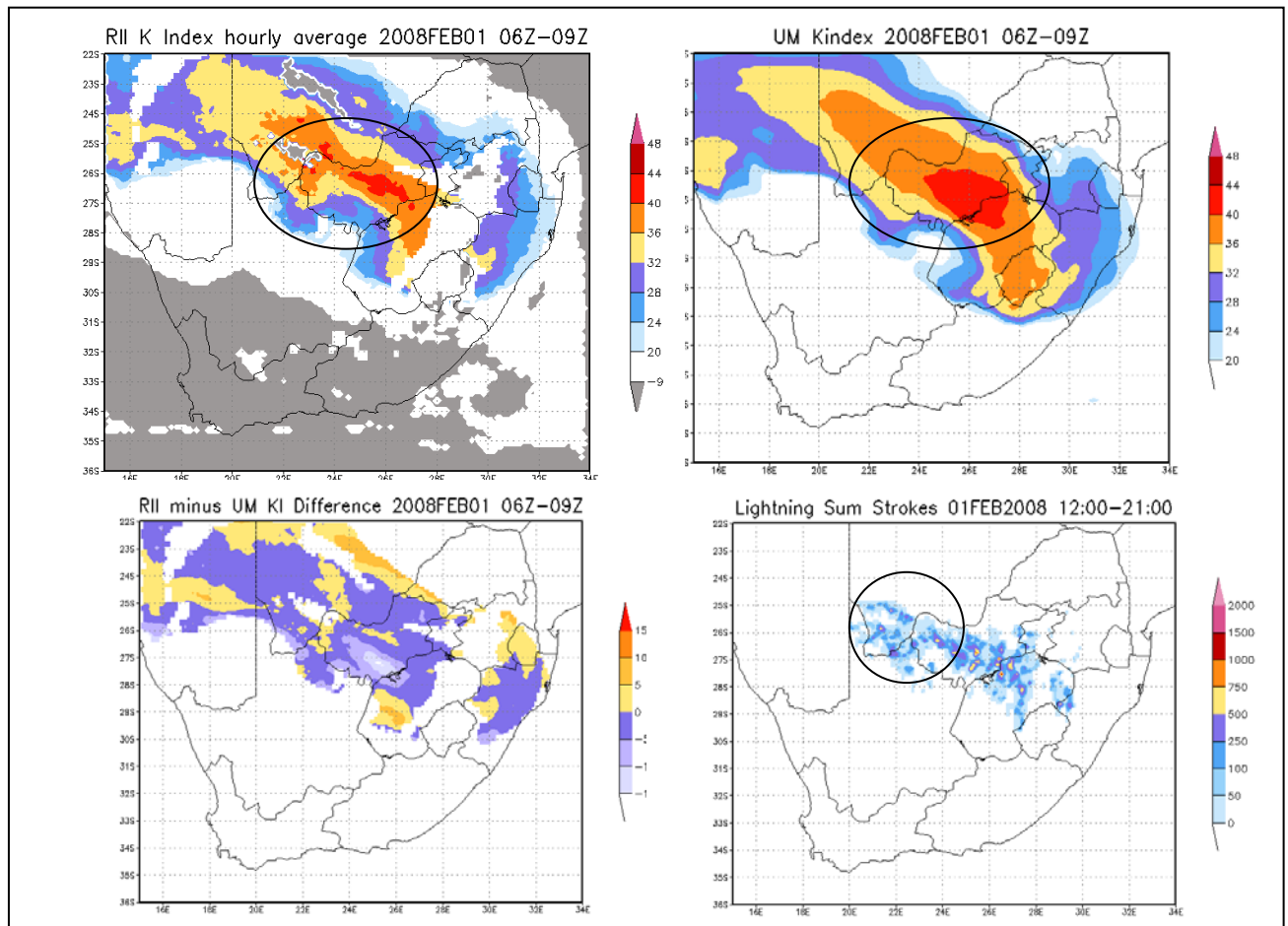


Figure 3.6 RII K Index (top left), Unified Model K Index (top right), difference field (bottom left) and the total number of lightning strokes which occurred later in the day (bottom right) for 1 February 2008

In this second example (Figure 3.6), it is clear that, despite the similarities (top left and right), subtle differences are again evident:

4. The difference field (bottom left) shows mostly values of +5 to -5°C, except over the Botswana region where there are values greater than 5°C.
5. The Model K Index field (top right) has the highest values (>40°C) over the Northwest Province and northwestern Free State while the area of high values (>40°C) for the RII K Index (top left) extends further northwestward into Botswana.
6. The RII K Index has no values over the eastern Free State and the surrounding high lying areas, due to the fact that it is dependent on the temperature at 850 hPa and those areas are

above 850 hPa. The “normal” K Index could thus NOT be computed there. The Unified Model uses the “normal” K Index and not the Mixed K Index (Chapter 2, Figure 2.5). In order to compare the K Index from the Unified Model to the K Index from the RII, the Mixed K Index was thus NOT used in this comparison.

7. Note that lightning is not accurately detected in northern Botswana and Namibia and can thus not be shown in the lightning data view (bottom right). Lightning occurred over the northern Free State, Northwest Province and into southern Botswana.
8. The RII field of maximum K Index (top left) adds more focus in an area where more lightning (bottom right) was detected.

### **3.4 EVALUATION OF RII AGAINST OCCURRENCE OF LIGHTNING**

#### **3.4.1 Initial evaluation of the GII**

As in studies by Koenig *et al.* (2007) a more quantitative evaluation method is used in this study to show the accuracy of the RII parameters when compared to the occurrence of lightning over South Africa. Initially a contingency table approach was used to calculate the Probability of Detection (POD) and the False Alarm Ratio (FAR) of the K Index and the Lifted Index from the GII product. The formulas for POD and FAR are listed in Table 3.2. This approach places the events into four categories (Wilks, 2005):

Hit: event was forecast to occur and did occur (A),

Missed: event was not forecast to occur but did occur (C),

False Alarm: event was forecast to occur but did not occur (B) and

Correct Negative: event was forecast not to occur and did not occur (D).

**Table 3.2 Statistical scores calculated for evaluation purposes adapted from <http://www.cawcr.gov.au/projects/verification/>**

Score	FORMULA	Answers the question:	Range	Perfect score
Probability of Detection	$A / (A+C)$	What fraction of the observed 'yes' events were correctly forecast?	0 to 1	1
False Alarm Ratio	$B / (A + B)$	What fraction of the predicted 'yes' event actually did NOT occur?	0 to 1	0

The maximum values of K Index and minimum values of Lifted Index from the 15X15 MSG pixel (corresponding to ~ 50 km X 50 km) over the period 0400 to 0800 UTC were compared to the occurrence of lightning between 1100 and 1800 UTC. The occurrence of lightning was regarded as confirmation of convective activity. If the Lifted Index was less than  $-5^{\circ}$  early in the morning and more than five lightning strokes occurred in the 15X15 pixels block later in the day, the forecast was considered to be a "hit". Similarly, if the K Index exceeded  $35^{\circ}\text{C}$  early in the morning and more than five strokes occurred in this block later in the day, the forecast was considered a "hit". Five case studies in the summer of 2006/7 were chosen when convective events took place. The average Probability of detection (POD) for the K Index was 77% and the False Alarm Ratio (FAR) 33% (Table 3.3).

**Table 3.3 Evaluation results for K Index for five cases**

Case Date	POD	FAR
15 Jan 2007	0.47	0.31
16 Jan 2007	0.91	0.42
17 Jan 2007	0.73	0.33
28 Dec 2006	0.83	0.21
4 Mar 2007	0.93	0.38
Average	0.77	0.33

The K Index fields for 0400 to 0800 UTC for 15 January 2007 are given in Figure 3.7 while Figure 3.8 shows the same fields for 16 January 2007. The case of 15 January did not evaluate well as indicated by the scores in Table 3.3. Figure 3.7 shows that the high cloud incidence decreased the number of

cloud free blocks which could be used to calculate the GII. The case of 16 January 2007 evaluated much better, coinciding with more cloud free pixels which could be used to calculate the GII. The degree of cloud cover might thus explain the difference in performance to some extent. Based on these few cases the GII product was considered as possibly being a valuable tool for short range forecasting of thunderstorms (de Coning, 2007) and worthy of further investigation.

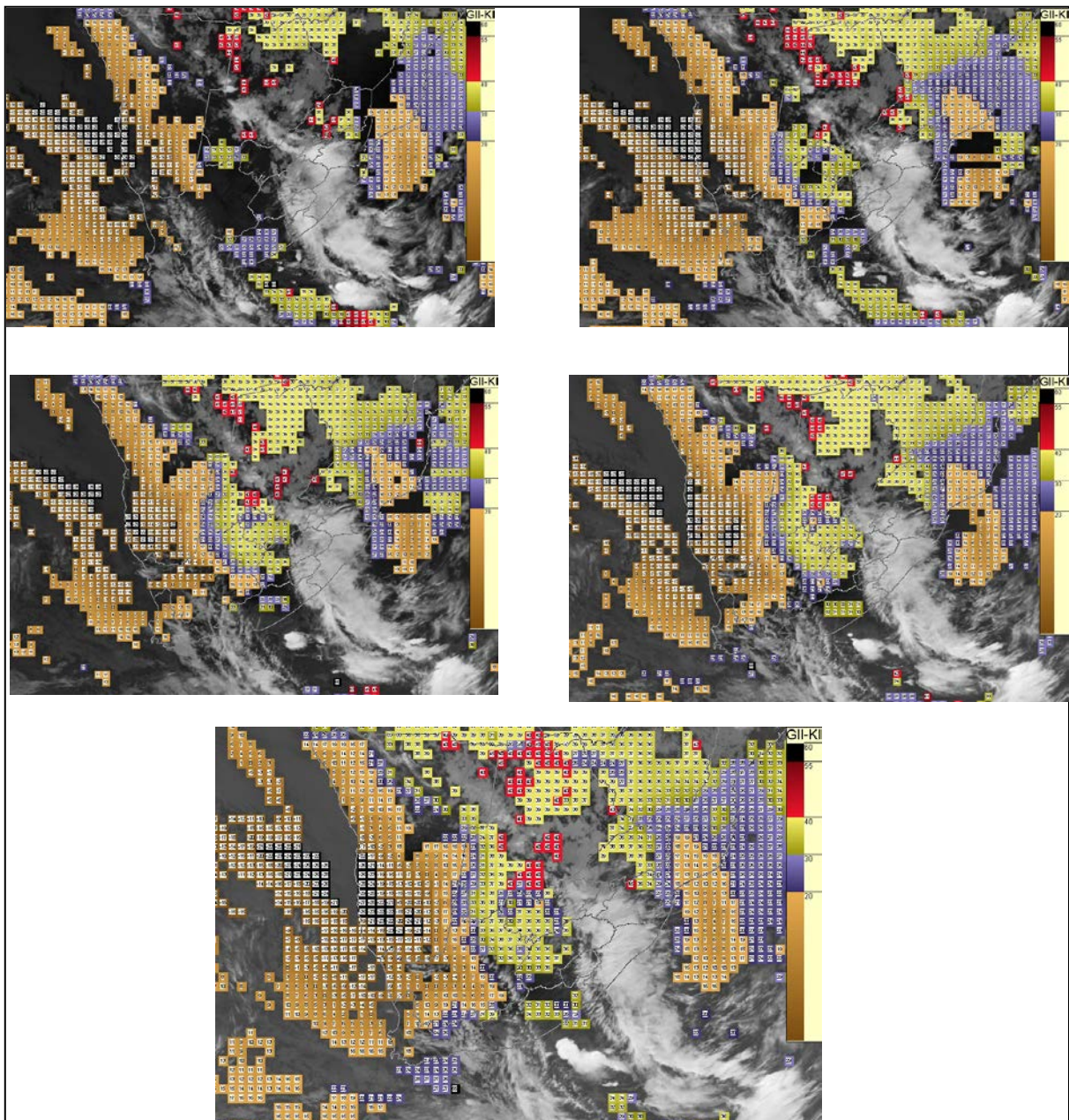


Figure 3.7 K Index at 0400 UTC (top left), 0500 UTC (top right), 0600 UTC (middle left), 0700 UTC (middle right) and 0800 UTC (bottom) for 15 January 2007

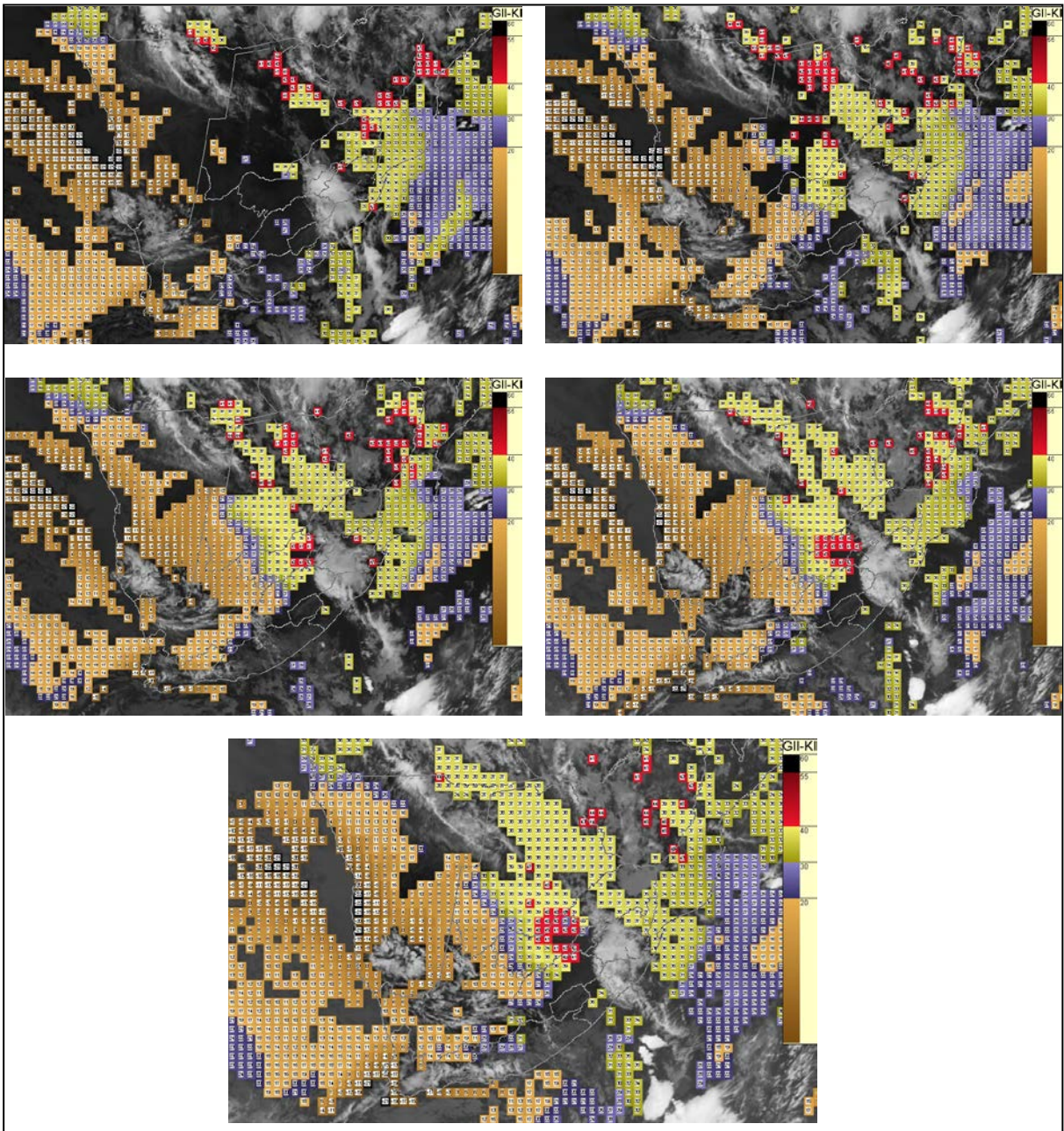


Figure 3.8 K Index at 0400 UTC (top left), 0500 UTC (top right), 0600 UTC (middle left), 0700 UTC (middle right) and 0800 UTC (bottom) for 16 January 2007

### 3.4.2 Evaluation of individual RII against lightning

After the installation of the local version of the GII in South Africa in 2007, the evaluation scheme was adjusted to use a  $0.1^{\circ} \times 0.1^{\circ}$  block, since the resolution of the model input had increased. Instead of using the *extreme* values of the indices in a six hour period and  $15 \times 15$  pixel block, the *average* value of each index over a three hour period from 0600 to 0900 UTC in a  $3 \times 3$  pixel block was chosen. In this way the spatial resolution was improved and the most cloud free period of the day was selected. Each index was then compared to the occurrence of lightning (*one* lightning stroke in this smaller block of  $0.1^{\circ} \times 0.1^{\circ}$ ). Based on the contingency table approach additional statistical values were calculated for each meaningful value of the index (Table 3.4). For each of the indices, all fifty cases from November 2007 to March 2009, were used to verify against the occurrence of lightning. Instead of using certain thresholds for each index as before, the evaluation was done for every value of the respective index. Two additional scores were also calculated, the Probability of False Detection (POFD), also known as the False Alarm Rate (FAR), as well as the Hanssen-Kuipers Discriminant (HK), also known as the True Skill Statistic (TSS). These scores are defined in Table 3.4.

If *all* the boxes with K Indices above  $20^{\circ}\text{C}$  are evaluated against the occurrence of lightning, the probability of detection of all the lightning will probably be 100%. At K Index values of more than  $25^{\circ}\text{C}$ , the probability of anticipating all the lightning will be less since areas with K Index values of less than  $25^{\circ}\text{C}$  would also have had lightning. At K Index values of more than  $30^{\circ}\text{C}$  the POD of anticipating all lightning becomes less, and for K Index values of more than  $35^{\circ}\text{C}$ , the probability of being able to capture all the lightning is even less. In essence one is looking to identify the area where it is most likely to see all lightning; the bigger the area (lower threshold for K Index), the higher the POD will be, but the FAR and POFD will be large too. In order to balance these scores, it is necessary to find the area where POD is high and FAR and POFD are low. This approach should not be confused with calculating the POD, FAR or POFD for *single values* of an index, but rather for *an area where the index exceeds a certain value* in order to get to a probability map. This is also indicated in the following graphs on the x-axis, with the use of ">" for each value.

**Table 3.4 Additional statistical scores calculated for evaluation purposes adapted from <http://www.cawcr.gov.au/projects/verification/>**

Score	FORMULA	Answers the question:	Range	Perfect score
Probability of False Detection (or False Alarm rate)	$B / (B+D)$	What fraction of the observed 'no' events were incorrectly forecast as 'yes'?	0 to 1	0
Hanssen-Kuipers discriminant (or True Skill Statistic)	$POD - POFD$	How well did the forecast separate the 'yes' events from the 'no' events?	-1 to 1	1

### 3.4.2.1 Evaluation of Mixed K Index (Figure 3.9)

1. POD:  
If the area of all Mixed K Index (MK) values above 15°C is considered, a POD of almost 1 will be obtained, i.e. almost all lightning will occur within this area. This value, of course, decreases as one looks at higher and higher values of Mixed K Index, since the area becomes smaller and smaller.
2. POFD:  
The POFD starts just above 0.2 (or 20%) and decreases with higher values of Mixed K Index.
3. FAR:  
The False Alarm Ratio starts at 70% and decreases to around 50%, after which there are not enough data points to make a calculation possible.
4. HK:  
This indicator starts at 0.75 and remains above 0.6 until Mixed K Index becomes more than 30°C, when it decreases steadily.

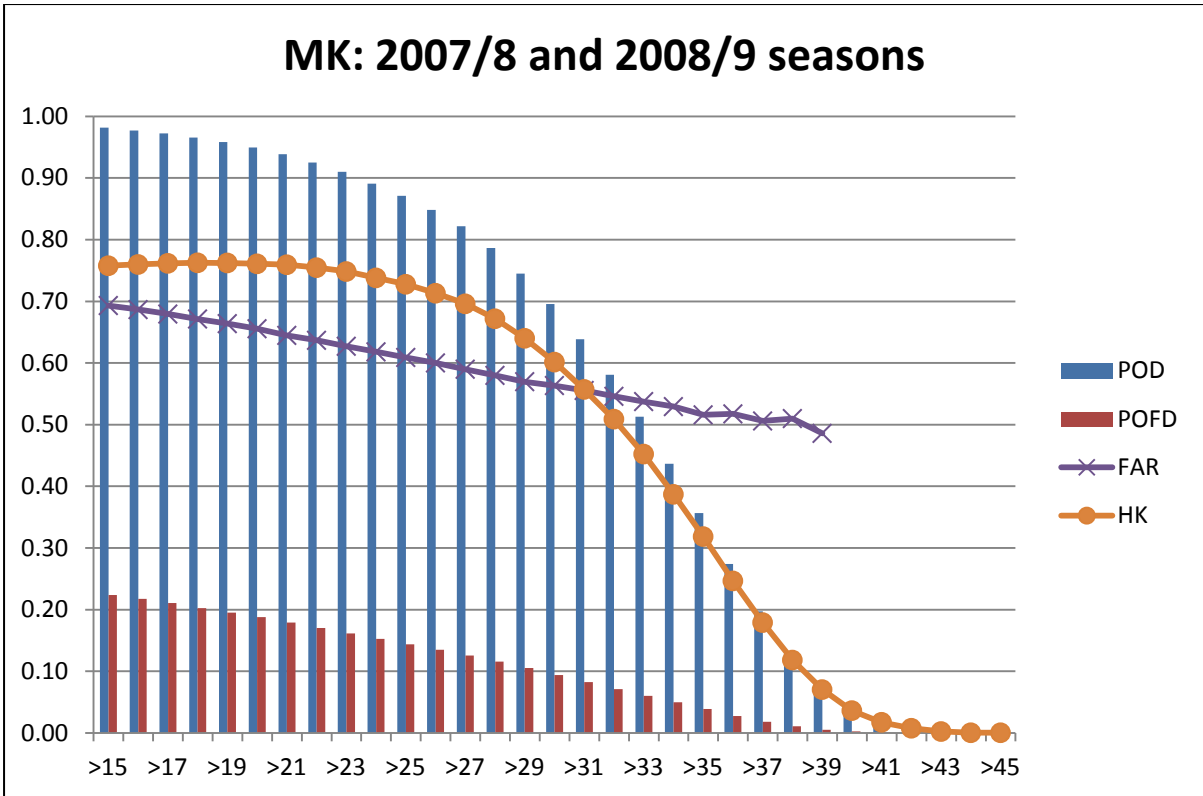


Figure 3.9 Statistical scores for Mixed K Index for all fifty cases

**3.4.2.2 Evaluation of Mixed Total Totals (Figure 3.10)**

- 5. POD:  
If the area of all Mixed Total Totals (MT) values above 35°C is considered, a POD of 1 is noted and all lightning will occur in this area. This value decreases with higher and higher values of MT.
- 6. POFD:  
The POFD starts just above 0.3 (or 30%) and decreases with higher values of MT.
- 7. FAR:  
The False Alarm Ratio starts just below 80% and decreases to just above 50% where Mixed Total Totals is about 51°C.
- 8. HK:  
This indicator starts below 0.70, increases slightly to about 0.75 (where Mixed Total Totals is more than 42°C) and then decreases steadily.

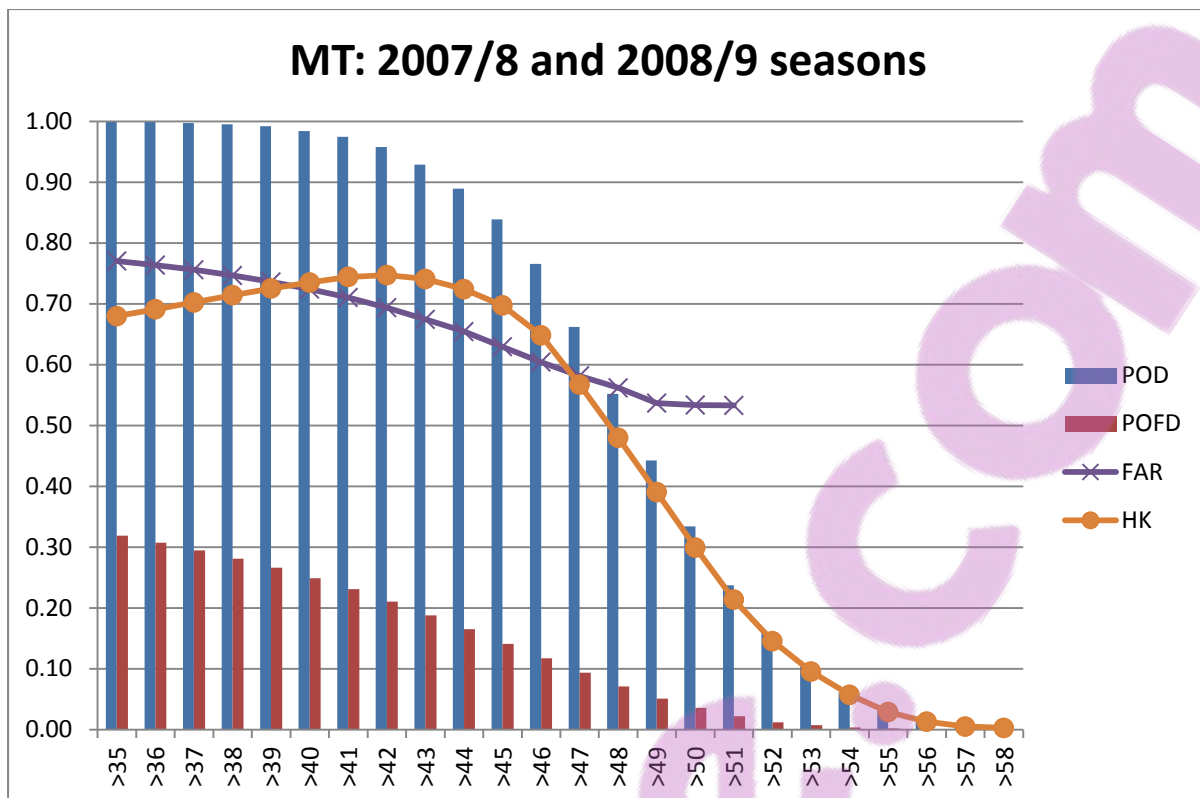


Figure 3.10 Statistical scores for Mixed Total Totals for all fifty cases

### 3.4.2.3 Evaluation of Lifted Index (Figure 3.11)

9. POD:  
If the area of all Lifted Index (LI) values of  $>+2^{\circ}\text{C}$  is considered POD is almost 1 and thus all lightning will occur in such a region.
10. POFD:  
The POFD starts high at almost 80% when Lifted Index is positive, which makes physical sense, since then there is no instability. As soon as Lifted Index is less than  $0^{\circ}\text{C}$ , POFD becomes less than 20% and continues to diminish.
11. FAR:  
The False Alarm Ratio starts at 90%, drops quickly to just above 60% when Lifted Index is negative and ends at around 50% where Lifted Index is about  $-6^{\circ}\text{C}$ .
12. HK:  
This indicator only has favourable values when Lifted Index is below zero, where it is above 70% and then it decreases steadily.

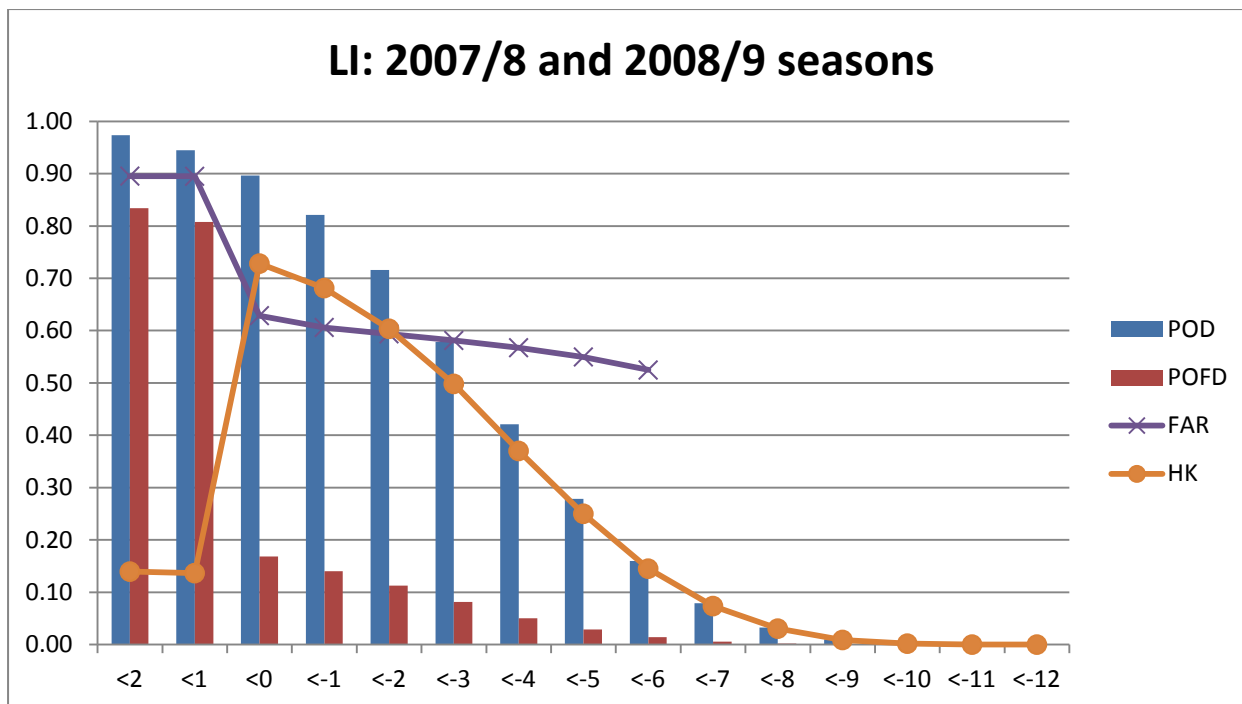


Figure 3.11 Statistical scores for Lifted Index for all fifty cases

### 3.4.2.4 Evaluation of Precipitable Water (Figure 3.12)

13. POD:  
If the area of all Precipitable Water (PW) values above 10mm is considered POD is almost 1 and thus all lightning will occur in such a region.
14. POFD:  
The POFD starts above 30% and decreases.
15. FAR:  
The False Alarm Ratio starts below 80%, drops to below 70% where Precipitable Water is about 22 mm and then increases, contrary to all the other parameters. Evett *et al.* (2008) in a study on the effect of monsoonal atmospheric moisture on lightning fire ignitions in southwestern North America found that the average number of lightning flashes per day increased with increasing atmospheric moisture and thunderstorm activity, but at higher values of daily minimum relative humidity (more than 50%) there was a slight decrease in the number of lightning flashes. One explanation could be that there is too little data at these higher relative humidity values, but it can also be that high humidity days are often overcast, limiting the necessary convective heating required for thunderstorm development and intensification.
16. HK:  
This indicator starts between 60% and 70% and remains high until Precipitable Water exceeds 16 mm and then decreases steadily.

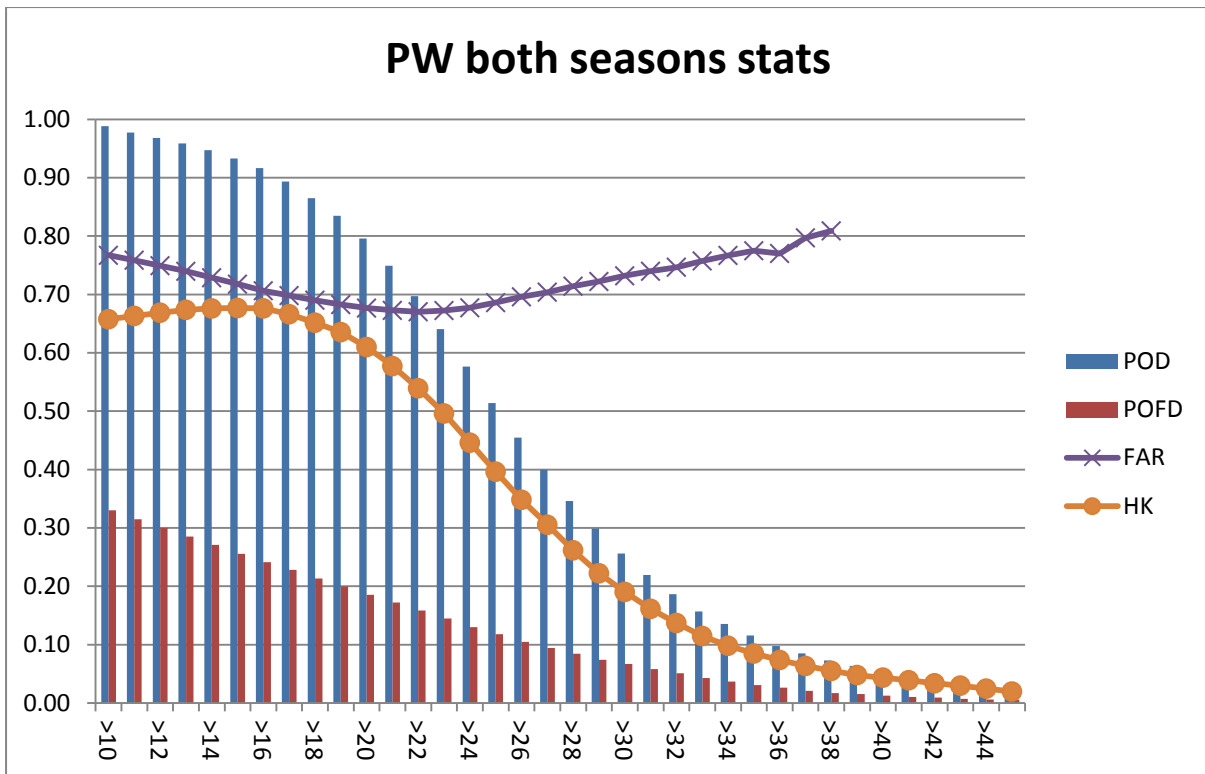


Figure 3.12 Statistical scores for Precipitable Water for all fifty cases

### 3.4.3 Comparison with similar work done in Poland

Several countries are using the GII product. Only a few have attempted a quantitative evaluation procedure. In Poland Struzik *et al.* (2006) carried out an evaluation for the GII K Index and Lifted Index against occurrence of lightning in Poland using several cases from April and May 2006. A threshold of 20°C was used for the K Index and Lifted Index was evaluated below 0°C in their contingency table approach. A summary of their results is shown in Table 3.5.

The circumstances as well as weather systems in South Africa and Poland are not exactly the same and for South Africa, the Mixed K Index is shown here but the normal K Index for Poland. In South Africa, a meaningful threshold for the Lifted Index is -2°C and for the K Index 25°C is more relevant. The thresholds used in the Poland study (0° and 20°C) are thus very 'weak' compared to the meaningful values in South Africa. This explains the differences in the statistics.

**Table 3.5 Comparison between evaluation scores for K Index and Lifted Index in Poland and South Africa**

	K Index with a threshold of 20°C (Poland)	Lifted Index with a threshold of 0°C (Poland)	Mixed K Index with a threshold of 20°C (South Africa)	Lifted Index with a threshold of 0°C (South Africa)
POD	0.75	0.71	0.95	0.90
FAR	0.25	0.12	0.66	0.63
POFD	0.44	0.16	0.19	0.17

### **3.5 SUMMARY**

In this chapter, after a discussion of data used for the study, some verification of results was presented. Fifty cases when convection occurred were listed mentioning where damage to property or loss of life was reported. The handling of lightning data in terms of space and time was described. The initial verification of the GII provided the basis for an evaluation method with a contingency table approach, which was expanded and refined when the RII came into operation. Two of the RII were compared with model fields of the same variables and some examples were shown. Finally, the four modified RII were evaluated against the occurrence of cloud-to-ground lightning over South Africa over two summer seasons by means of four statistics. In general the statistics for the individual RII look like good indicators of the occurrence of convection (or lightning) and could thus be useful for short term forecasts of thunderstorms. Keeping in mind that cloud-ground-lightning does not reflect all lightning, the favourable statistics are especially encouraging. In the next chapter the results obtained so far will be used to develop a new index for the probabilistic forecasting of convection.

# CHAPTER 4

## PRINCIPLES OF A NEW COMBINED INSTABILITY INDEX

---

### 4.1 BACKGROUND

The first three chapters supplied background for work done in South Africa to regionalize the principles of GII. The Lifted Index was adjusted for South African circumstances. Total Totals was added as an additional parameter. Due to the high terrain in South Africa the eastern escarpment is often excluded from K Index and Total Totals calculations because it is higher than the 850 hPa level. The Modified K Index and Total Totals principles were applied in this region, and the normal K Index and Total Totals everywhere else, to provide a Mixed K Index and Mixed Total Totals (Chapter 2). The four RII, namely Mixed K Index, Mixed Total Totals, Precipitable Water and adjusted Lifted Index, were subsequently evaluated as a way to provide at least a three hour lead time on the occurrence of lightning. Lightning was assumed to be a confirmation of convection. All the indices evaluated well and statistical values from a contingency table proved that they all add value in the process of anticipation of convection.

In this chapter these principles will be expanded upon to develop a new index, a combination of the other four indices, to provide forecasters with a single probabilistic map showing where convection is most likely to occur. Examples will be shown where this parameter was found useful according to visual verification techniques.

### 4.2 USING THE FOUR REGIONAL INSTABILITY INDICES IN THE DEVELOPMENT OF A NEW INDEX

In working towards the development of a single probability map for convection it becomes obvious that combining the four RII into one parameter is not a simple matter, if only because each has its own unit (mm for Precipitable Water and °C for the rest) and that an indirect type of combination is required. For the same reason that the occurrence of lightning was chosen as a way to evaluate the RII, it will now be used as a stepping stone in the combination of the four RII. The frequency of lightning occurrence was thus calculated for values of each of the four RII. For each index the time average between the 0600 and 0900 UTC fields was found for each of the fifty case study days. This was compared to the occurrence of lightning between 1200 and 2100 UTC later in the same day. The

results of these calculations are given in this section in terms of cumulative frequency, i.e., the frequency of lightning occurrence for all the values of the RII below a particular threshold. These cumulative frequencies are displayed in the form of cumulative frequency polygons or graphs as described by Burington and May (1970) and are given here as percentages (vertical axis). A combination involving the cumulative frequencies of lightning related to the four RII, rather than the RII they would allow the final index also to be expressed in terms of percentages.

#### 4.2.1 Cumulative frequency graphs for Mixed K Index and lightning

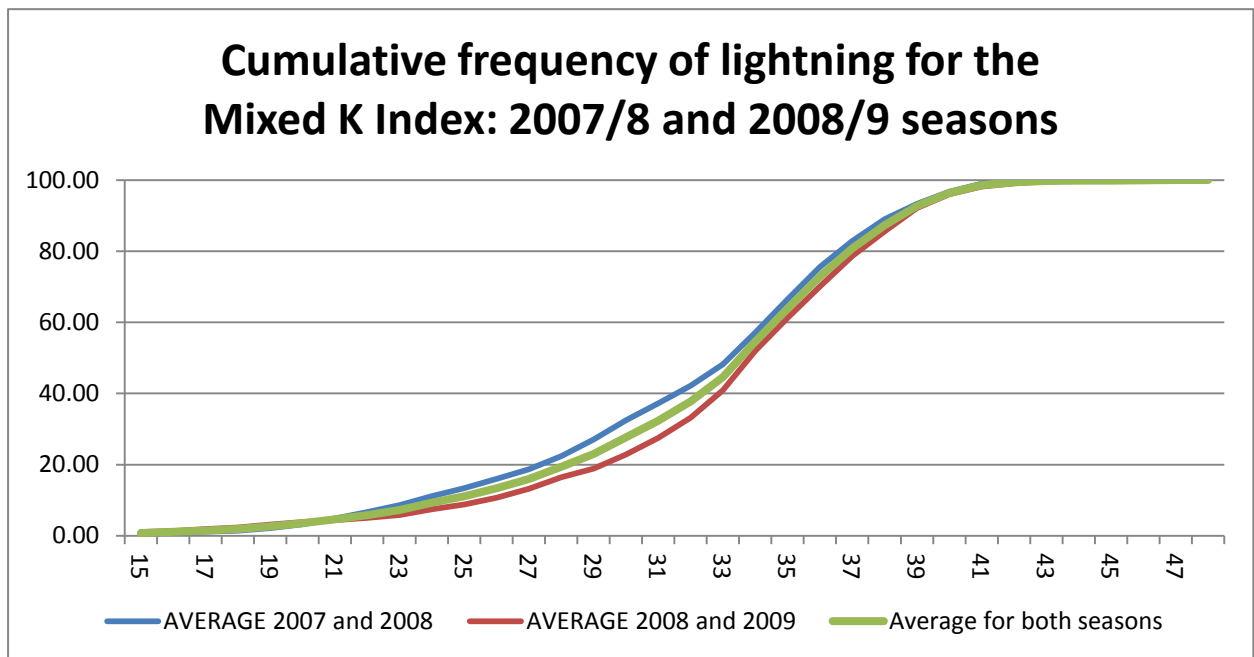


Figure 4.1 Cumulative frequency graph for Mixed K Index values (°C) for 2007/8 and 2008/9 seasons

From Figure 4.1 it is clear that:

17. For Mixed K Index values of less than 15°C, no lightning has occurred.
18. When the Mixed K Index is less than or equal to 33°C, 50% of the lightning has occurred.
19. When the Mixed K Index reaches 43°C, all the lightning has occurred.
20. The Mixed K Index values for the two seasons are very similar (blue and red lines) and the average for the two seasons (green line) differs only slightly around the Mixed K Index values of 30°C.

## 4.2.2 Cumulative frequency graphs for Mixed Total Totals and lightning

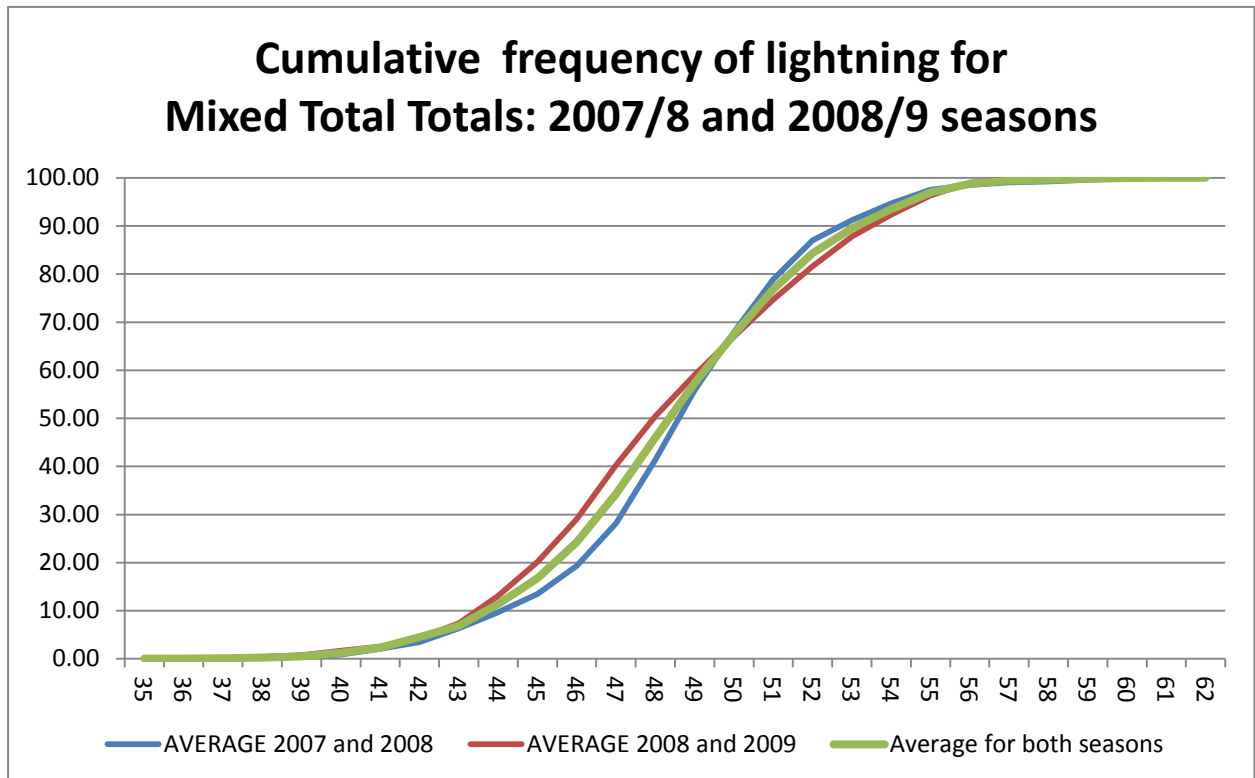


Figure 4.2 Cumulative frequency graph for Mixed Total Totals values (°C) for 2007/8 and 2008/9 seasons

From Figure 4.2 it is clear that:

1. For Mixed Total Totals values of less than 35°C, no lightning has occurred.
2. When the Mixed Total Totals is less or equal to 48°C, 50% of the lightning has occurred.
3. When the Mixed Total Totals reaches 57°C, all the lightning has occurred.
4. The Mixed Total Totals values for the two seasons are very similar (blue and red lines) and the average for the two seasons (green line) centres between them.

### 4.2.3 Cumulative frequency graphs for Lifted Index and lightning

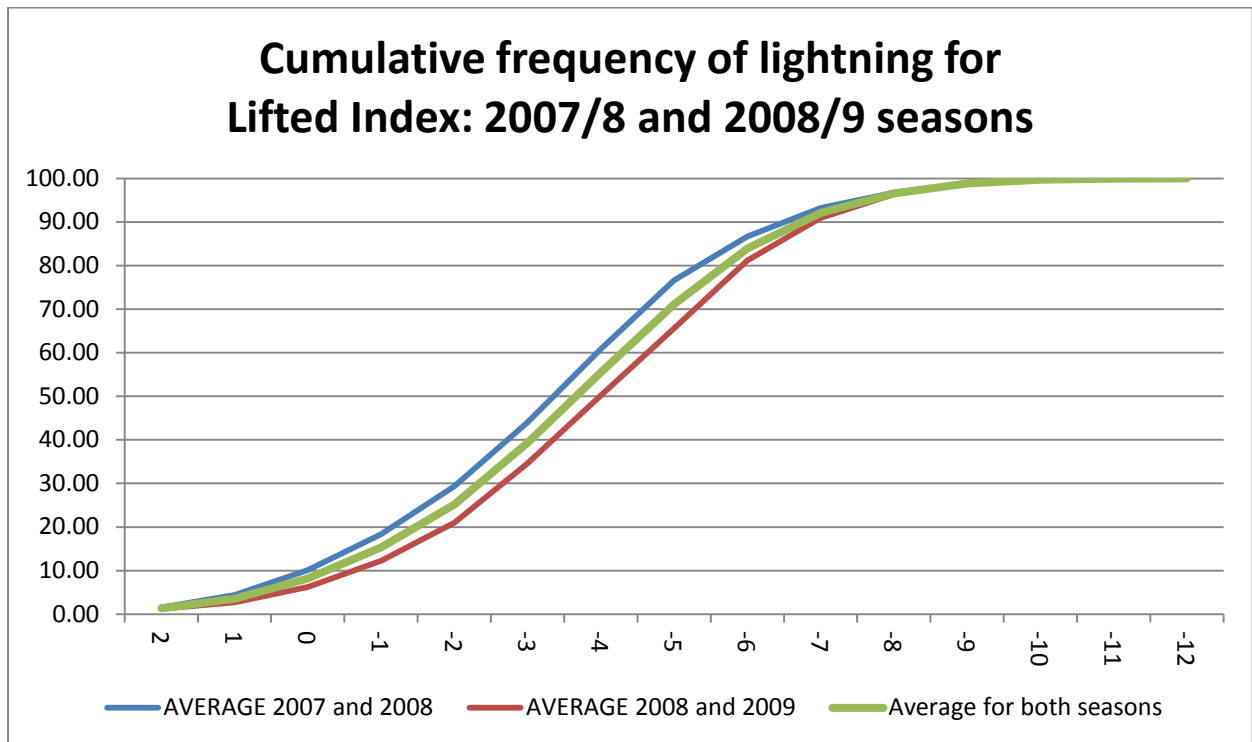


Figure 4.3 Cumulative frequency graph for Lifted Index values (°C) for 2007/8 and 2008/9 seasons

From the Lifted Index graph (Figure 4.3), it is clear that:

5. For Lifted Index values of more than +2°C, very little lightning has occurred.
6. When the Lifted Index is less than or equal to -4°C, 50% of the lightning has occurred.
7. When the Lifted Index reaches -10°C, all the lightning has occurred.
8. The Lifted Index values for the two seasons are very similar (blue and red lines) and the average (green line) lies in between for the two seasons.

#### 4.2.4 Cumulative frequency graphs for Precipitable Water and lightning

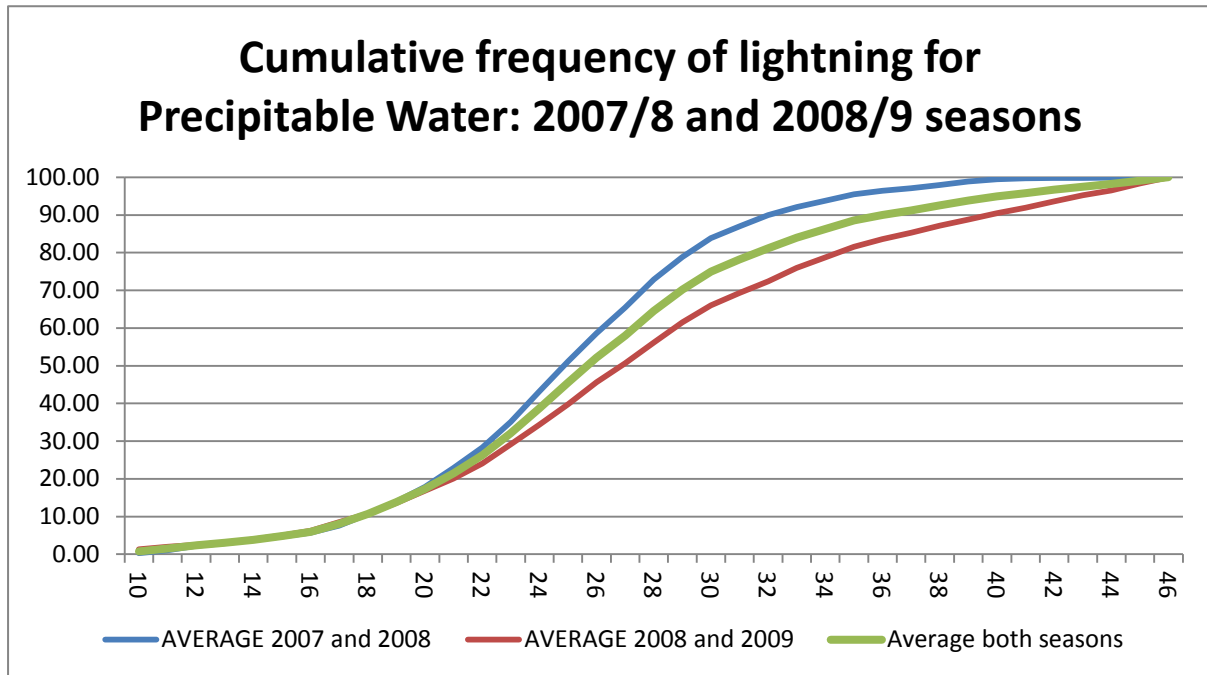


Figure 4.4 Cumulative frequency graph for Precipitable Water values (mm) for 2007/8 and 2008/9 seasons

Finally, from the Precipitable Water graph (Figure 4.4) it is clear that:

9. For Precipitable Water values of less than 10 mm, no lightning has occurred.
10. When Precipitable Water is less than or equal to 26 mm, 50% of the lightning has occurred.
11. When Precipitable Water reaches 46 mm, all the lightning has occurred.
12. The cumulative frequency of lightning differs for the two seasons, especially at the higher values of Precipitable Water (greater than 24 mm). Without going into much detail, it can be noted that the 2007/8 season started with above normal rainfall (first three months) and ended drier. The 2008/9 season started drier and ended (last three months) with large parts of South Africa receiving above normal rainfall. Climatologically speaking, South Africa experienced near La Nina conditions in the 2008/9 season, which is usually associated with more rain over the summer rainfall regions.

Based on these cumulative frequency polygon relationships between the individual RII and the occurrence of lightning, a look up table could then be created for each value of the respective RII, relating it the probability of seeing lightning.

### 4.3 CUMULATIVE FREQUENCY GRAPHS FOR TOPOGRAPHY AND LIGHTNING

Kotroni and Lagouvardos (2008) investigated lightning occurrence in relation with elevation, terrain slope and vegetation over the Mediterranean and found a positive relation between lightning activity and elevation during spring and summer. Schulz and Diendorfer (1999) also noted more lightning with increasing terrain height in Austria. Gill (2008b) studied flash densities across South Africa in 2006/7 and found that the highest densities occur in spring and summer along the eastern escarpment onto the Highveld region of the interior plateau (Figure 1.4, Chapter 1). This is the result of the orographic enhancement of convection in combination with surface heating and abundant moisture. The average amount of lightning strokes which occurred in 2008 based on a 0.1°X0.1° grid is shown in Figure 4.5 (left) and is related to topography shown in Figure 4.5 (right).

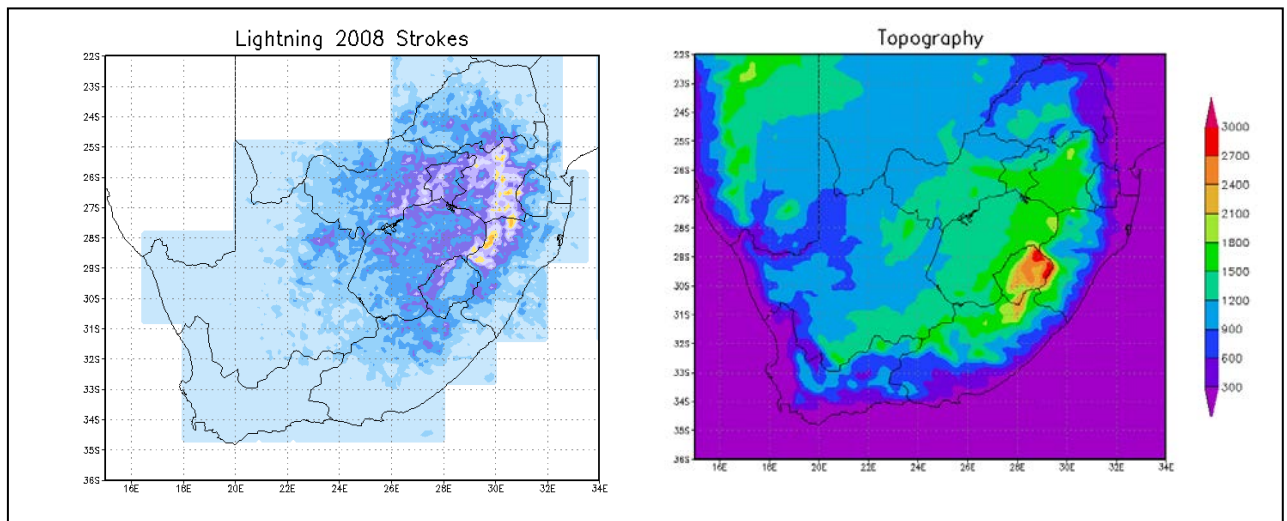


Figure 4.5 Average amount of lightning for 2008 (left) and topography of South Africa (right)

This confirms the fact that the orography is closely related to lightning occurrence, but also that the highest number of lightning strokes does *not* occur where the highest terrain is seen. This agrees with the findings of Schulz and Diendorfer (1999). They used data from 1995 to 1998 from their lightning detection network in Austria and showed that from 500 m to 2000 m there is an increase in the amount of lightning, but if the terrain is higher than 2000 m there is a rapid decrease. Their explanation is that regions at these altitudes are inside or at least very close to the thunderstorm clouds and that only some flashes might be recorded. Alternatively, there might be a real decrease in lightning. Similar findings were made by Reap (1986) for the United States and Orville (1994) for the Appalachian mountains.

Using the 2008 data from the South African lightning detection network (excluding areas over the ocean), Figure 4.6 shows the frequency histogram and cumulative frequency polygon for topography and lightning.

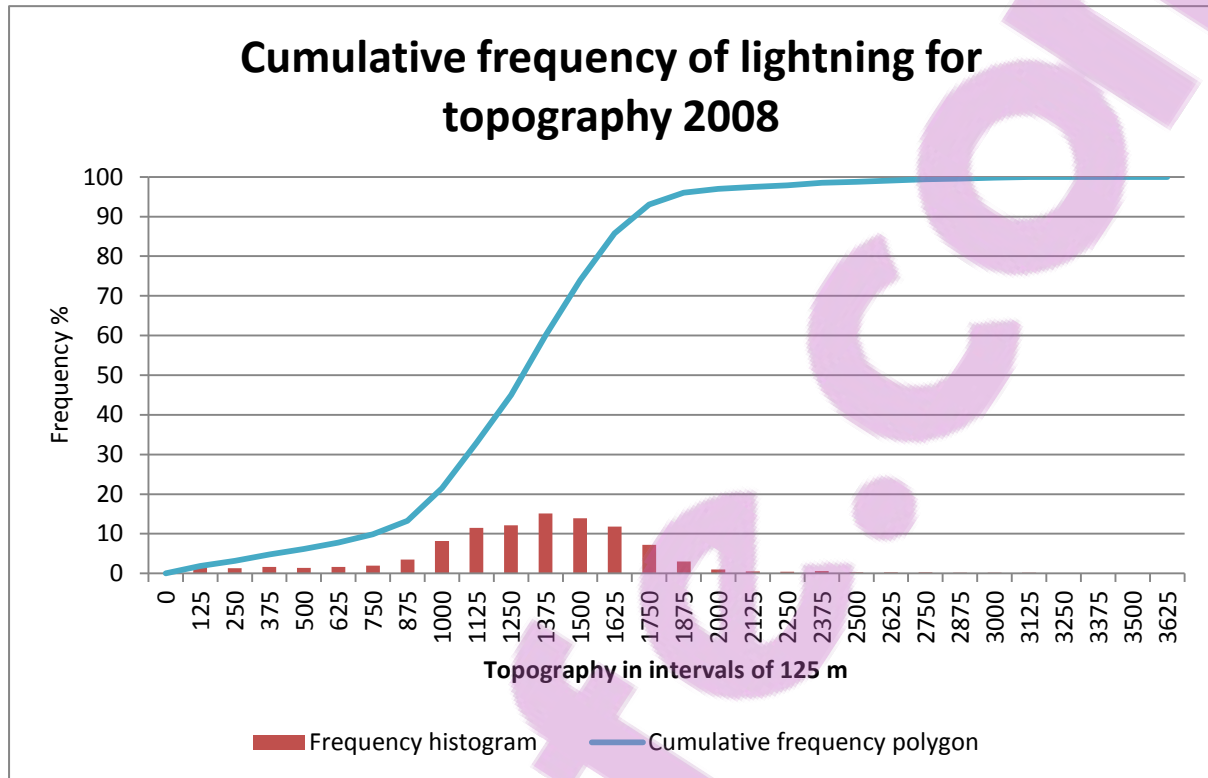


Figure 4.6 Frequency histogram of lightning for 2008 (red) and cumulative frequency graph (blue) related to topography of South Africa, indicated in intervals of 125 m.

The same tendency is seen here in the South African data namely that there is an increase in lightning occurrence up to 1375 m, where 50% of the lightning has occurred. Although some lightning still occurs at higher altitudes, there is marked decrease after about 1625 m. Gill (2008a) noted that the mountain ranges in the southeastern parts of South Africa have a flash density of four to five flashes per square kilometre per year compared to the five to ten flashes per square kilometre per year in the surrounding areas. Gill (2008a) suggests that thunderstorms possibly form at a level below these very high mountain peaks, which would make lightning detection difficult. Another possibility is that the thunderstorms, which developed on the windward side of the mountain, may have lost most of their moisture content on lower parts of the mountains.

Based on this cumulative frequency polygon relationship between topography and the occurrence of lightning, a look up table could also be created for each interval of the topography, relating it the probability of seeing lightning.

#### 4.4 COMBINING THE FOUR RII AND TOPOGRAPHY FOR A NEW INDEX

Based on the lightning frequency look up tables for each of the RII and for topography, which related each RII to the occurrence of lightning, the scene was set to combine the RII into one parameter. Acknowledging the fact that convection is formed when warm, moist air and instability as well as a trigger mechanism are present, the approach followed was that the Mixed K Index, Mixed Total Totals and Lifted Index (instability indices), Precipitable Water (moisture) as well as topography (height above sea level) could be combined into a single value. A possibility would be taking a simple average of the cumulative frequencies related to each of these quantities, with equal weight for each parameter (20%). The problem is that according to the statistical values calculated by means of the contingency table in Chapter 3, the indices' performance does not always improve with higher values. For Precipitable Water the false alarm ratio increases with time and thus one would not want higher values of Precipitable Water to play a large role. The Hanssen-Kuipers discriminant (HK) initially increased for some of the RII and then decreased. The solution would be to assign some kind of performance- related weight to the individual parameters in the combination process. Together with the cumulative frequency values for all meaningful values of each RII, the HK score for that value of the RII would also be taken into account. Taking this approach the final look up tables for each RII could then be compiled, including the HK, as listed in Tables 4.1 to 4.4.

**Table 4.1 Look up table for Mixed K Index**

Mixed K Index value	Percentage probability of seeing lightning (based on Figure 4.1) for two summer seasons	HK (based on Figure 3.9)
15	0.8	0.76
16	1.1	0.76
17	1.49	0.76
18	1.91	0.76
19	2.68	0.76
20	3.57	0.76
21	4.64	0.76
22	5.82	0.75
23	7.27	0.75
24	9.31	0.74
25	11.07	0.73
26	13.34	0.71

Mixed K Index value	Percentage probability of seeing lightning (based on Figure 4.1) for two summer seasons	HK (based on Figure 3.9)
27	15.96	0.7
28	19.39	0.67
29	23	0.64
30	27.67	0.6
31	32.39	0.56
32	37.72	0.51
33	44.57	0.45
34	54.56	0.39
35	63.86	0.32
36	72.86	0.25
37	80.76	0.18
38	87.3	0.12
39	92.74	0.07
40	96.38	0.04
41	98.58	0.02
42	99.35	0.01
43	99.74	0.01
44	99.87	0.01
45	99.89	0.01
46	99.97	0
47	100	0

Table 4.2 Look up table for Mixed Total Totals

Mixed Total Totals value	Percentage probability of seeing lightning (based on Figure 4.2) for two summer seasons	HK (based on Figure 3.10)
35	0.03	0.68
36	0.04	0.69
37	0.1	0.7
38	0.29	0.71

Mixed Total Totals value	Percentage probability of seeing lightning (based on Figure 4.2) for two summer seasons	HK (based on Figure 3.10)
39	0.53	0.73
40	1.27	0.74
41	2.3	0.74
42	4.54	0.75
43	6.87	0.74
44	11.38	0.72
45	16.77	0.70
46	24.2	0.65
47	34.25	0.57
48	45.96	0.48
49	57.36	0.39
50	67.45	0.3
51	76.77	0.21
52	84.31	0.15
53	89.47	0.1
54	93.51	0.06
55	96.94	0.03
56	98.73	0.01
57	99.41	0.01
58	99.61	0.01
59	99.8	0
60	99.95	0
61	100	0

**Table 4.3 Look up table for Lifted Index**

Lifted value	Index	Percentage probability of seeing lightning (based on Figure 4.3) for two summer seasons	HK (based on Figure 3.11)
+2		1.38	0.14

Lifted value	Index	Percentage probability of seeing lightning (based on Figure 4.3) for two summer seasons	HK (based on Figure 3.11)
+1		3.55	0.14
0		8.2	0.73
-1		15.33	0.68
-2		25.18	0.6
-3		39.3	0.5
-4		55.5	0.37
-5		71.13	0.25
-6		83.95	0.15
-7		92.09	0.07
-8		96.58	0.03
-9		98.88	0.01
-10		99.76	0
-11		99.97	0
-12		100	0

**Table 4.4 Look up table for Precipitable Water**

Precipitable value	Water	Percentage probability of seeing lightning (based on Figure 4.4)	HK (based on Figure 3.12)
10		1.32	0.66
11		1.98	0.66
12		2.46	0.67
13		3.12	0.67
14		3.95	0.68
15		4.95	0.68
16		6.21	0.68
17		8.5	0.67
18		10.76	0.65

Precipitable value	Water	Percentage probability of seeing lightning (based on Figure 4.4)	HK (based on Figure 3.12)
19		13.6	0.64
20		16.83	0.61
21		20.06	0.58
22		24.07	0.54
23		29.16	0.5
24		34.31	0.45
25		39.75	0.4
26		45.61	0.35
27		50.63	0.31
28		56.2	0.26
29		61.56	0.22
30		66.05	0.19
31		69.37	0.16
32		72.38	0.14
33		75.96	0.11
34		78.76	0.10
35		81.58	0.08
36		83.56	0.07
37		85.32	0.06
38		87.12	0.06
39		88.8	0.05
40		90.44	0.04
41		91.91	0.04
42		93.65	0.03
43		95.18	0.03
44		96.51	0.02
45		98.33	0.02

Since topography is an invariant field, it was not weighted according to its performance, but just related directly to its percentage probability of lightning occurrence, as listed in Table 4.5.

**Table 4.5 Look up table for topography**

Topography value (m)	Percentage probability of seeing lightning (based on Figure 4.6)
125	1.9
250	3.2
375	4.8
500	6.2
625	7.8
750	9.9
875	13.3
1000	21.5
1125	33
1250	45
1375	60.1
1500	74
1625	85.8
1750	93
1875	96
2000	97
2125	97.9
2250	98.5
2375	98.8
2500	99.1
2625	99.4
2750	99.6
2875	99.8
3000	100

The Combined Instability Index (CII) is now defined as an 80% contribution by the lightning frequencies of the four RII and a 20% contribution by those related to topography. The contribution related to each value of each RII respectively is the product of its cumulative frequency value and its ability to distinguish the 'yes' and 'no' events as reflected in the Hanssen-Kuipers discriminant. The CII is calculated only in areas where all five role players make a contribution (i.e. have a cumulative frequency greater than zero), in order to include the effects of instability (Mixed K Index, Mixed Total Totals and Lifted Index), moisture (Precipitable Water) and elevation (topography) at all times. The inclusion of height above sea level has the consequence that the CII can only be calculated over continental areas and exclude ocean areas.

As an example, using the values highlighted in the respective tables,

for a 0.1°X0.1° block, with a 3 h time average from 0600 to 0900 UTC, with

Mixed K Index = 30°C,

Mixed Total Totals = 50°C,

Lifted Index = -3°C and

Precipitable Water = 20 mm,

at an altitude of 1500 m:

$$\begin{aligned}
 \text{CII} &= 0.8 \times [\text{Mixed K Index contribution} + \text{Mixed Total Totals contribution} + \text{Lifted Index contribution} + \text{Precipitable Water contribution}] + 0.2 \times [\text{Topography contribution}] \\
 &= 0.8 \times [(27.67 \times 0.6) + (67.45 \times 0.3) + (39.3 \times 0.5) + (16.83 \times 0.61)] + 0.2 \times [74] \\
 &= 0.8 \times [16.6 + 20.24 + 19.65 + 10.266] + 0.2 \times [74] \\
 &= 23.93 + 14.8 \\
 &= 38.73\%
 \end{aligned}$$

Given these values, there would thus be a 38.73% chance of seeing lightning later in the day. This calculation was carried out for all fifty cases and again a three hour time average was used to ensure time consistency as well as to use as many cloud free pixel blocks as possible.

The CII created in this way can be seen as a pseudo “ensemble” of ingredients for convection over land. Since deterministic forecasts will never be perfect, ensembles provide scenarios of possibilities for an event to happen with the associated estimates of uncertainty (Ebert *et al.*, 2006). The CII methodology moves away from a deterministic threshold for different parameters and aims at a probabilistic forecast to enable better decision making for the very short range forecasting of convection.

## **4.5 EXAMPLES OF THE NEW COMBINED INSTABILITY INDEX (CII) WITH VISUAL VERIFICATION**

In the following examples the CII will be given in percentages above 10% as shown on the colour scale on the right hand side of the figures. This is a probabilistic map indicating areas where there are varying degrees of probability for convection to develop. The grey shading depicts the areas where clouds were present during the three hour period and the CII could not be calculated.

To aid in the interpretation of real time MSG images, forecasters and researchers often make use of colour combinations of the different channels. Two of these Red-Green-Blue (RGB) combinations will be used here:

1. The MSG Convection RGB product consists of the difference between Channel 5 (WV6.2) and Channel 6 (WV7.3) in the red beam, the difference between Channel 4 (IR3.9) and Channel 9 (IR10.8) in the green beam and the difference between Channel 3 (NIR1.6) and Channel 1 (VIS0.6) in the blue beam. Combining the Water Vapour channels (WV6.2 and WV6.3), Infrared channels (IR3.9 and IR10.8) and Visible channels (VIS0.6 and NIR1.6) in this way, makes it possible to identify areas of convection more clearly. The reddish areas indicate deep, precipitation clouds at a high level with large ice particles. The yellow areas indicate Cumulonimbus clouds with small ice particles in the top layer, which implies strong updrafts and possible severe weather (Kerkmann, 2005).
2. The MSG High Resolution Visible RGB product uses the High Resolution Visible channel in the red and green beams and the infrared channel in the blue beam. This combination depicts Cumulonimbus (Cb) and Nimbostratus clouds in bright white, cirrus clouds in blue and middle and low clouds in greenish-yellowish colours (Kerkmann, 2005).

EXAMPLE 1: 2 NOVEMBER 2008

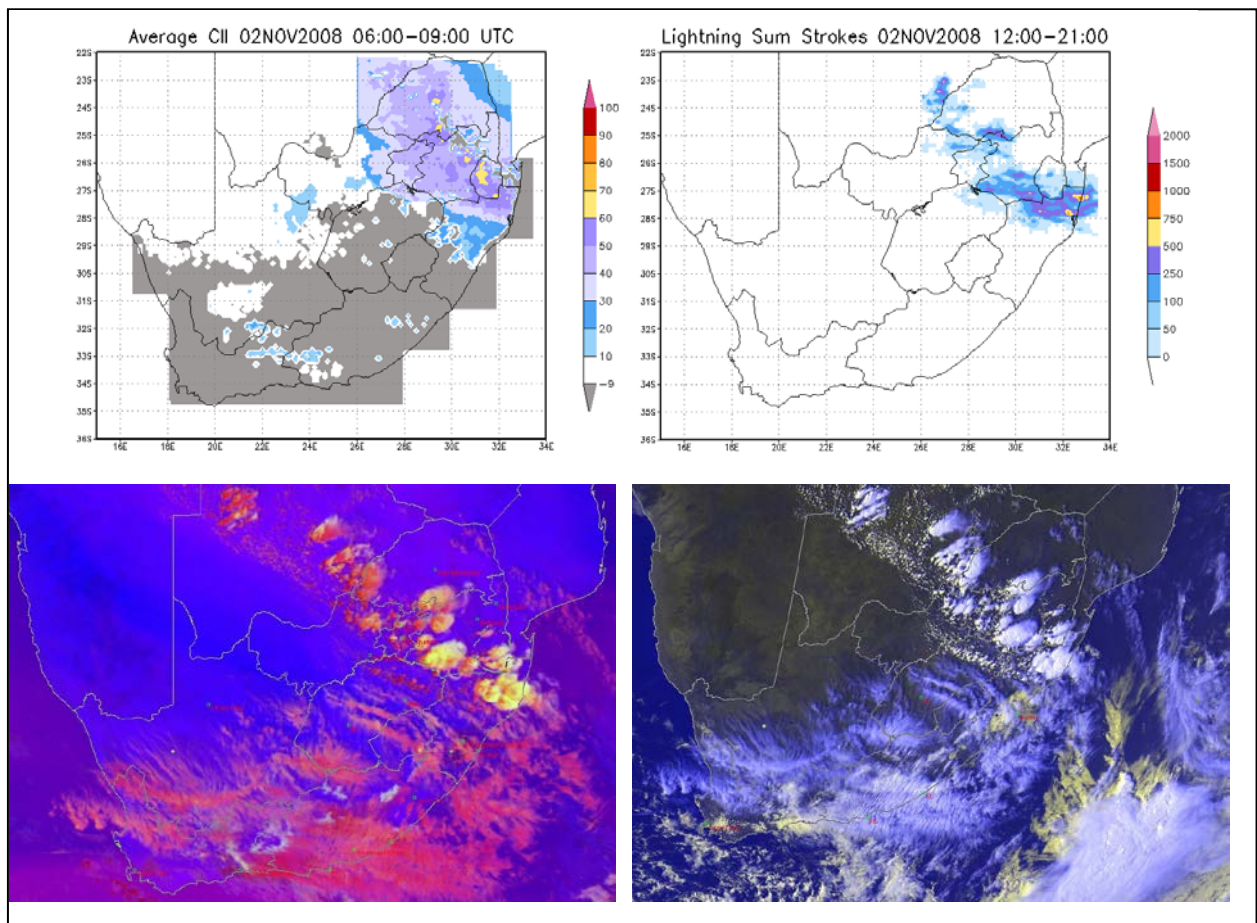


Figure 4.7 CII time average between 0600 and 0900 UTC (top left), occurrence of lightning between 1200 and 2100 UTC (top right), Convection RGB product (bottom left) at 1400 UTC and the High Resolution Visible RGB product (bottom right) at 1400 UTC for 2 November 2008

In Figure 4.7 the yellow areas of the Convection RGB (bottom left), the bright white in the HRV RGB (bottom right) and the most lightning (top right) coincide to a large extent with the area where the CII has the highest percentages (purple and yellow in top left) and most lightning occurred (top right).

EXAMPLE 2: 3 March 2009

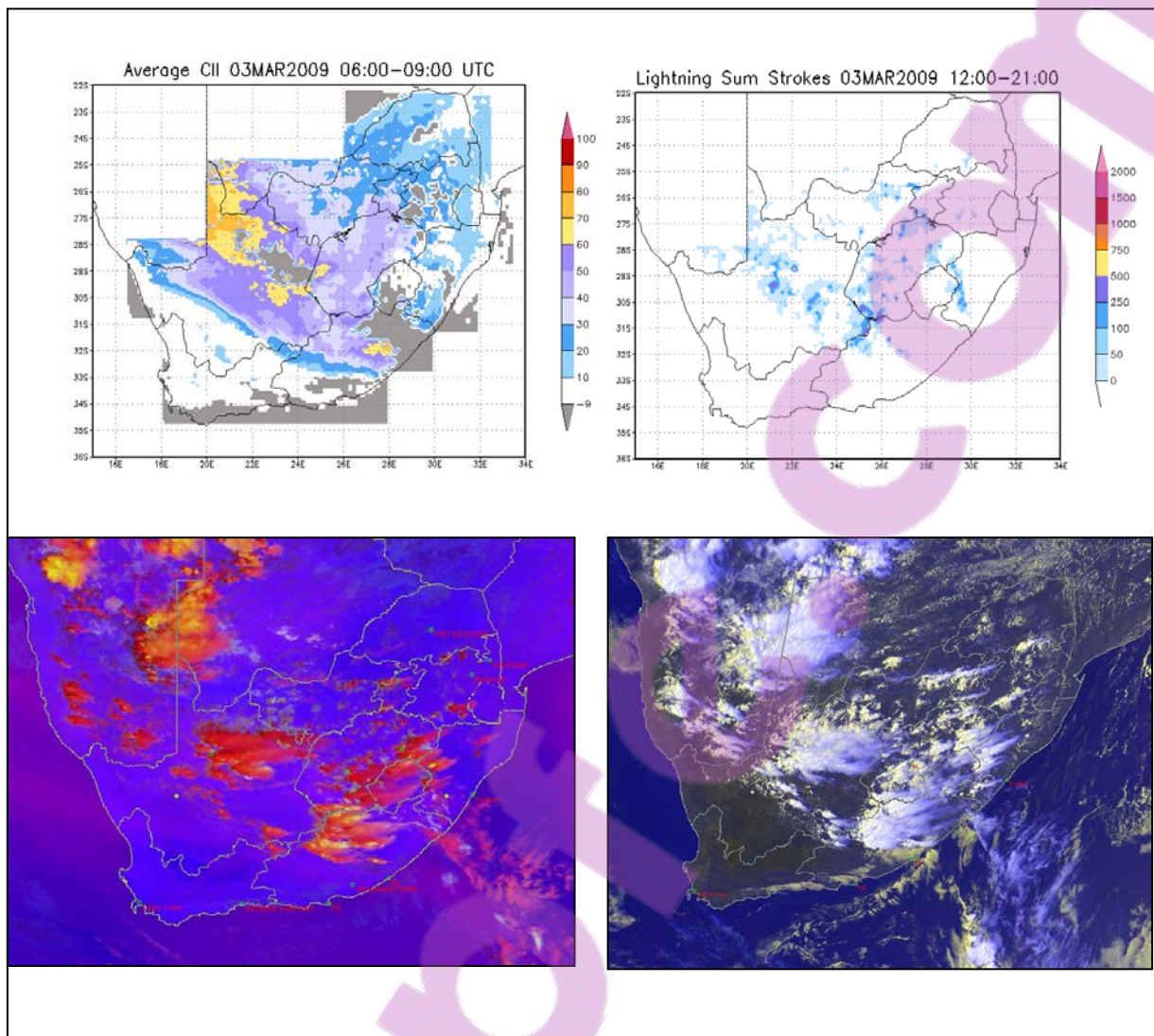


Figure 4.8 CII time average between 0600 and 0900 UTC (top left), occurrence of lightning between 1200 and 2100 UTC (top right), Convection RGB product (bottom left) at 1300 UTC and the High Resolution Visible RGB product (bottom right) at 1300 UTC for 3 March 2009

In Figure 4.8 the areas where the CII gives the highest probabilities (purple and yellow in top left) look very similar to the observations of convection (MSG RGB products at the bottom) and lightning observations (top right) later in the day. In this case high probabilities of convection are given for the Northern Cape, on the border with Namibia, where the convection RGB at 1300 UTC does not show signs of deep convection, but at 1900 UTC and 2000 UTC (not shown) convective activity is indeed evident coinciding with the lightning also shown in that area.

## **4.6 SUMMARY**

In this chapter the data and methodology used to develop a new instability indicator were described. Cumulative frequencies of lightning occurrence related to each of the RII as well as to topography were calculated. Look up tables for the various contributors were set up and the formula for the Combined Instability Index was postulated, using weighting provided by the Hanssen-Kuipers discriminant. Finally, two examples were shown to demonstrate the usefulness of the CII based on visual verification. Chapter 5 will provide a more thorough evaluation of the CII against the occurrence of lightning and in Chapter 6 the CII will be evaluated against the Hydroestimator product.

# CHAPTER 5

## EVALUATION OF THE CII AGAINST THE OCCURRENCE OF LIGHTNING OVER SOUTH AFRICA

---

### 5.1 BACKGROUND

In the first four chapters the background and development leading to a new combined indicator of convective activity with at least a three hour lead time was described. From a visual verification point of view, the new indicator, CII, seems able to focus attention very well on the areas where convection occurred later in the day. A more quantitative evaluation of the CII, similar to the evaluation carried out for the individual RII, will be the focus of this chapter.

### 5.2 EVALUATION OF THE CII

In the same way as was described in Chapter 3, the early morning CII is evaluated against the occurrence of lightning later in the day. A three hourly average of the CII from 0600 to 0900 UTC is used in order to ensure consistency in time as well as to fill as many pixels as possible with data. The sum of lightning strokes for the period 1200 to 2100 UTC is used as verification because this is the most likely time for occurrence of convection in South Africa, as mentioned previously. The contingency table approach is used and the same statistics as mentioned in Chapter 3, are computed.

Of the fifty cases studied over the summer seasons of 2007/8 and 2008/9, ten cases, one from each of the months (November, December, January, February and March) of the two seasons, were chosen to demonstrate the accuracy of the CII. The only prerequisite for the choice of the ten days was that reasonable convective activity had to be present over a reasonably large area of South Africa. Next, CII statistics for all fifty cases are presented and then compared to the statistics of the individual RII.

CASE 1: 29 November 2007

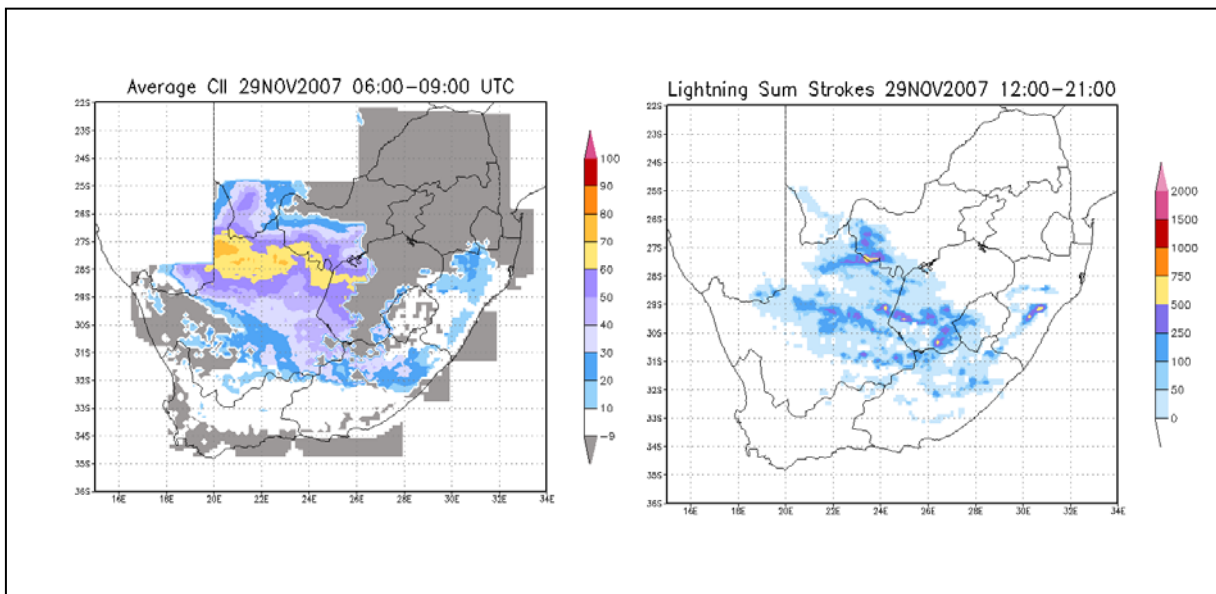


Figure 5.1 CII (left) and occurrence of lightning (right) for 29 November 2007

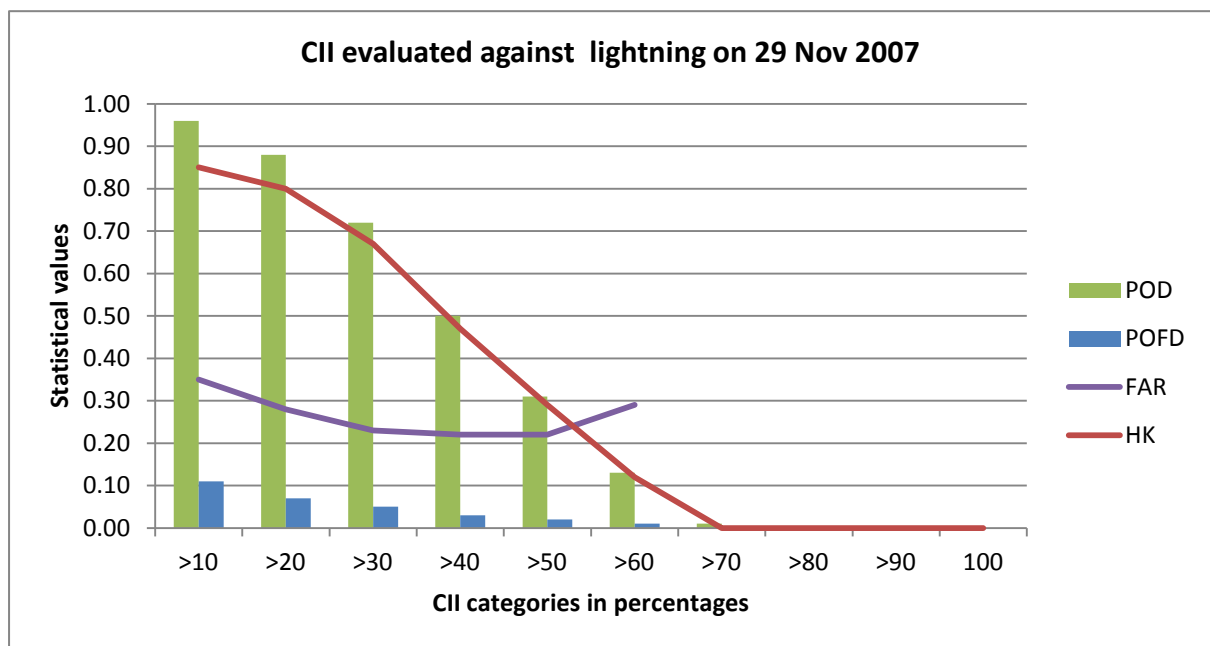


Figure 5.2 CII statistical scores against the occurrence of lightning for 29 November 2007

From Figures 5.1 and 5.2 it can be concluded that:

1. There appears to be a high degree of visual agreement between the areas where the CII was more than 10% in the early morning and where lightning occurred later in the day. The higher probabilities given by the CII (more than 60%) also coincide with a high amount of lightning over a considerable area of the Northwest Province and Northern Cape (Figure 5.1).
2. POD for CII greater than 10% is above 0.95 and decreases slowly to just above 0.1 when CII exceeds 60% (Figure 5.2).
3. POFD starts just above 0.1 and diminishes with higher values of CII (Figure 5.2).
4. FAR starts at 0.35, decreases to 0.22 and increases when CII exceeds 50%, after which there are too few values for calculation (Figure 5.2).
5. HK starts just below 0.9 and decreases gradually (Figure 5.2).

**CASE 2: 14 December 2007**

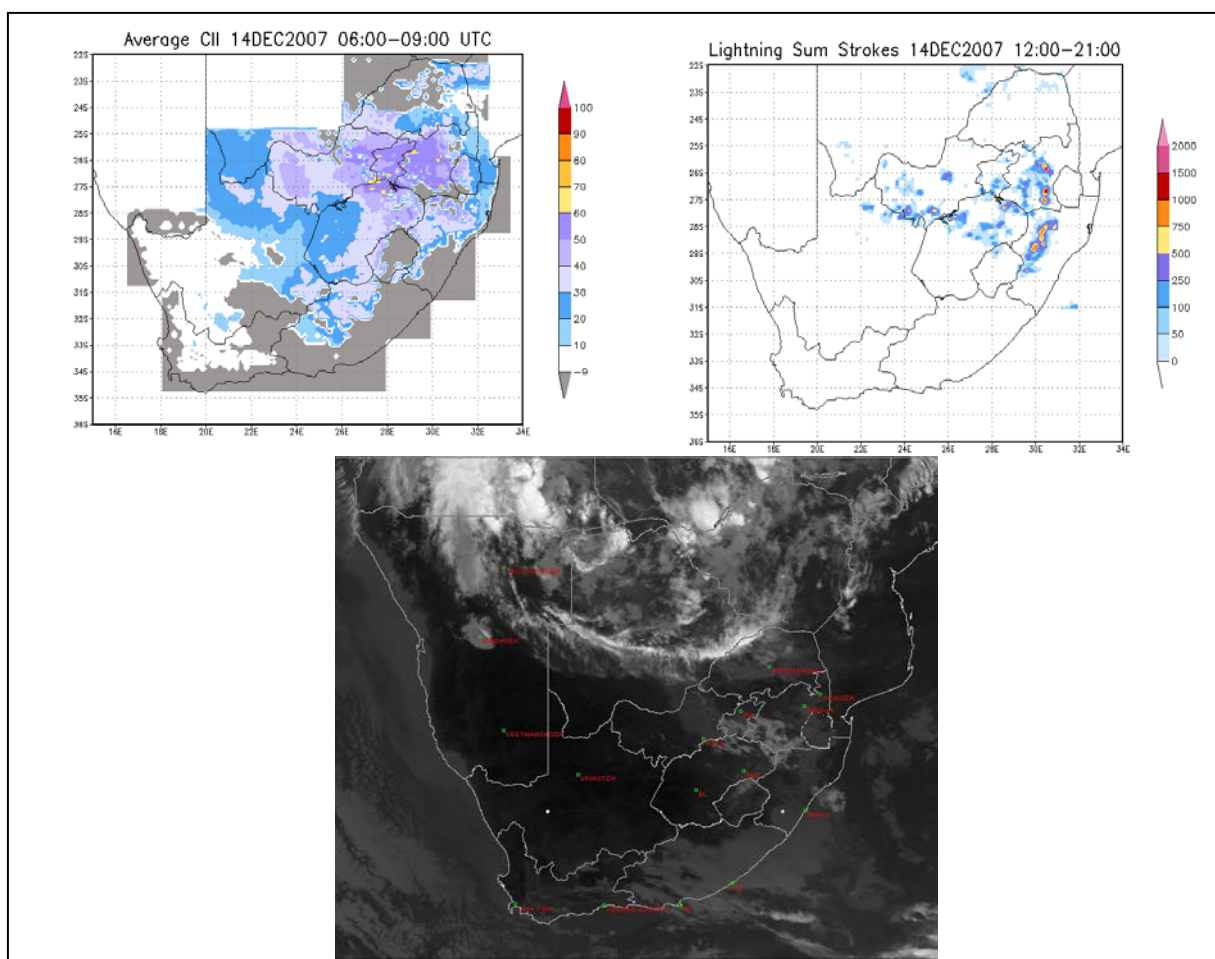


Figure 5.3 CII (top left) and occurrence of lightning (top right). Areas covered by cloud so that CII values are not available are shown in the 0600 UTC IR108 image below and also indicated by the grey areas in the CII graphic for

14 December 2007

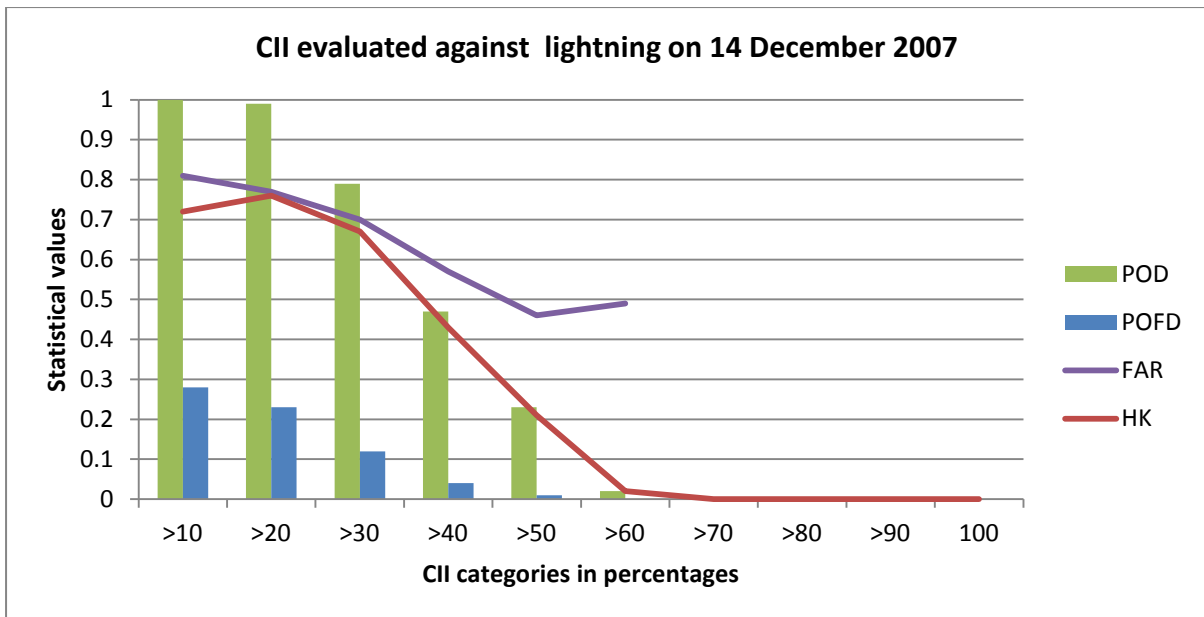


Figure 5.4 CII statistical scores against the occurrence of lightning for 14 December 2007

From Figures 5.3 and 5.4 it can be concluded that:

6. The areas where the CII was more than 10% and the area where lightning occurred show a high degree of correspondence (Figure 5.3), although the CII might have overestimated the area. The CII indicated areas of up to 40% over the Eastern Cape and southern Free State where no lightning occurred in this nine hour period.
7. POD for CII greater than 10% is 1.0 and decreases slowly to just above 0.2 when CII exceeds 50% (Figure 5.4).
8. POFD starts just below 0.3 and diminishes with higher values of CII (Figure 5.4).
9. FAR starts at 0.8 and decreases to below 0.5 when CII exceeds 50% and then increases slightly, after which there are too few values for calculation (Figure 5.4).
10. HK starts at about 0.7, increases slightly and then decreases gradually (Figure 5.4). The overestimation of the CII is reflected in the lower HK and the higher FAR for this case.

CASE 3: 6 January 2008

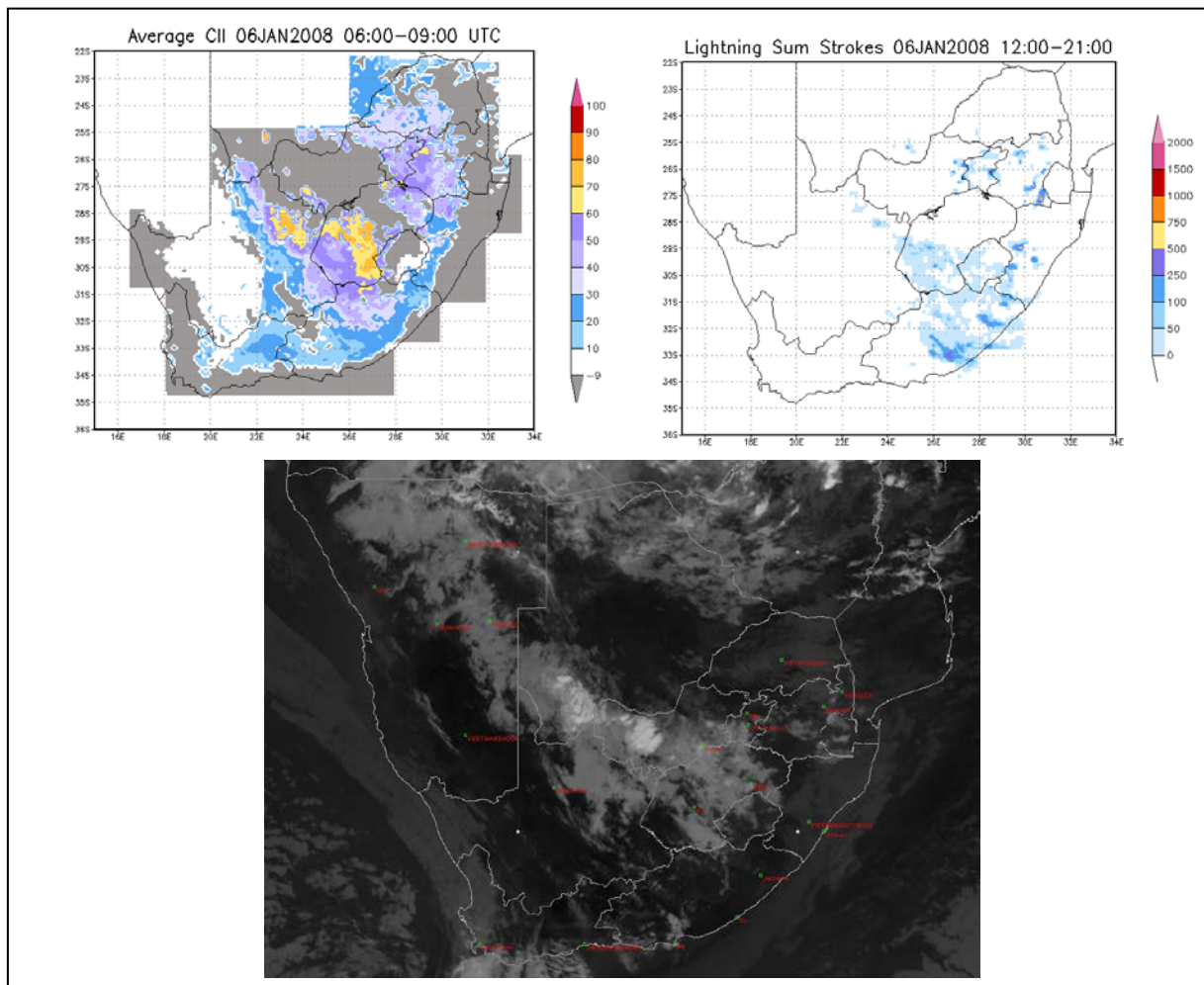


Figure 5.5 CII (top left) and occurrence of lightning (top right). Areas covered by cloud so that CII values are not available are shown in the 0600 UTC IR108 image below and also indicated by the grey areas in the CII graphic for 6 January 2008

From Figures 5.5 and 5.6 it can be concluded that:

11. There is good visual agreement between the areas where the CII was more than 10% in the early morning and the occurrence of lightning later in the day (Figure 5.5), bearing in mind the early morning cloud cover. Some areas in the Limpopo Province and the southwestern Cape were given a 20% probability of convection by the CII and no lightning occurred in that area in the nine hour period. The lightning in the Eastern Cape was well predicted.
12. POD for CII greater than 10% is 1.0 and decreases slowly (Figure 5.6).
13. POFD starts below 0.2 and diminishes with higher values of CII (Figure 5.6).
14. FAR starts above 0.6 and decreases to less than 0.1 when CII exceeds 70% after which there are too few values for calculation (Figure 5.6).

15. HK starts just above 0.8, increases slightly and decreases gradually (Figure 5.6).

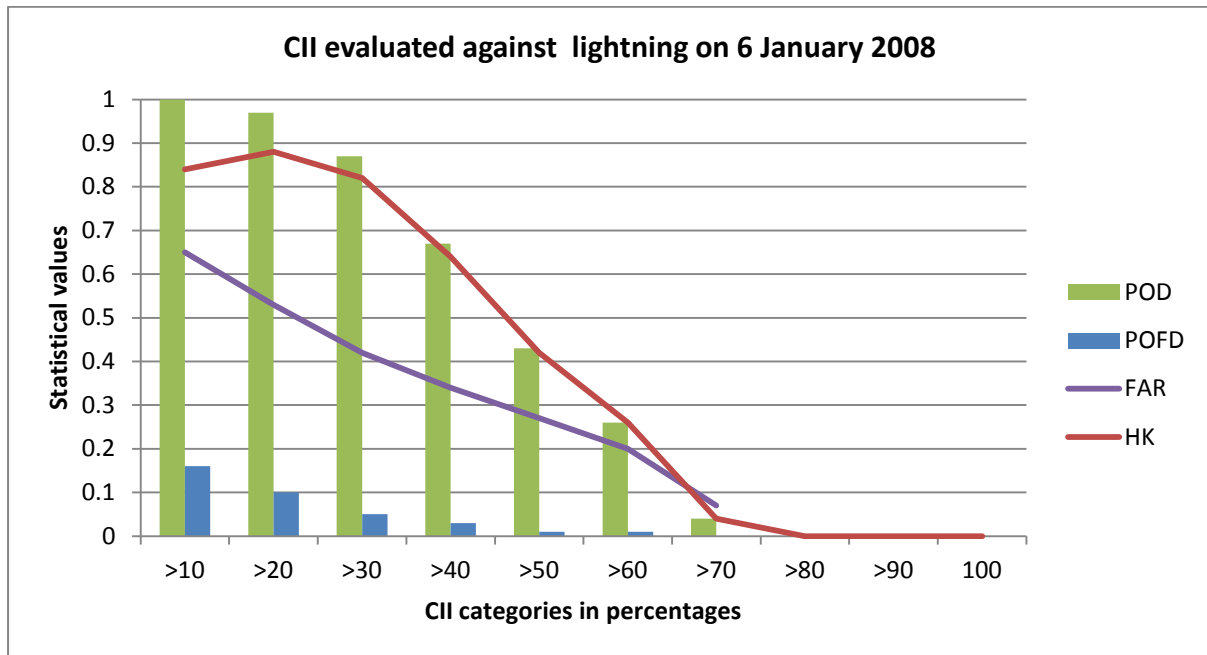


Figure 5.6 CII statistical scores against the occurrence of lightning for 6 January 2008

CASE 4: 7 February 2008

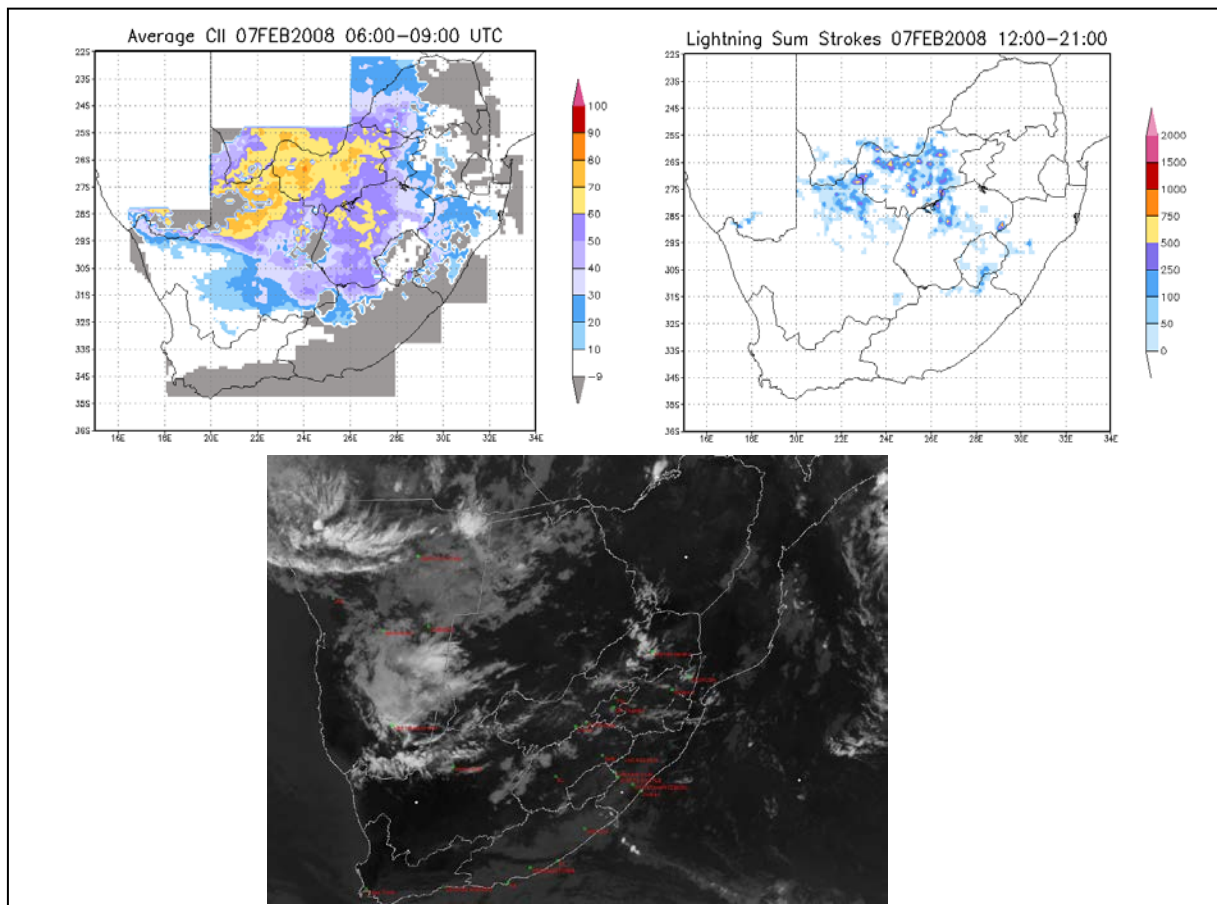


Figure 5.7 CII (top left) and occurrence of lightning (top right). Areas covered by cloud so that CII values are not available are shown in the 0600 UTC IR108 image below and also indicated by the grey areas in the CII graphic for 7 February 2008

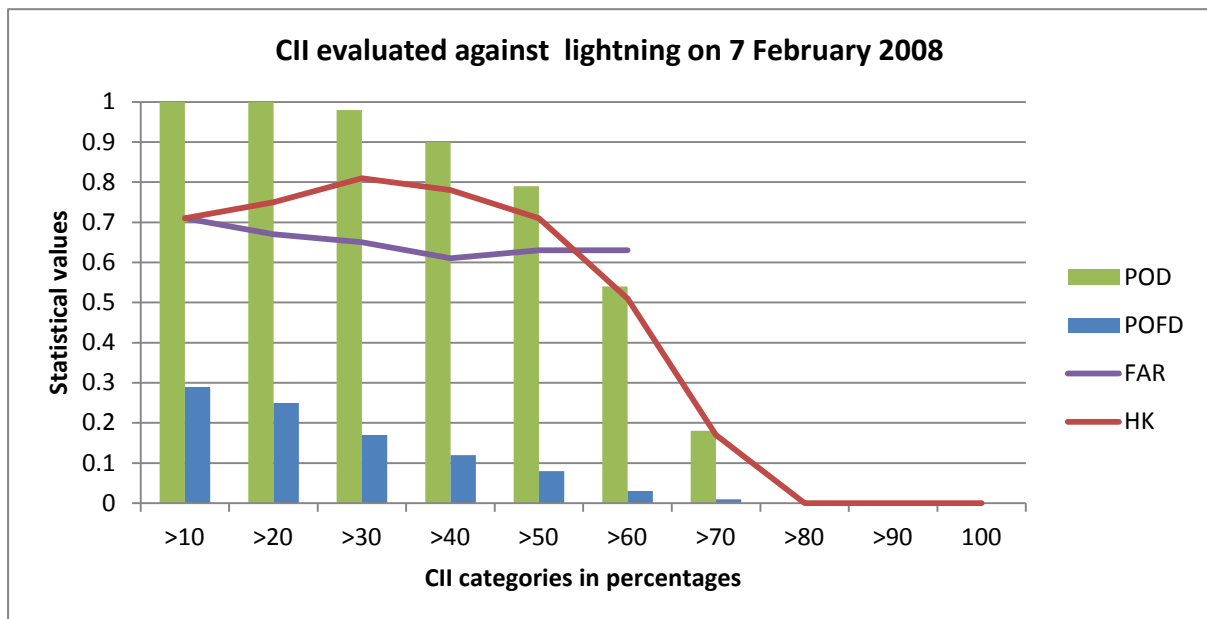


Figure 5.8 CII statistical scores against the occurrence of lightning for 7 February 2008

From Figures 5.7 and 5.8 it can be concluded that:

16. There is good visual agreement between the area indicated by the CII early in the morning as favourable for convection and the occurrence of lightning after 1200 UTC (Figure 5.7). Higher amounts of lightning occurred over the Northwest Province, Northern Cape and northern Free State, which coincided with the higher probabilities (greater than 60%) given by the CII. Lower probabilities of the CII were seen over areas where no lightning occurred in the nine hour period.
17. POD for CII greater than 10% is 1.0 and decreases slowly (Figure 5.8).
18. POFD starts below 0.3 and diminishes with higher values of CII (Figure 5.8).
19. FAR starts at 0.7 and decreases to 0.6 when CII exceeds 40%, increases slightly and then there are too few values for calculation (Figure 5.8).
20. HK starts above 0.7, increases slightly to 0.8 and then decreases gradually (Figure 5.8).

CASE 5: 5 March 2008

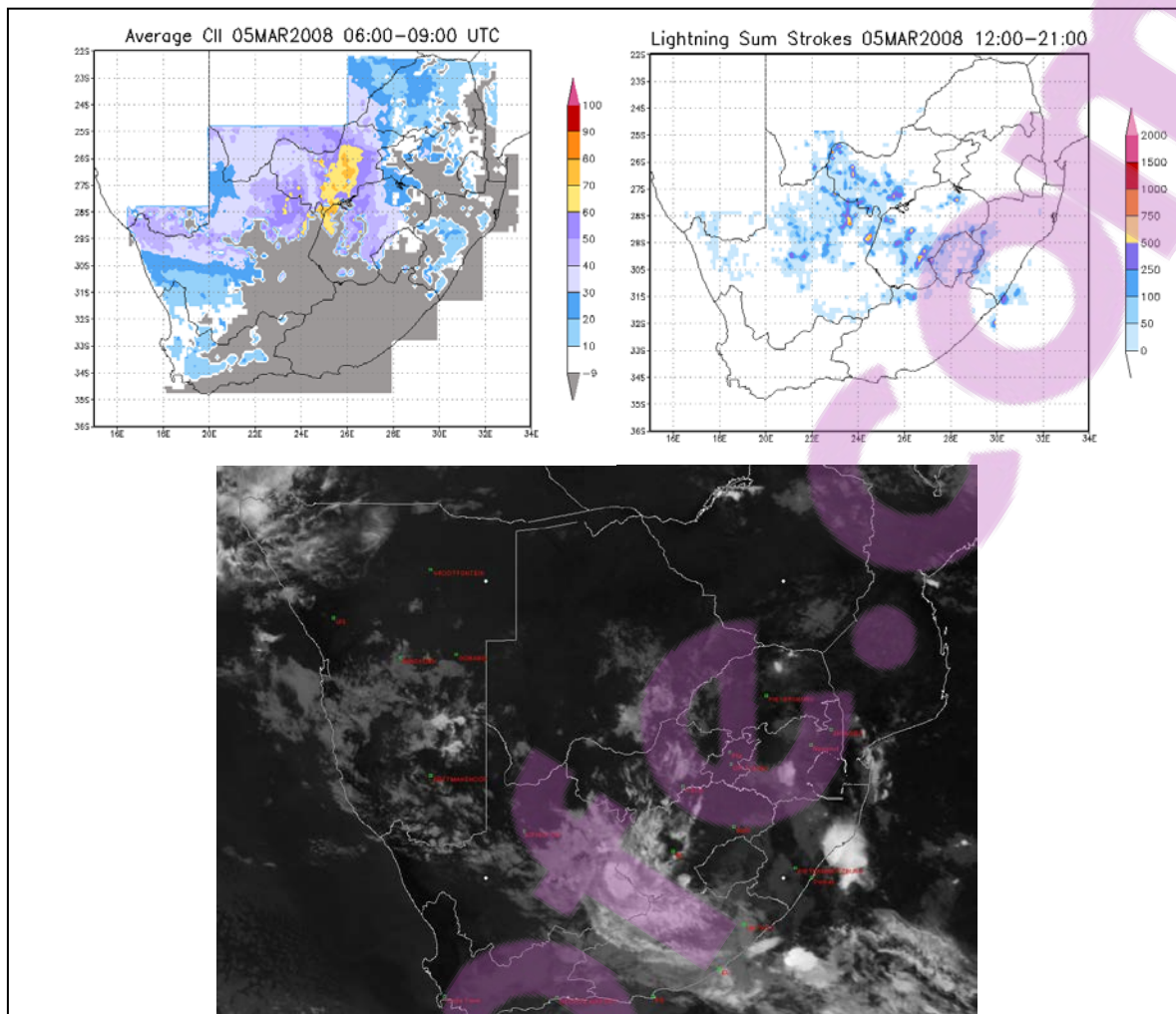


Figure 5.9 CII (top left) and occurrence of lightning (top right). Areas covered by cloud so that CII values are not available are shown in the 0600 UTC IR108 image below and also indicated by the grey areas in the CII graphic for 5 March 2008

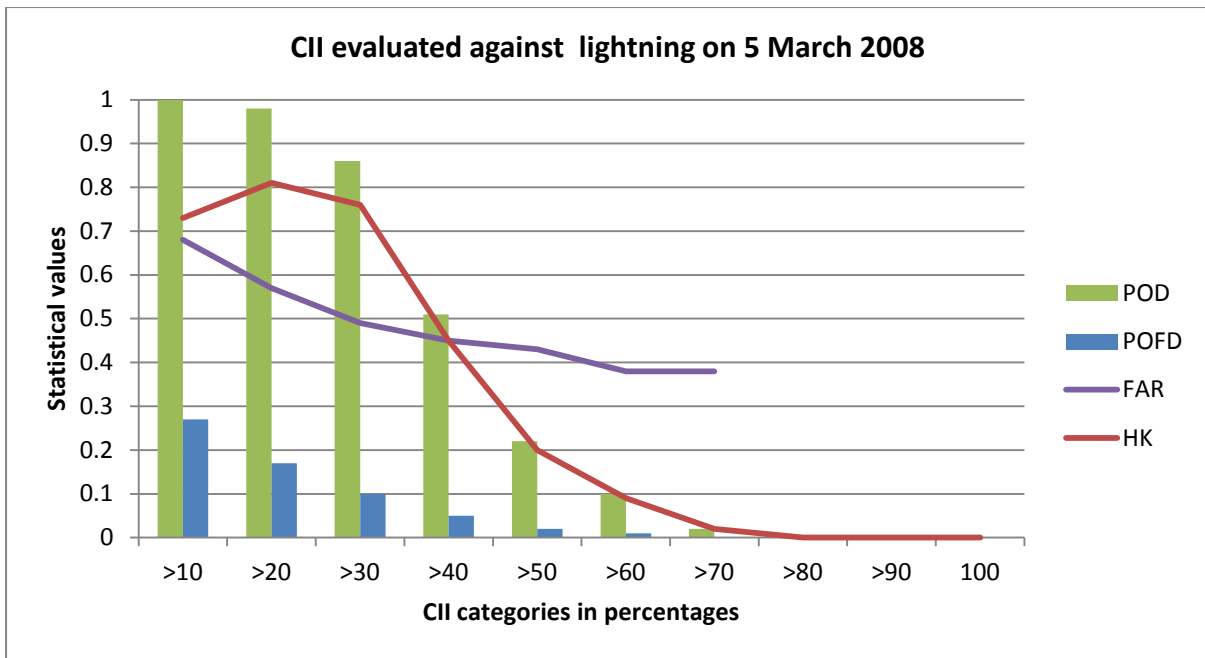


Figure 5.10 CII statistical scores against the occurrence of lightning for 5 March 2008

From Figures 5.9 and 5.10 it can be concluded that:

21. There is good visual agreement between the area indicated as favourable by the CII early in the morning and the occurrence of lightning later in the day (Figure 5.9). Higher amounts of lightning occurred over the central parts of the country which coincided with the higher probabilities of the CII. Areas where lower probabilities were given by the CII (less than 20%) occurred in the Western Cape and Limpopo and no lightning was detected there in the nine hour period.
22. POD for CII greater than 10% is 1.0 and decreases slowly (Figure 5.10).
23. POFD starts below 0.3 and diminishes with higher values of CII (Figure 5.10).
24. FAR starts below 0.7 and decreases to below 0.4 when CII exceeds 70% (Figure 5.10).
25. HK starts above 0.7, increases slightly to 0.8 and then decreases gradually (Figure 5.10).

CASE 6: 9 November 2008

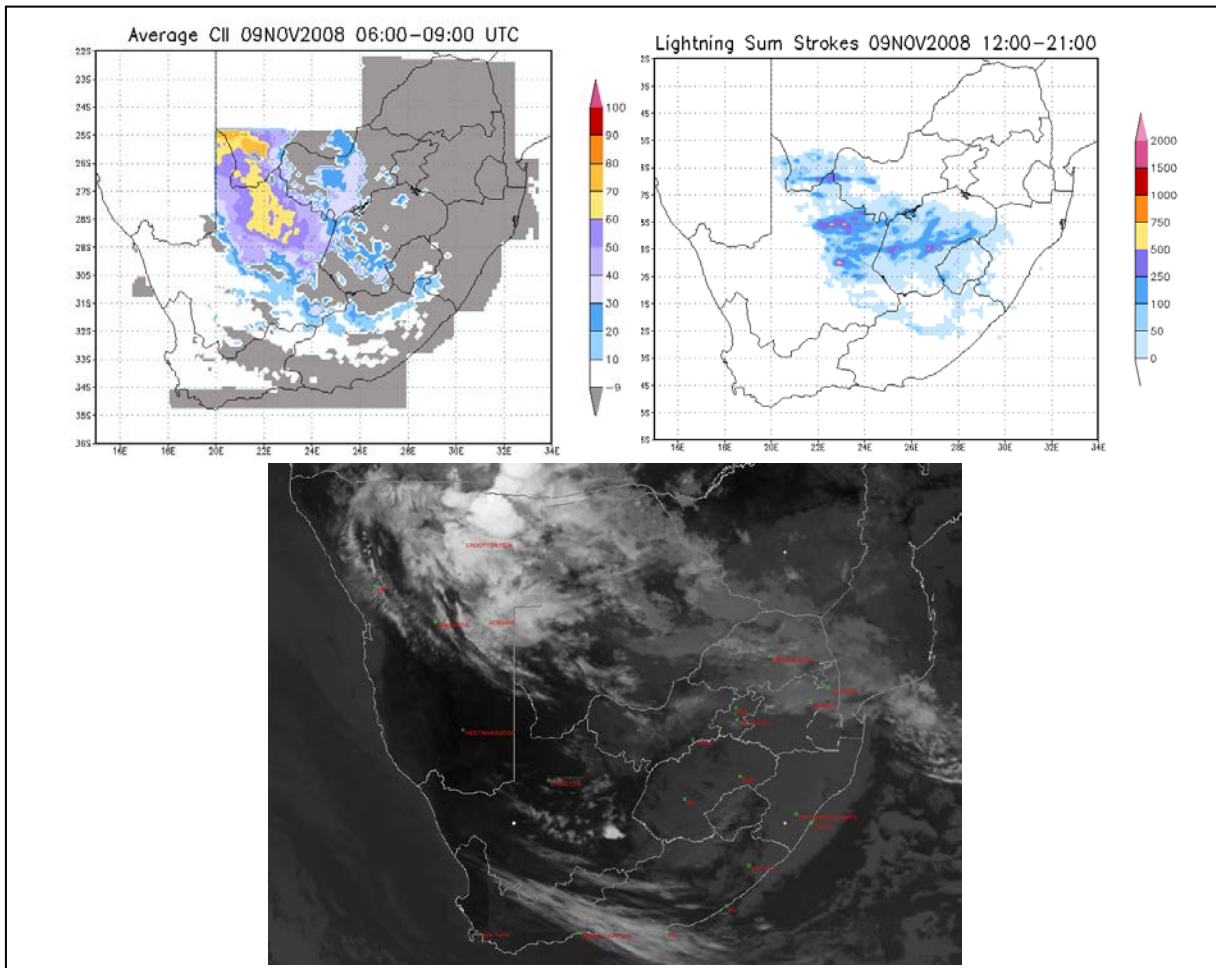


Figure 5.11 CII (top left) and occurrence of lightning (top right). Areas covered by cloud so that CII values are not available are shown in the 0600 UTC IR108 image below and also indicated by the grey areas in the CII graphic for 9 November 2008

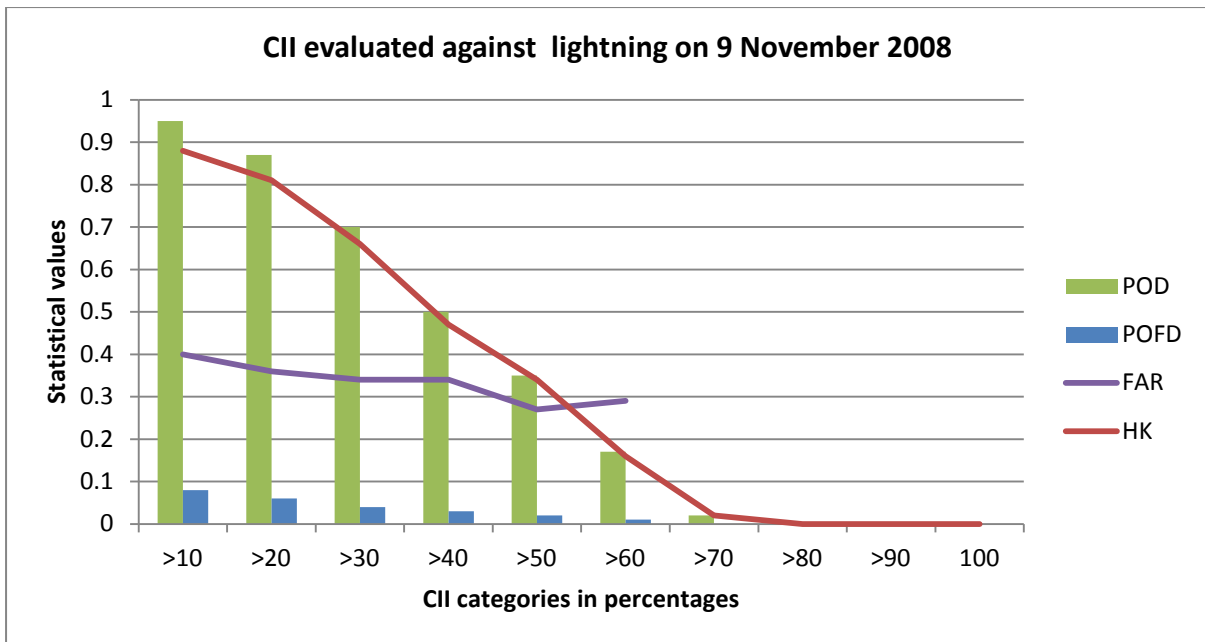


Figure 5.12 CII statistical scores against the occurrence of lightning for 9 November 2008

From Figures 5.11 and 5.12 it can be concluded that:

26. The areas where early in the morning the CII gave a more than 10% probability for convection to occur and where the lightning occurred later in the day are in good agreement, keeping in mind the cloud cover (indicated in grey). Spatial agreement is good with higher probabilities of CII (greater than 60%) and the areas with the highest amount of lightning agreeing in the Northern Cape (Figure 5.11). Over the northern Free State high amounts of lightning also occurred but no CII could be calculated there due to the cloud cover early that morning.
27. POD for CII greater than 10% is above 0.9 and decreases slowly (Figure 5.12).
28. POFD starts below 0.1 and diminishes with higher values of CII (Figure 5.12).
29. FAR starts at 0.4 and decreases to less than 0.3 when CII exceeds 50% after which it increases slightly (Figure 5.12). When CII exceeds 60% there are not enough values for calculation.
30. HK starts just below 0.9 and then decreases gradually (Figure 5.12).

CASE 7: 23 December 2008

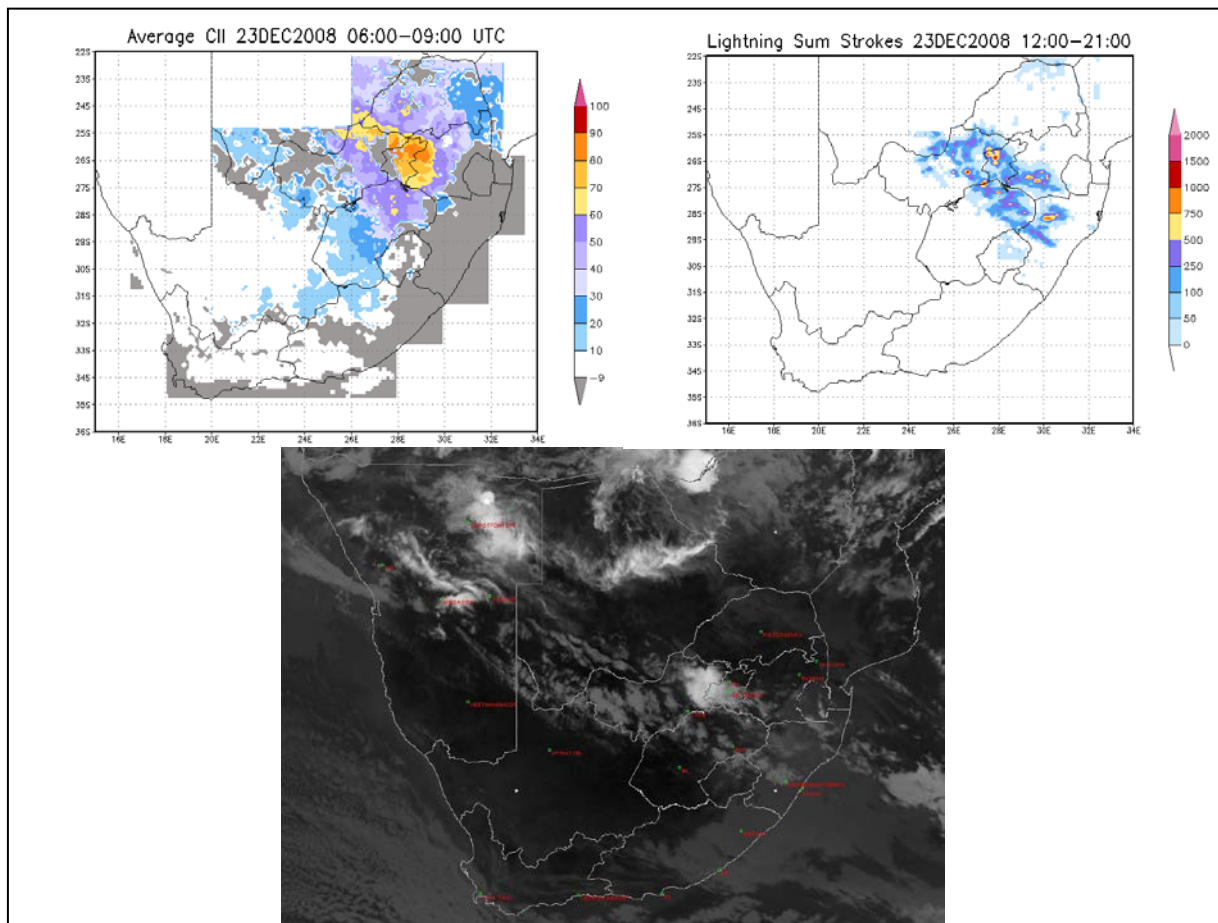


Figure 5.13 CII (top left) and occurrence of lightning (top right). Areas covered by cloud so that CII values are not available are shown in the 0600 UTC IR108 image below and also indicated by the grey areas in the CII graphic for 23 December 2008

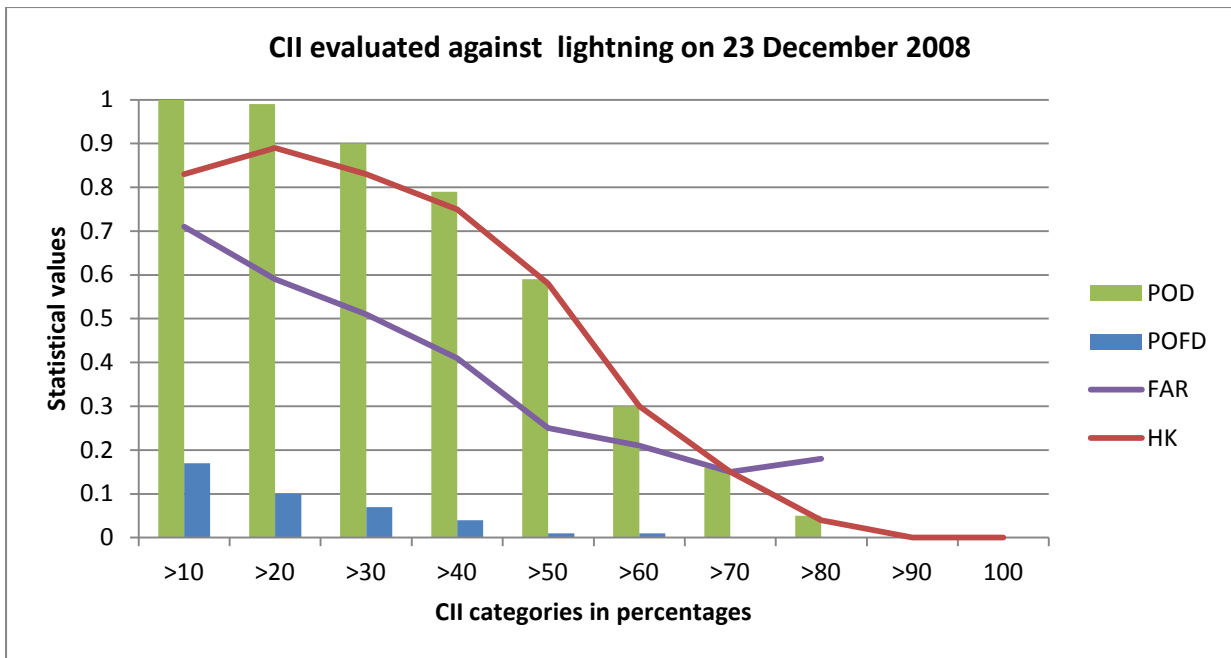


Figure 5.14 CII statistical scores against the occurrence of lightning for 23 December 2008

From Figures 5.13 and 5.14 it can be concluded that:

31. Spatial agreement between CII (greater than 10%) and occurrence of lightning later in the day is good, with the higher amounts of lightning in the same areas as the higher values of CII across Gauteng (Figure 5.13). Some of the lightning in KwaZulu-Natal could not be captured by CII due to cloud cover earlier that morning.
32. POD for CII greater than 10% is 1.0 and decreases slowly (Figure 5.14).
33. POFD starts below 0.2 and diminishes with higher values of CII (Figure 5.14).
34. FAR starts just above 0.7 and decreases to less than 0.2 when CII exceeds 70% (Figure 5.14). The fairly high FAR reflects the areas where lower probabilities of CII were given and no lightning occurred over Limpopo and southern Free State.
35. HK starts above 0.8, increases slightly and then decreases gradually (Figure 5.14).

CASE 8: 13 January 2009

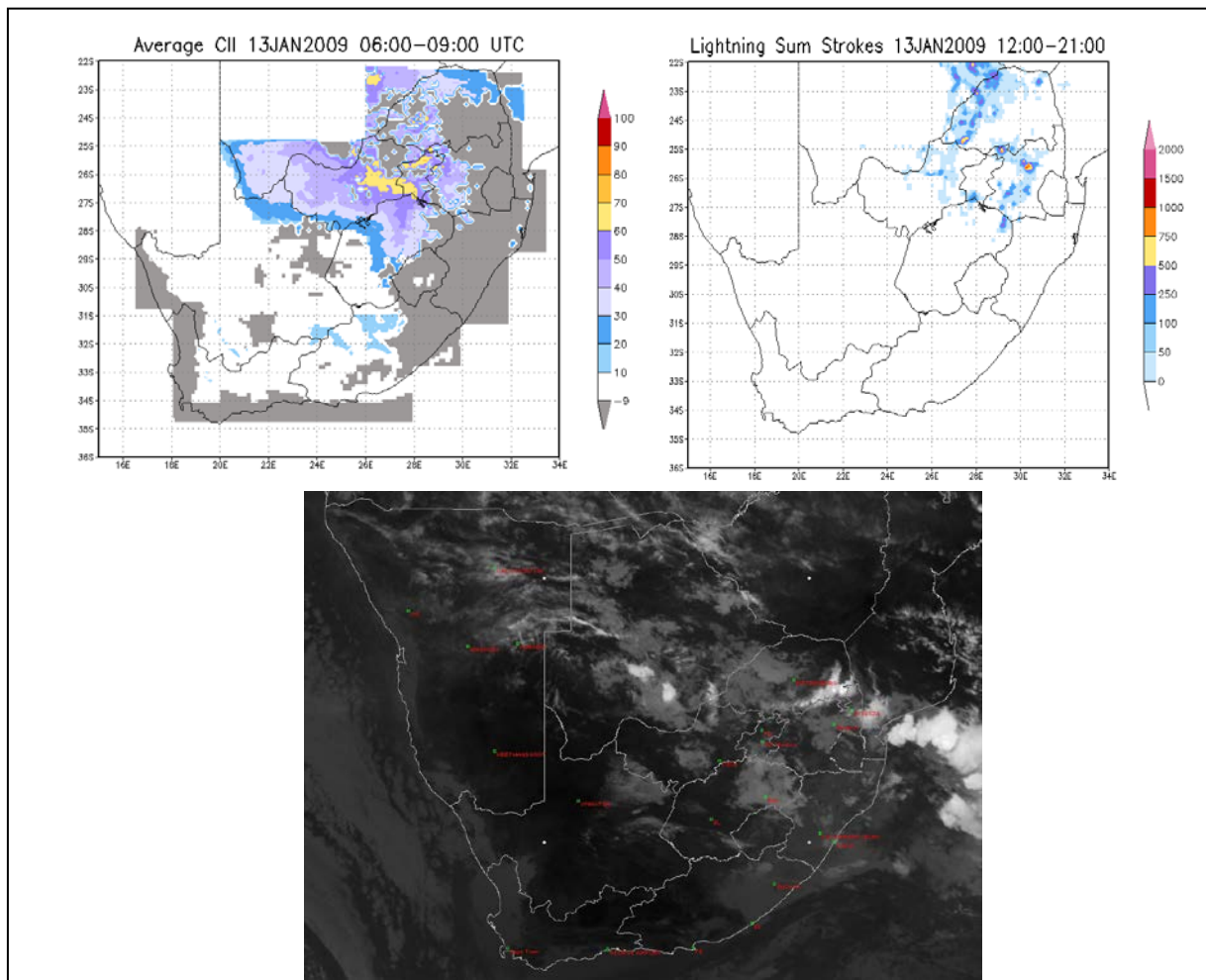


Figure 5.15 CII (top left) and occurrence of lightning (top right). Areas covered by cloud so that CII values are not available are shown in the 0600 UTC IR108 image below and also indicated by the grey areas in the CII graphic for 13 January 2009

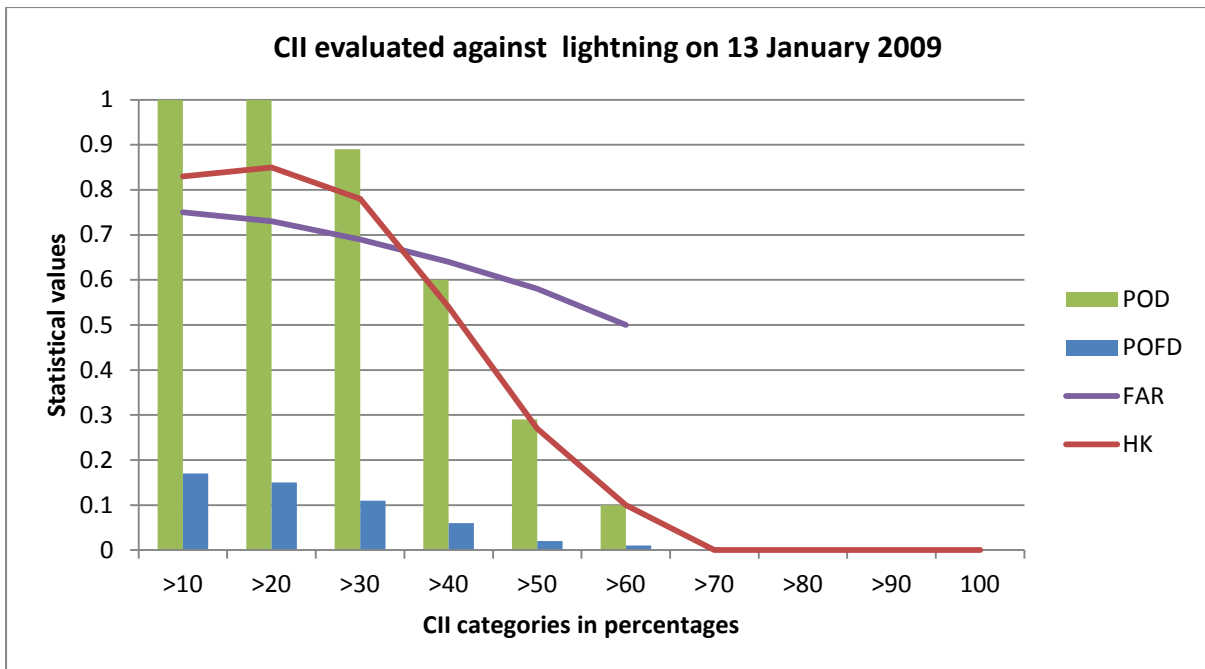


Figure 5.16 CII statistical scores against the occurrence of lightning for 13 January 2009

From Figures 5.15 and 5.16 it can be concluded that:

36. Spatial agreement between areas where the CII had values greater than 10% early in the morning and lightning occurrence later in the day is good (Figure 5.15). Clouds were already present early in the morning in Mpumalanga where a high amount of lightning also occurred later in the day. Lower probabilities were predicted by the CII over the Northwest Province, where no lightning occurred in the nine hour period.
37. POD for CII greater than 10% is 1.0 and decreases slowly (Figure 5.16).
38. POFD starts below 0.2 and diminishes with higher values of CII (Figure 5.16).
39. FAR starts below 0.8 and decreases to less than 0.5 when CII exceeds 60% (Figure 5.16), after which there are not enough values for calculations.
40. HK starts above 0.8, increases slightly and then decreases gradually (Figure 5.16).

CASE 9: 20 February 2009

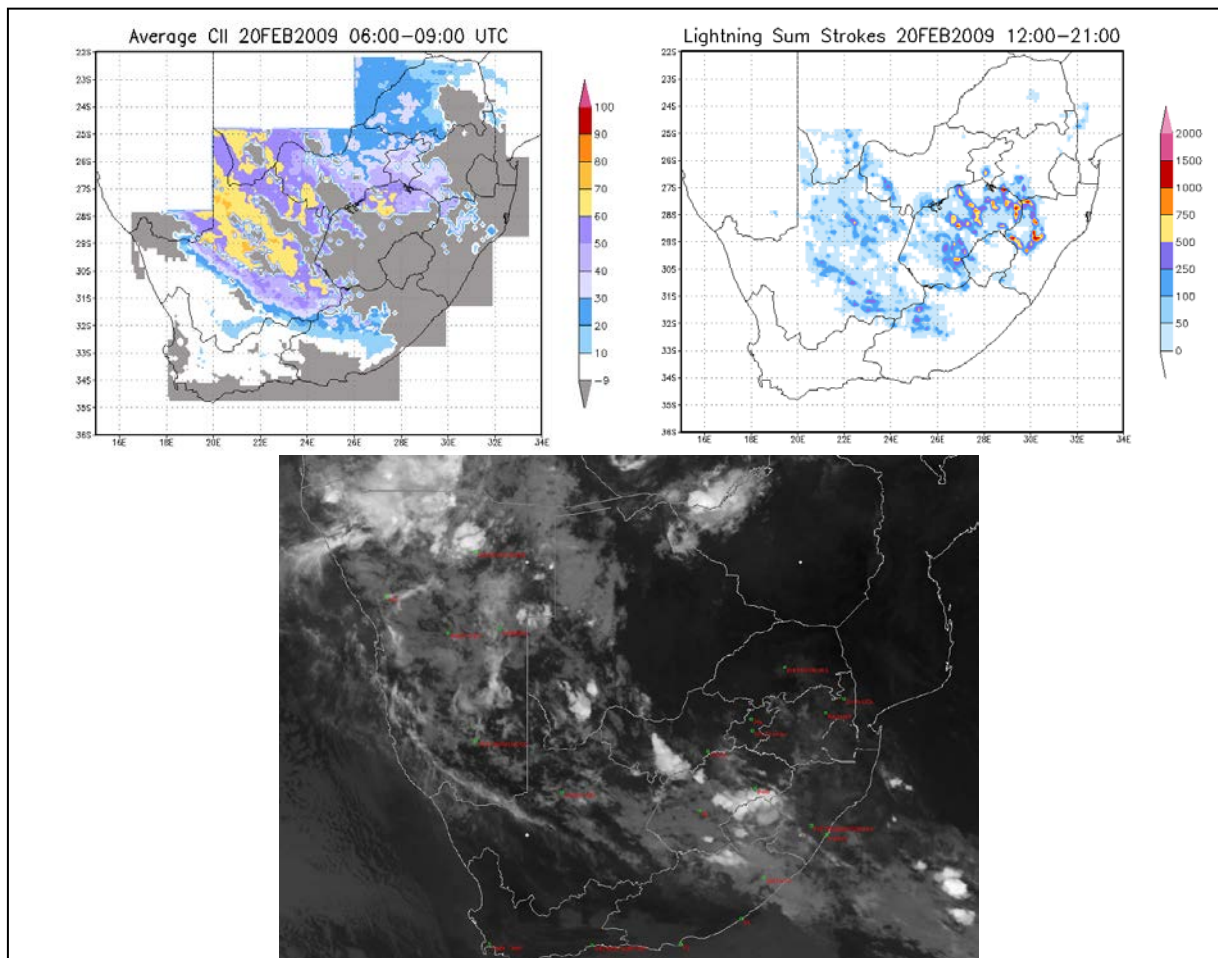


Figure 5.17 CII (top left) and occurrence of lightning (top right). Areas covered by cloud so that CII values are not available are shown in the 0600 UTC IR108 image below and also indicated by the grey areas in the CII graphic for 20 February 2009

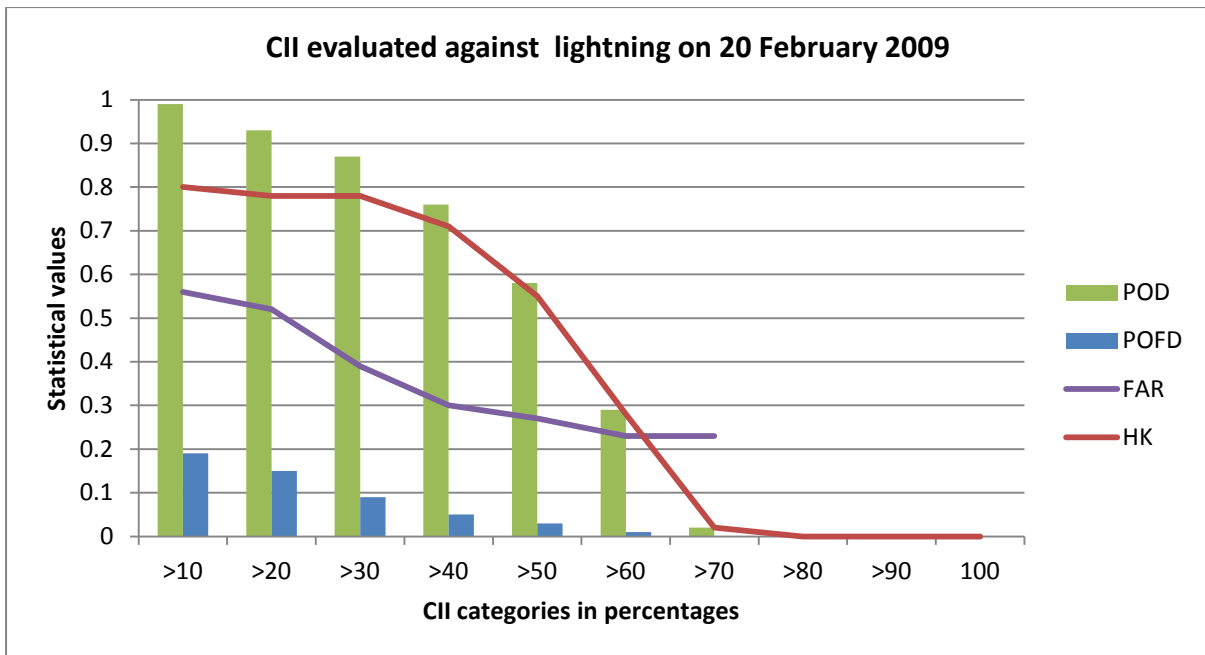


Figure 5.18 CII statistical scores against the occurrence of lightning for 20 February 2009

From Figures 5.17 and 5.18 it can be concluded that:

41. Spatial agreement between the area where the CII was more than 10% in the morning and where lightning occurred later in the day is good, taking the early morning cloud cover into consideration (Figure 5.17). Lower probabilities were forecast for Limpopo where very little lightning occurred in this period. Higher probabilities of the CII (more than 60%) coincided with areas where more lightning strokes occurred over the Free State, Northern Cape and Northwest Province.
42. POD for CII greater than 10% is above 0.9 and decreases slowly (Figure 5.18).
43. POFD starts below 0.2 and diminishes with higher values of CII (Figure 5.18).
44. FAR starts just below 0.6 and decreases to just above 0.2 where CII is more than 70% (Figure 5.18).
45. HK starts just at 0.8 and then decreases gradually (Figure 5.18).

CASE 10: 13 March 2009

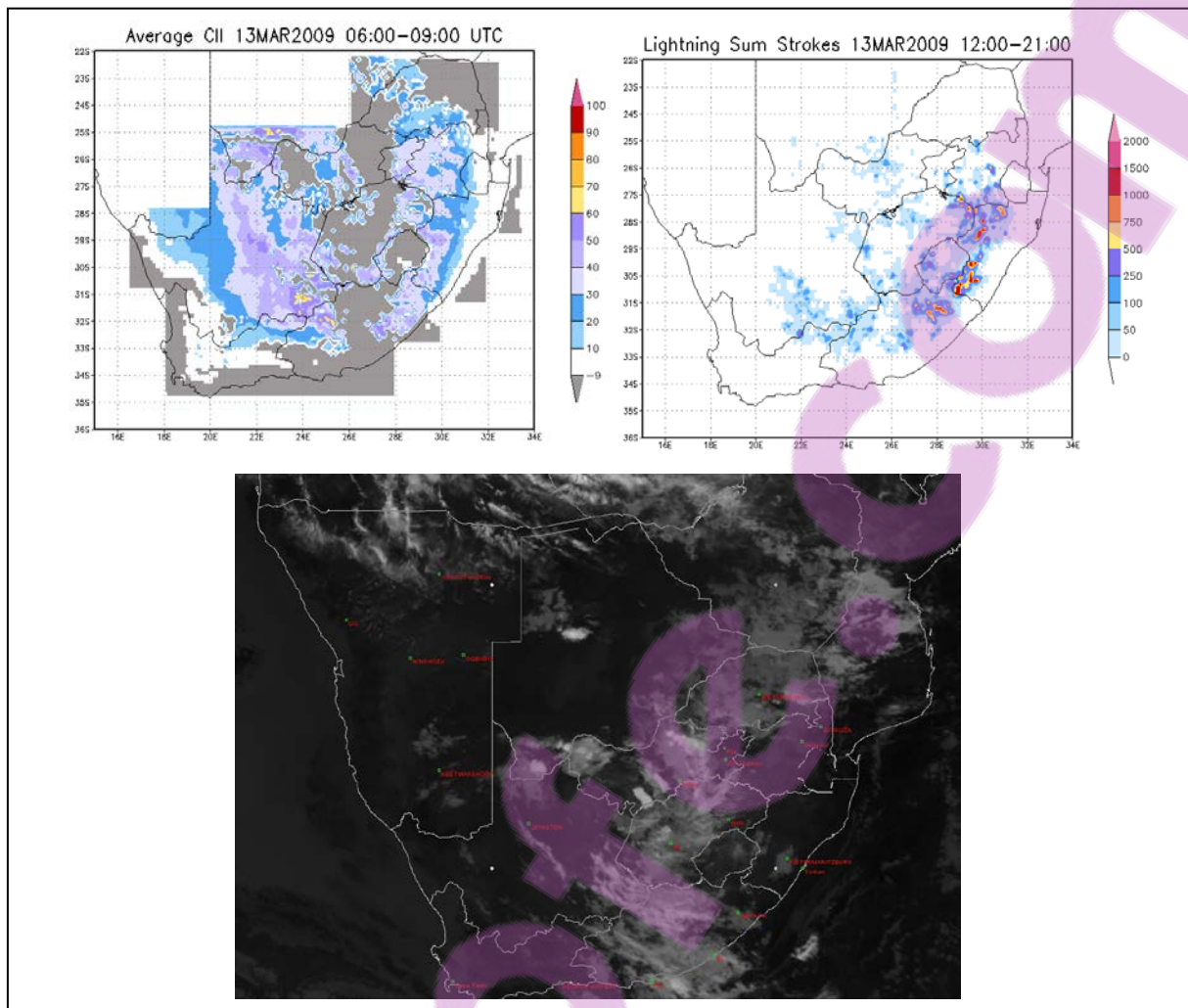


Figure 5.19 CII (top left) and occurrence of lightning (top right). Areas covered by cloud so that CII values are not available are shown in the 0600 UTC IR108 image below and also indicated by the grey areas in the CII graphic for 13 March 2009

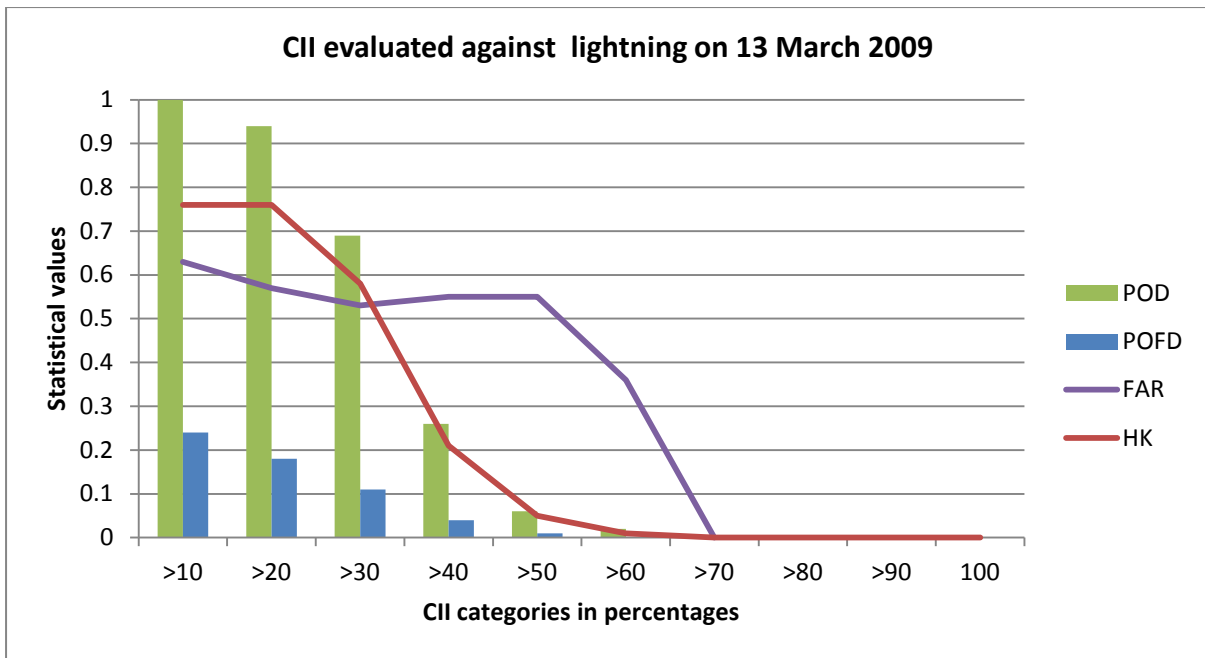


Figure 5.20 CII statistical scores against the occurrence of lightning for 13 March 2009

From Figures 5.19 and 5.20 it can be concluded that:

46. This case evaluates well from a spatial distribution point of view although the Northern Cape did not have as much lightning as the CII would have suggested (Figure 5.19). Good agreement is, however, evident in the Eastern Cape, KwaZulu-Natal and Mpumalanga as well as in the Northwest Province.
47. POD for CII greater than 10% is 1.0 and decreases slowly (Figure 5.20).
48. POFD starts just above 0.2 and diminishes with higher values of CII (Figure 5.20).
49. FAR starts just above 0.6 and decreases. It remains between 0.5 and 0.6 until CII exceeds 50% and then diminishes (Figure 5.20).
50. HK starts below 0.8 and then decreases gradually (Figure 5.20).

### 5.3 CII STATISTICS FOR ALL FIFTY CASES

In summary the statistical evaluation done for all fifty cases is shown in Figure 5.21. It is evident that:

1. POD starts very high when CII is more than 10% and decreases slowly to very small values when CII reaches 70%.
2. POFD starts below 0.2 and decreases with higher values of CII.

3. FAR starts just above 0.6 at CII values of 10%, but decreases to more or less 0.45 when CII is greater than 60%.
4. HK is greater than 0.8 for the first two intervals, and then decreases gradually. The CII has the highest possibility to distinguish between the 'yes' and 'no' events when all the boxes with a probability of more than 10-20% are considered, showing that it is meaningful even for low values.

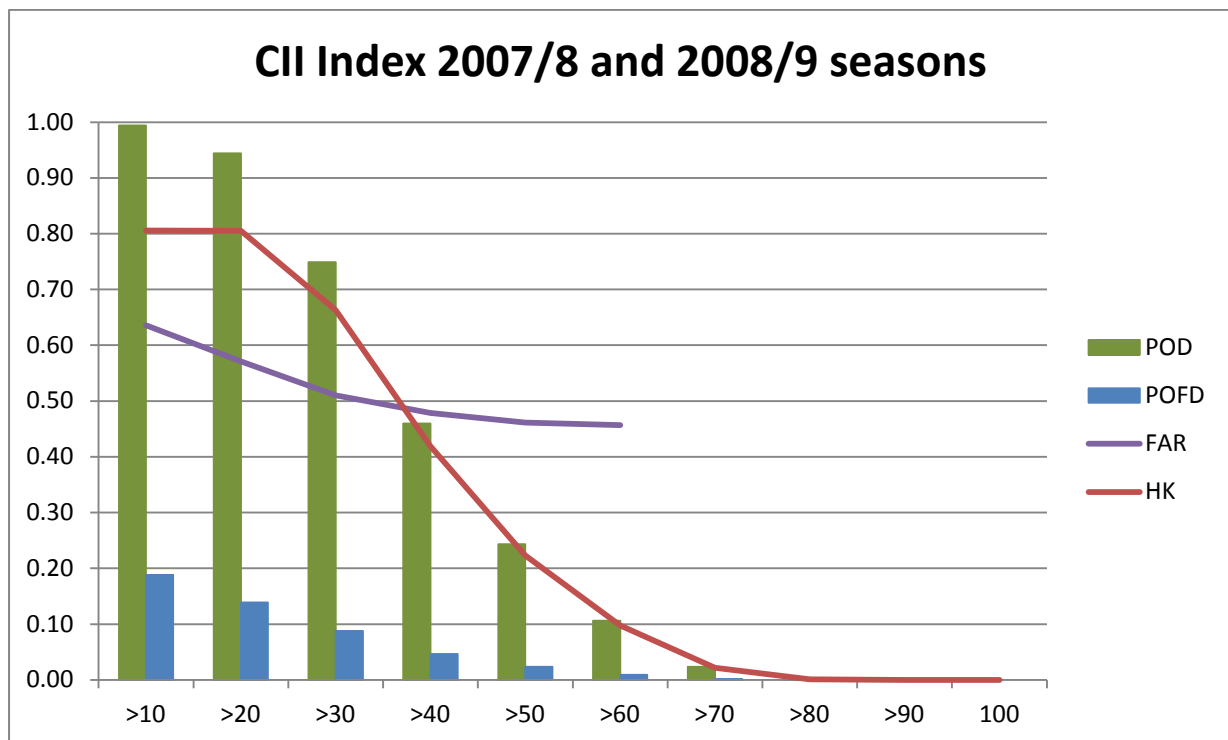


Figure 5.21 Statistical scores for CII for fifty case studies

As shown for the individual RII in Chapter 3, the statistical evaluation of the CII is influenced by the occurrence of clouds early in the morning since convection might already be on the way in those areas while CII cannot be calculated. Spatially, the area where CII is more than 10% is usually in good agreement with the area where lightning occurred later the same day. There were areas where lower probabilities of CII were given where no lightning occurred in the nine hour period after 1200 UTC, which accounts for the higher FAR. Often the higher probabilities of CII coincided with the areas where higher amounts of lightning occurred, which is very good. One should bear in mind that lightning also occurs before 1200 UTC and after 2100 UTC, although the bulk of the lightning occurs inside this nine hour period. The fact that the statistics are still so good is consequently very encouraging. Forecasters have the greatest difficulty to determine where convection will occur when skies are clear early in the morning. Currently they use the instability indicators from the upper air soundings. These are only available at midnight and midday at less than ten weather stations around the country. Similarly, to the upper air sounding data, the CII offers a vertical profile of the atmosphere

based on the MSG imagery and model input. The CII improves the spatial and temporal coverage of these types of indicators considerably and thus aids the forecasters in their early morning decision making process. Once clouds are present, the MSG RGB combination imagery as well as radar images can be utilized to determine the nature of the clouds and whether there will be convection or not.

## 5.4 CII PERFORMANCE COMPARED TO THE PERFORMANCE OF THE INDIVIDUAL RII

The final test was to see whether the CII performs better than the individual RII. Like an “ensemble” principle it is hypothesized that the combined product will outperform the individual products. In order to evaluate the CII against the individual RII, it was necessary to compare the various statistical scores for the four RII and the CII separately. The CII ranges from 0% to 100% and the RII ranges used thus far in the study are:

1. 10 mm to 45 mm for Precipitable Water,
2. +2°C to -12°C for Lifted Index,
3. 35°C to 58°C for Mixed Total Totals and
4. 15°C to 45°C for Mixed K Index.

It was necessary to normalize all of the ranges for all the indices to ensure that the values fall between 0 and 1. Judging by the *meaningful* values listed in Chapter 2 (Tables 2.2, 2.3, 2.4 and 2.5) as per the definitions of the indices from literature sources, the following were seen as the *meaningful ranges* with a chance for thunderstorm development for each index:

1. Precipitable Water: 13 to 31 mm (low moisture content),
2. Lifted Index: -1° to -4° (marginal instability),
3. Total Totals: 44° to 50° (thunderstorms likely) and
4. K Index: 15° to 25° (small convective potential).

Taking the cumulative frequency graphs (Figures 4.1, 4.2, 4.3 and 4.4 from Chapter 4) into consideration, it can be seen that more than 80% of the lightning in South Africa occurs for Lifted Index values less than -2°C, Precipitable Water values more than 21mm, Mixed Total Totals values more than 46°C and Mixed K Index values more than 28°C. The values listed in Tables 2.2 to 2.5 and Table 5.1 are in similar ranges, with the advantage that Table 5.1 lists the *meaningful values for South African conditions*, based on the fifty cases during the summers of 2007/8 and 2008/9. The

upper threshold was taken as the value of the respective RII where the HK was less than 0.01, i.e. no skill was shown at values higher than that. The lower and upper thresholds for each RII for the purpose of the normalized scale were as listed in Table 5.2.

**Table 5.1 Threshold values for each RII corresponding to more than 80% of lightning (from Chapter 4)**

RII	During the two summer seasons more than 80% of the lightning in South Africa occurred at a value of:
Lifted Index	<- 2°C
Mixed K Index	>28°C
Mixed Total Totals	>46°C
Precipitable Water	>21 mm

**Table 5.2 Lower and upper threshold values for each RII on the normalized scale**

RII	Lower threshold corresponding to 0	Upper threshold corresponding to 1
Precipitable Water	21 mm	46 mm
Lifted Index	-2°C	-9°C
Mixed Total Totals	46°C	58°C
Mixed K Index	28°C	45°C
CII	10%	100%

Figures 5.22 to 5.26 show the individual scores for each of the parameters. Figure 5.22 shows the POD for all fifty case studies for all the indices. The POD for all the indices starts above 0.7. The POD for Mixed K Index seems to be better than for the other indices, but still not as good as the POD for CII. When CII is greater than 0.6, its POD is less than the POD for all the individual parameters, but at that point the POD is less than 0.1 for all indices. The POD for CII, however, is higher than most of the

RII until 0.5, after which of the POD of individual RII are higher, but at that point the POD is around 10%.

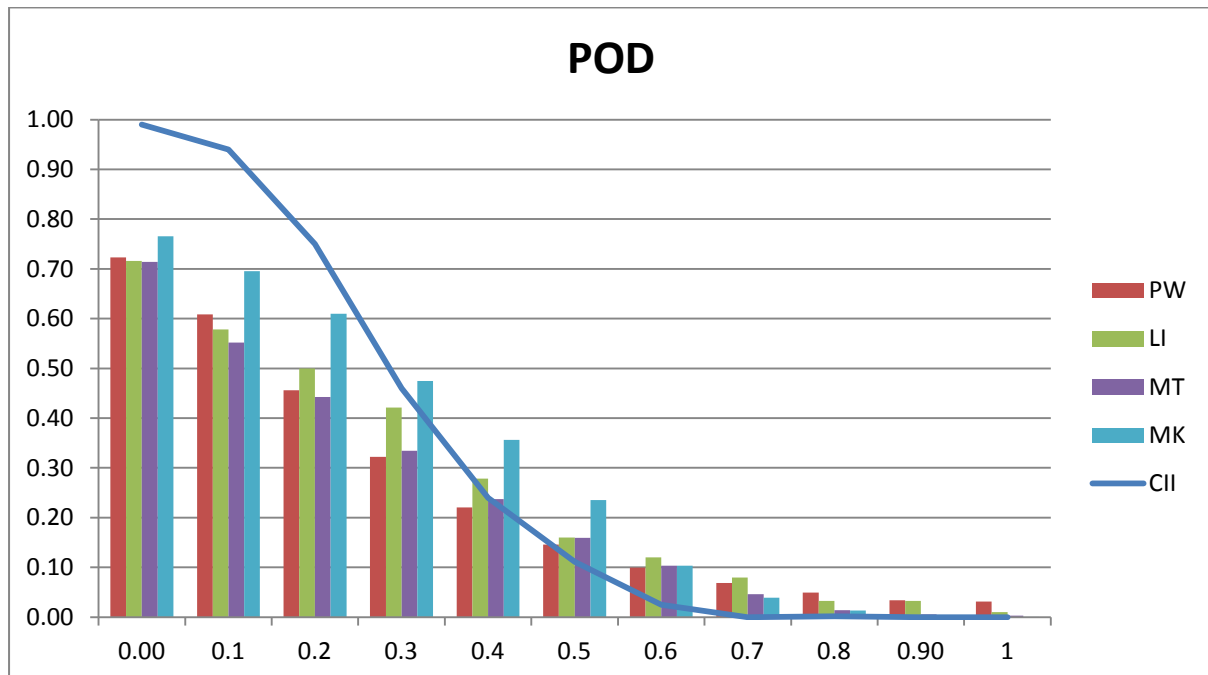


Figure 5.22 POD for the RII and CII

The POFD for all the indices is shown in Figure 5.23. All the indices have low values for POFD, starting at less than 20% and decreasing. The CII POFD is the highest at 0 where CII equals 10% but still less than 0.2, and diminishes to a lower value than the other indices at 0.4.

Most of the values for FAR start between 0.5 and 0.6 and then decrease (Figure 5.24), but remain above 0.5. The only exception is PW, which starts close to 0.7 and increases to 0.8. This tendency was also seen and noted in Chapter 3. The FAR for CII starts just above 0.6 at 0 and diminishes to 0.45 at 0.5 where CII equals 55%. This is lower than the FAR for all the other indices.

The HK (Figure 5.25) starts off well for all the indices, with Mixed K Index again being the highest of the four RII (just above 0.6). The HK for CII is, however, well above the values of all the other RII, starting at just above 0.8. The HK of the CII remains better than all the individual indices with a value of HK above 0.4. However, at values higher than 0.3 the Mixed K Index slightly outperforms the CII. At 0.6 the CII is outperformed by all the individual indices when the HK is around 0.1

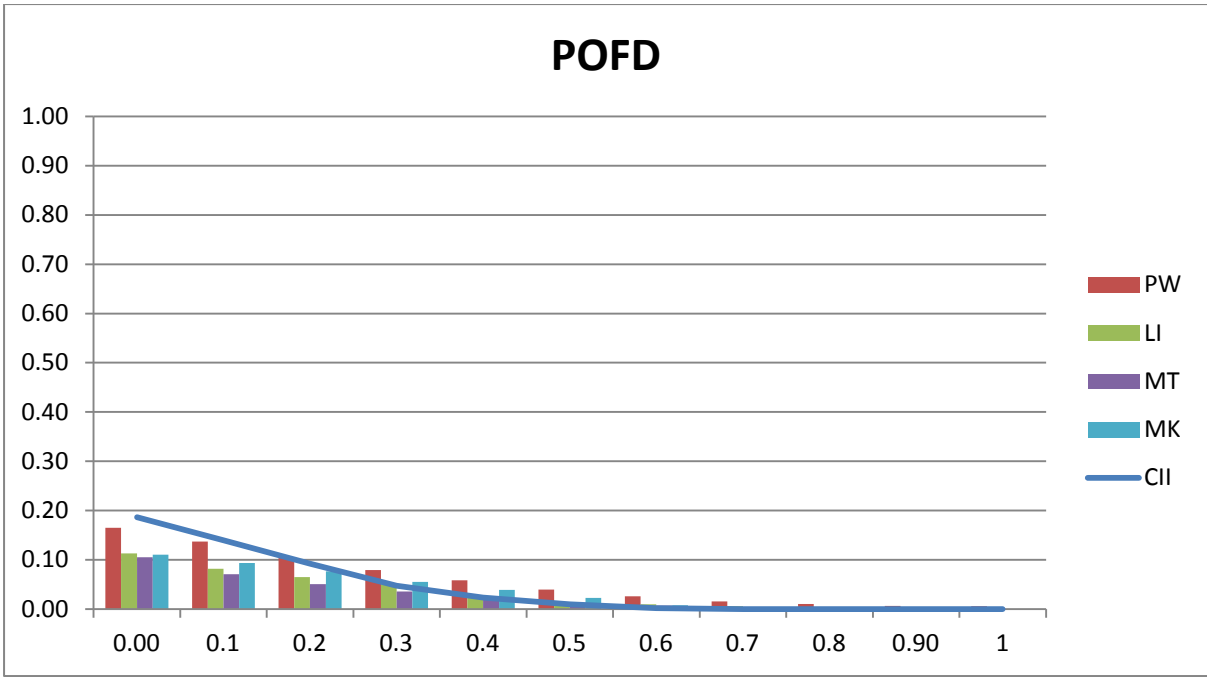


Figure 5.23 POFD for the RII and CII

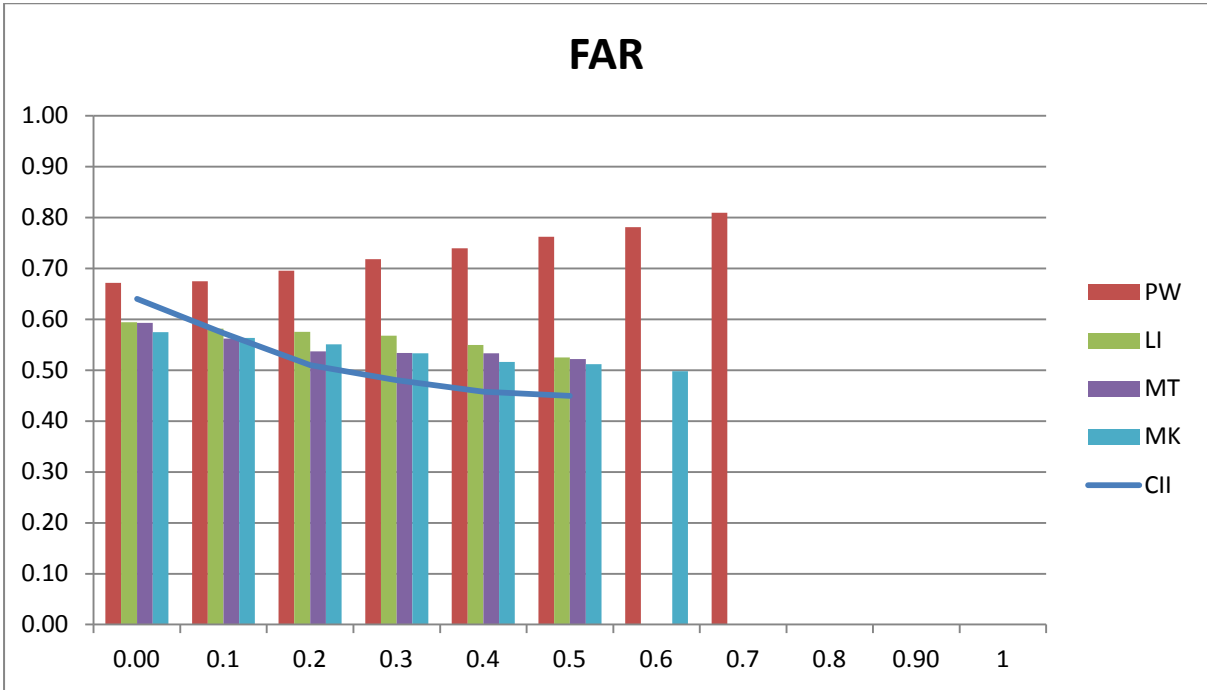


Figure 5.24 FAR for the RII and CII

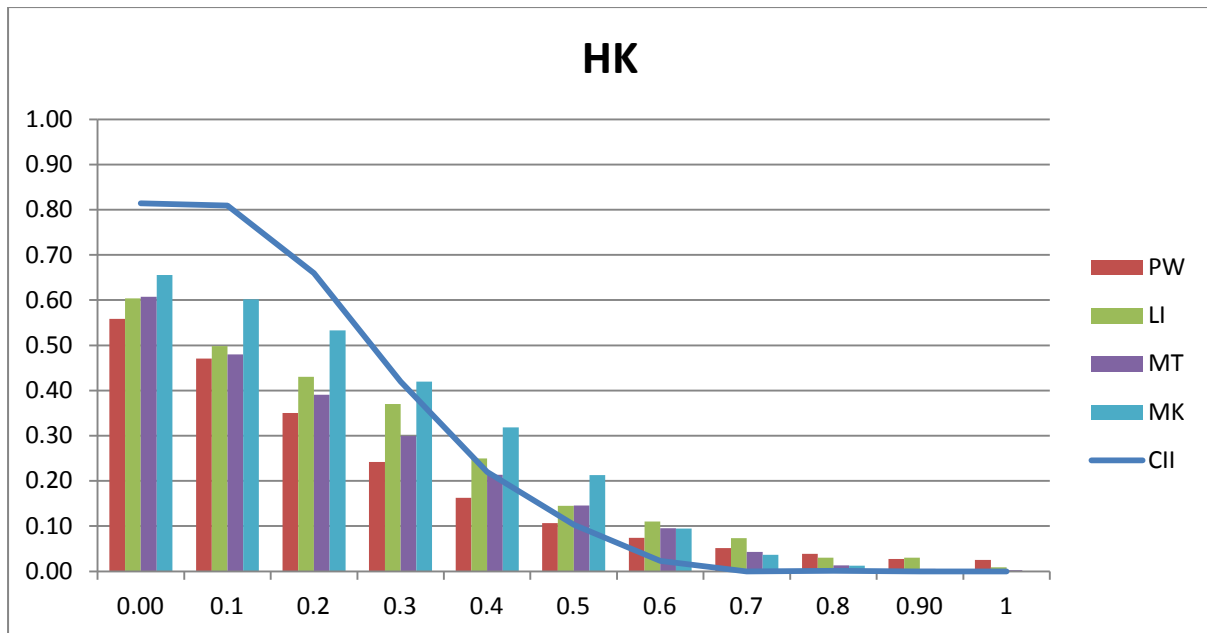


Figure 5.25 Hanssen-Kuipers discriminant for the RII and CII

It can be concluded that the CII is not only in good visual agreement with the area where lightning occurs later in the day, but also evaluates well statistically and outperforms the scores of the individual indices for the fifty test cases. If the area where CII is more than 10 to 20% is considered (0 - 0.1 on the normalized scale), CII performs better than all the indices. It is only at the higher values where the individual RII might outperform the CII but then the area to consider is small. The combination of indices thus evaluates better than the individual indices for a large proportion of the cases, reminiscent of an “ensemble” principle. The CII should thus be beneficial for operational forecasters in anticipating convection in the early morning hours when skies are clear and a decision on convective activity has to be made.

## 5.5 SUMMARY

In this chapter a quantitative evaluation of the CII was shown for ten cases, as well as in general for all fifty test cases. The same method and statistical scores were used as before, based on a contingency table approach. Based on the statistics, CII performs well and when the area with a probability of more than 10-20% is considered, the CII has the best ability to anticipate convective activity (this is where the HK is at its highest). The CII also outperforms the individual RII for most meaningful values. The newly developed index should thus be beneficial to operational forecasters in focussing their attention on the correct area for the development of convection, taking instability and moisture as well a height above sea level into account in early morning cloud free conditions.

In Chapter 6 a final comparison will be made between the CII and the occurrence of precipitation. For the purpose of this type of evaluation, rain gauges and convective precipitation fields from the Unified

Model as well as the NOAA/NESDIS HE will be used to indicate whether the CII could also have value for countries outside South Africa.

# CHAPTER 6 EVALUATION OF CII AGAINST PRECIPITATION ESTIMATES

---

## 6.1 BACKGROUND

A new indicator for convection was developed and evaluated over fifty cases during the summer seasons of 2007/8 and 2008/9. In the previous chapter this new index (the Combined Instability Index, CII) was evaluated against the occurrence of lightning through a contingency table approach. Not only did the CII prove to have good evaluation statistics, but it also outperformed the individual RII (Chapter 5, paragraph 5.3). Another way of verifying the CII would be against the occurrence of precipitation, either measured or estimated, to assess whether the convection did indeed materialize. If successful, this method would be especially useful over areas such as southern Africa outside South Africa where there might not be a lightning detection network available.

The question is then posed: how is convective precipitation measured? Measuring precipitation is one of the most difficult observational challenges of meteorology as a result of the high variability with geography and time. Although rain gauges provide a direct measurement of rainfall, rain gauge networks are far too coarse to capture all the rainfall, especially at smaller scales. Rain gauges are unevenly distributed and, most importantly, they provide point source data and not a representation of a spatial domain (Kondragunta, 2007). Radars can be used to provide an indirect measurement of rainfall, but then the radars need to cover the entire area of interest, be well correlated and have a good radar rainfall relationship. Outside South Africa radars are a scarce commodity and thus not a feasible option for this purpose. Three other factors which complicate the use of radar rainfall fields are:

1. Radars only work well for precipitation measurement close to the radar unit,
2. In mountainous regions effective radar coverage is poor as a consequence of beam blockage and
3. Accuracy in radar rainfall is also influenced by bright band effects (Centre for Satellite Applications and Research website: <http://www.star.nesdis.noaa.gov/smcd/emb/ff/index.php>).

Although satellite based estimates of rainfall are not as accurate as gauges of radar, its major advantage is the high spatial resolution and coverage, even over oceans, in mountainous regions and sparsely populated areas where rainfall is not measured. Thunderstorms and flash floods often start and move in between gauges and other surface based networks and thus cannot be detected properly. In such cases satellite-derived rainfall can be a “critical tool for identifying hazards from smaller-scale rainfall and flood events.” (STAR Satellite Rainfall estimates, <http://www.star.nesdis.noaa.gov/smcd/emb/ff/index.php>).

In this chapter data from the satellite and model based hydroestimator (HE) operational in South Africa as well as gauges from the South African rain gauge network are used to verify the CII. Although the HE cannot be considered the “ultimate truth” in terms of precipitation measurement, it can be used to advantage at least in the quantitative testing of the performance of CII in forecasting convection over the entire southern African region where no other measure of precipitation exists, aside from very coarsely spaced rain gauges.

## 6.2 SOUTH AFRICAN RAIN GAUGE NETWORK

The SAWS observation network is indicated in Figure 6.1 and the rain gauge network in Figure 6.2. Rainfall is measured by about 1500 rain gauges for 24 hour periods from 0600 to 0600 UTC, and they are then listed as the day total in climatological records.

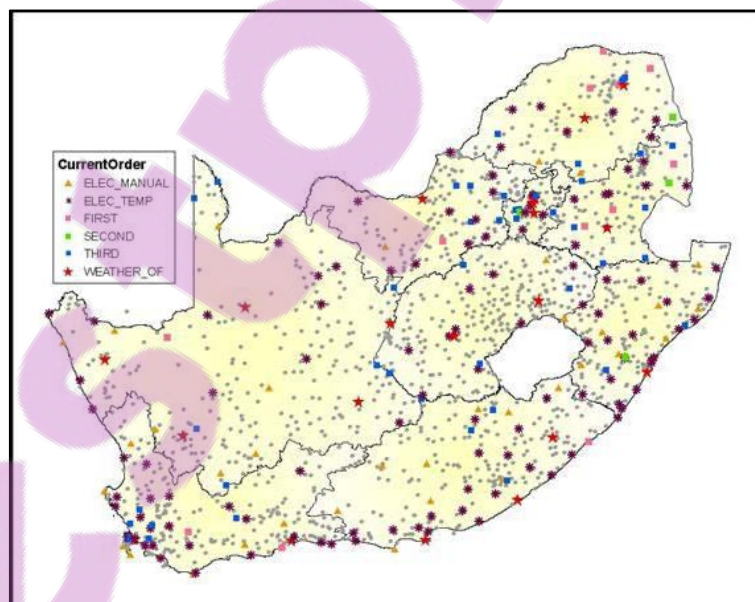


Figure 6.1 Climatological observation stations in South Africa

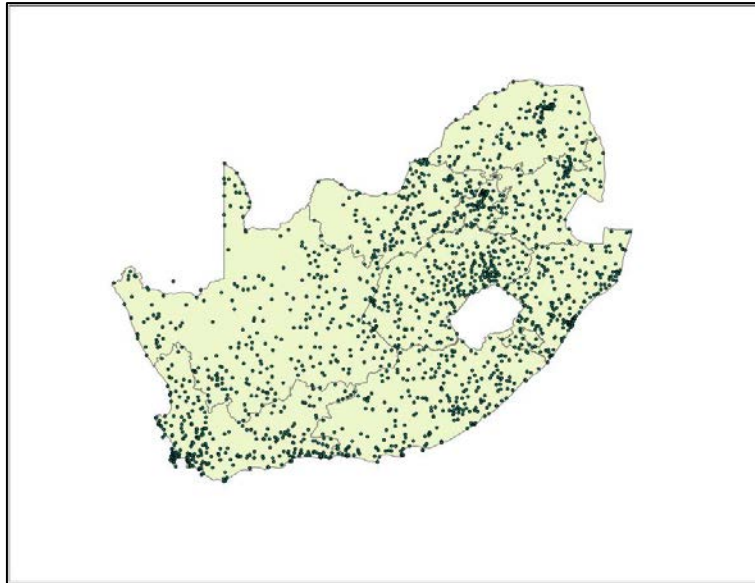


Figure 6.2 Rainfall stations in South Africa

### 6.3 HYDROESTIMATOR (HE)

As mentioned in Chapter 1, the HE is independent of radar and thus a very useful tool over areas of the southern African region where there are no radars. The HE is mainly dependent on temperature (the higher the cloud, the colder the temperature and the greater the rain rate). Scofield and Kuligowski (2003) described the following new features in the HE:

1. The definition of a “raining pixel” was adjusted to include only those pixels with an IR10.8 brightness temperature below the average value of the surrounding region. In this way the overestimation of rain area seen in the Autoestimator (AE) has been significantly reduced.
2. The rain rate curve used for the AE was adjusted according to the difference between the brightness temperature of the pixel and that of the pixels in the surrounding area. The highest rain rates are given to the pixels that are the coldest relative to their surroundings.
3. The dependence on Precipitable Water (PW) and Relative Humidity (RH) has been separated. PW was used to adjust the rain rate curve (higher PW means higher rain rate). RH was used to determine an amount which has to be subtracted from the calculated rain rate (drier low levels suggest rain will evaporate, i.e. the rain rate will be lowered). These adjustments have been beneficial in the handling of stratiform rain events with embedded convection as well as wintertime precipitation associated with lower PW.

More extensive information on the techniques used for the HE and recent improvements is available on the Centre for Satellite Applications and Research website (<http://www.star.nesdis.noaa.gov/smcd/emb/ff/HEtechnique.php>).

In general, experience and validation studies (Kuligowski *et al.*, 2001) have shown the following tendencies in the behaviour of infrared based Satellite Precipitation Estimates (SPE):

1. SPE tend to overestimate rainfall intensity and spatial coverage of the storm when it is slow moving and has a cold top.
2. SPE tend to underestimate rainfall from warm topped mesoscale convective systems.
3. SPE are less accurate spatially in regions of strong vertical wind shear.
4. SPE do not handle rain bursts early in the life cycle of mesoscale convective systems well.

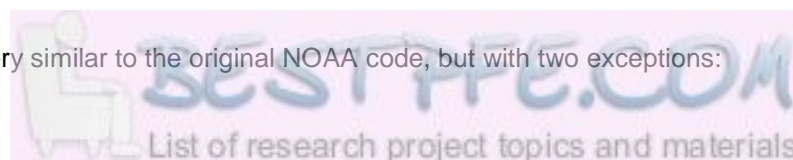
Comments by analysts at the NESDIS Satellite Analysis Branch (SAB) who work with the HE on an operational, real time basis (Kuligowski, 2009, personal communication) include:

1. The HE works best for convective events.
2. Stratiform events might be over/underestimated.
3. Very cold tops with significant Cirrus debris might be overestimated.
4. Warm cloud tops are often underestimated.
5. Rainfall totals over 1 to 6 hours should be most reliable, while 24 hour totals might be too high.

A local version of the HE has been running in South Africa since September 2007 and has been available to operational forecasters since then. Basic principles of the local HE include:

1. Input files consist of the IR10.8 channel brightness temperatures of the MSG satellite and model output fields of the SAWS local version of the Unified Model, including:
  1. Profiles of the temperature and humidity on 19 levels, from 1000 to 100 hPa, every 50 hPa,
  2. Surface pressure and
  3. 700 hPa wind field.
2. Before the actual HE code is run, parallax and zenith angle corrections are made. The parallax correction helps to position the rainfall cores more accurately, which plays an important role in smaller scale storms (Vicente *et al.*, 2002).
3. The HE is available in the same domain as the local version of the Unified model (i.e. between 0.48°N and 44°S and between 10°W and 56°E).

Most of the code is very similar to the original NOAA code, but with two exceptions:



a) Cloud top minimum temperature, which is fixed at to 213 K in the original code, is replaced by the tropopause temperature, taken from the given profile.

b) For the box averages, minima and standard deviations, the final rain rate is calculated only from the larger box (100X100 pixels), which was found to give somewhat smoother fields (Koenig, 2007).

Despite the simplicity of this precipitation estimation algorithm, it is still used in many countries around the world. There are, of course, more accurate and also more profound and involved precipitation algorithms available, but these algorithms are not available or operational in South Africa yet.

### **6.3.1 HE evaluated as part of the IPWG programme**

The International Precipitation Working Group (IPWG) is one of the working groups of the Coordination Group for Meteorological Satellites (CGMS). The work done in this group concentrates on “operational and research satellite based quantitative precipitation measurement issues and challenges” (<http://www.isac.cnr.it/~ipwg>).

Figure 6.3 shows an example from the IPWG website on the performance of the HE against rain gauges and radar rainfall. From the statistical evaluation performed on the data it is clear that the HE performs very well (a correlation between the HE and the rain gauges of more than 0.7 in this example). In South Africa similar studies have only just started, but has only been done for a small number of cases. It seems that similar trends exist, but extensive research in this regard is still ongoing. It is expected that the HE will perform better over the southern Africa region as soon as it has been tuned to local conditions. A bias-correction of the HE seemed appropriate and this forms part of research work currently done in South Africa (de Coning and Poolman, 2010). The HE is the only operational precipitation estimator available in southern Africa and is thus the only tool to use when a comparison with CII forecasts needs to be performed.

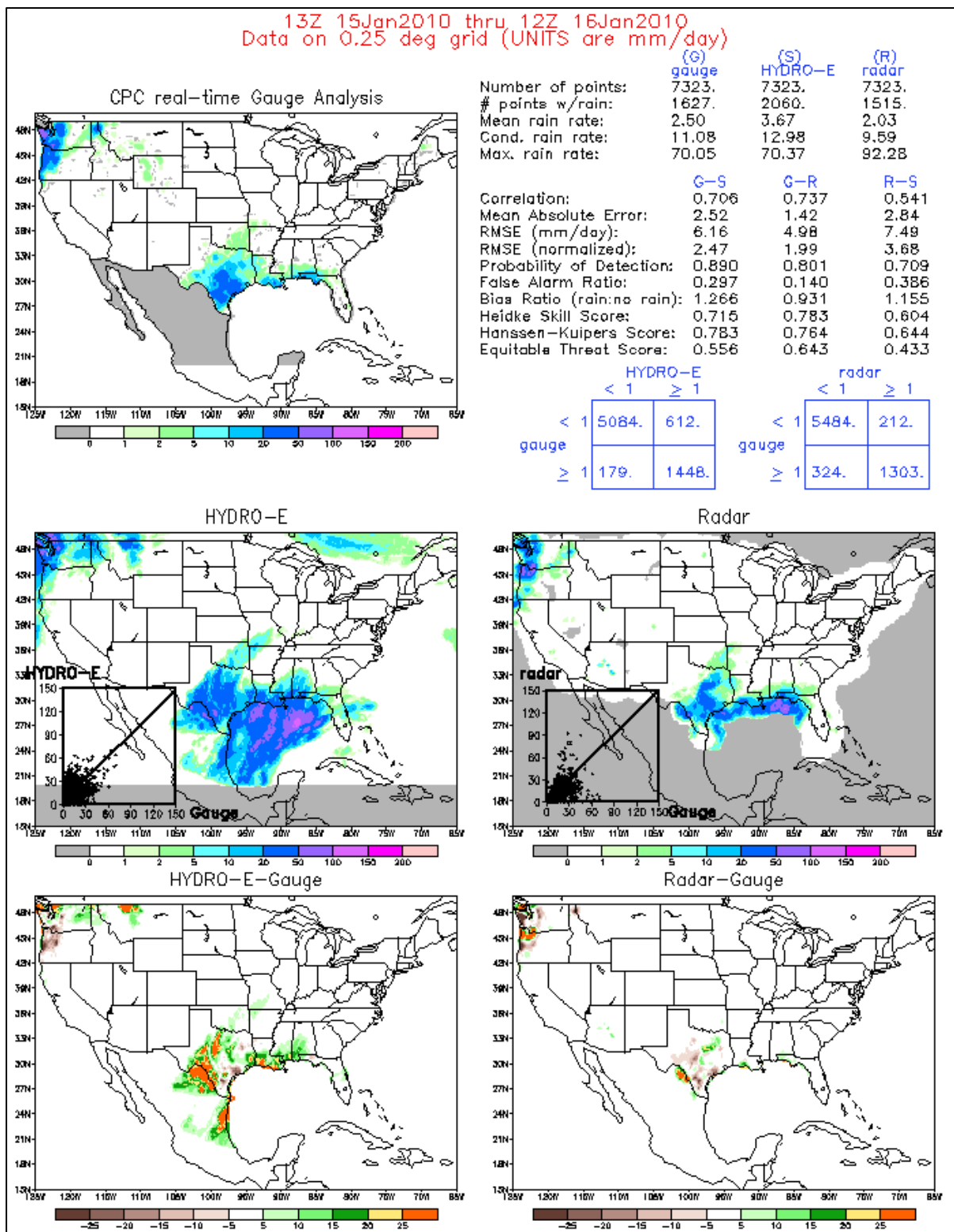


Figure 6.3 Example of IPWG evaluation of the Hydroestimator used in Northern America, from:

<http://cics.umd.edu/~johnj/us/gifs/hydroe+radar.20100110.gif>

### 6.3.2 Examples of 24 hour rain gauge totals versus 24 hour HE totals

In this section the 24 hour rain gauge totals will be compared to the 24 hour totals from the HE. Only rain gauges from South Africa are available and therefore the domain for comparison is confined to the areas within the border of South Africa. A factor to bear in mind is that the HE tends to overestimate 24 hour totals, as mentioned earlier in this chapter. Two examples will be shown to demonstrate the principles of this kind of comparison.

*EXAMPLE 1: 18 October 2008*

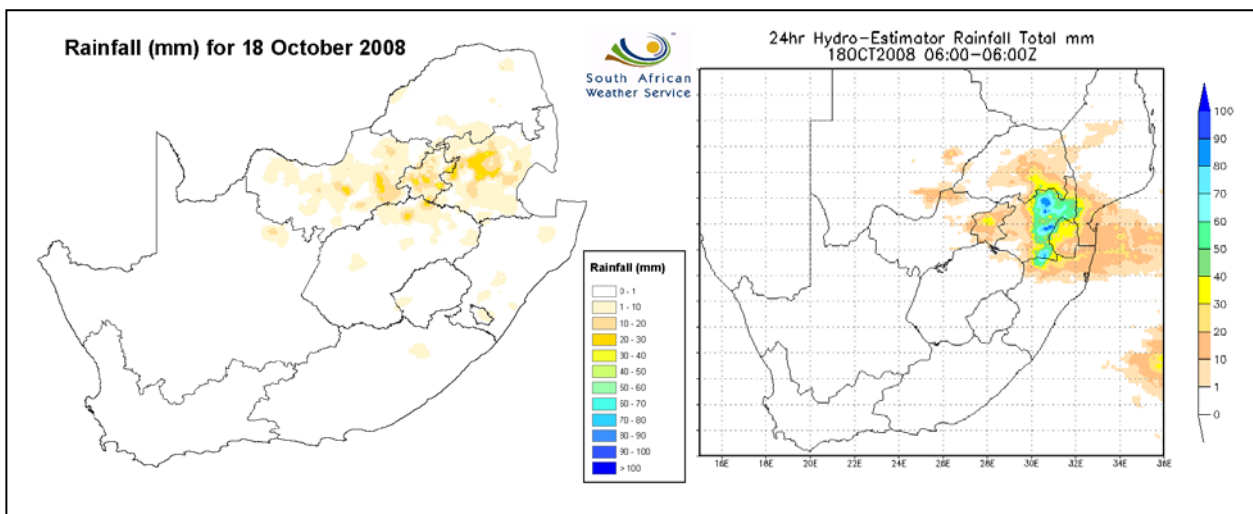


Figure 6.4 Rainfall totals over 24 hours from rain gauges (left) and HE (right) for 18 October 2008

The rain gauge totals for this day (left in Figure 6.4) show the rainfall mainly over the North West, Gauteng and Mpumalanga provinces. Amounts do not exceed 20 to 30 mm (light orange). The HE (Figure 6.4, right) shows less rain over North West, similar amounts of rain over Gauteng and totals reaching more than 70 mm in Mpumalanga. There is also an indication of more than 30 mm in the southern part of Limpopo which is not reflected by the gauge data. The amounts of rainfall given by the HE are generally too high.

In the second example the rain gauge totals (Figure 6.5, left) show widespread rain, except in the Northern Cape. The highest totals were recorded in the South Western Cape, on the east coast, in the northern parts of KwaZulu-Natal and Limpopo province. Spatially, the HE looks similar (Figure 6.4, right), but the rainfall in the southern Free State was not detected by the HE. The HE put the highest emphasis in the Limpopo Province, with rainfall totals close to 100 mm. The higher gauge totals in the Southwestern Cape and on the coast of KwaZulu-Natal were not reflected by the HE.

## EXAMPLE 2: 12 November 2008

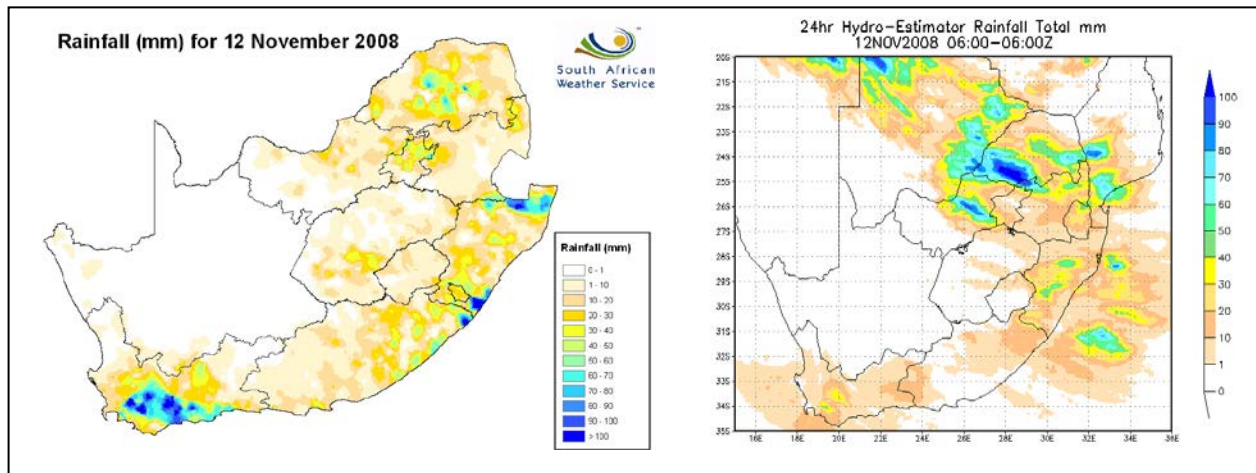


Figure 6.5 Rainfall totals over 24 hours from rain gauges (left) and HE (right) for 12 November 2008

From these examples it should be clear that the HE differs substantially from the rain gauge totals when using a 24 hour accumulation. Although the spatial distribution is in fair agreement, there are also areas where rain was reported and the HE did not show any rainfall. The HE often overestimates the amount of rain. The HE performs best for convective events and consequently stratiform rainfall is not always detected by the HE. This might explain some of the discrepancies in these examples.

## 6.4 COMPARING THE CII WITH THE HYDROESTIMATOR RAINFALL

In an effort to show that the CII might also have a role in countries other than South Africa, it was decided to compare the CII with the HE rainfall since, firstly, other southern African countries do not have lightning detection networks for comparison with the CII and, secondly, the HE is available and operational in southern Africa.

For the sake of uniformity the same nine hour period used for the lightning data was used for the HE estimates against which to evaluate the three hourly CII time averages. It has to be kept in mind that the CII cannot be calculated in cloudy areas, and thus rainfall and/or lightning can occur where the CII has no values to be used for a comparison. This is a disadvantage when comparing the CII to any observation field.

Figure 6.6 shows that the CII favoured an area surrounding Gauteng and Northwest Province. Although lightning occurred over a very similar region, rainfall as detected by the HE was shifted to a region further east. Evaluation statistics for this day, using the contingency table approach for rainfall of more than 1 mm are shown in Figure 6.7.

It is clear that, despite the high POD, the POFD is equally high and thus the HK is very low. The FAR starts low, but increases after CII reaches values of 50%. Although the FAR is low, the ability of the CII to distinguish between the rain and no rain events, evidenced by the low HK, is not good. The evaluation statistics for CII versus occurrence of lightning are much better (Figure 6.8).

*EXAMPLE 1: 18 October 2008*

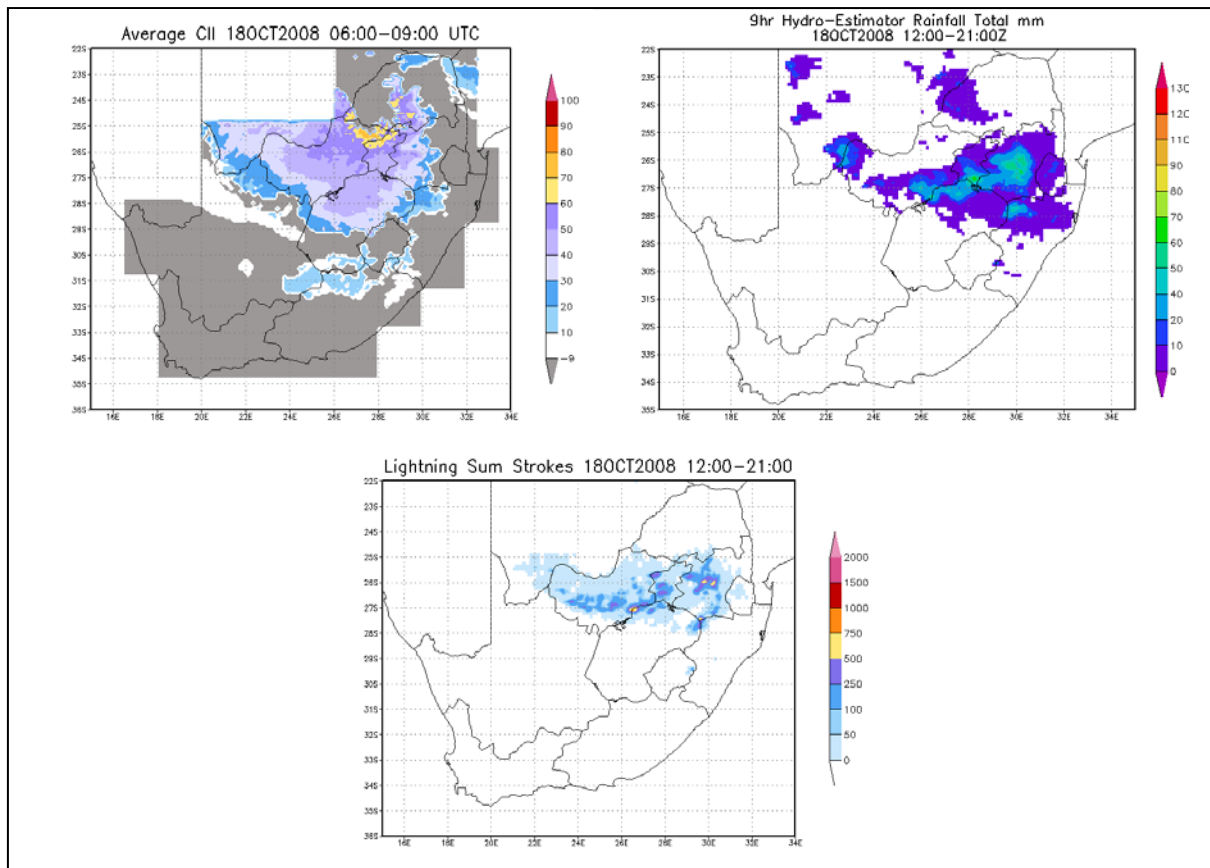


Figure 6.6 CII (top left), HE nine hour total (top right), sum of lightning strokes for nine hours (bottom) for 18 October 2008

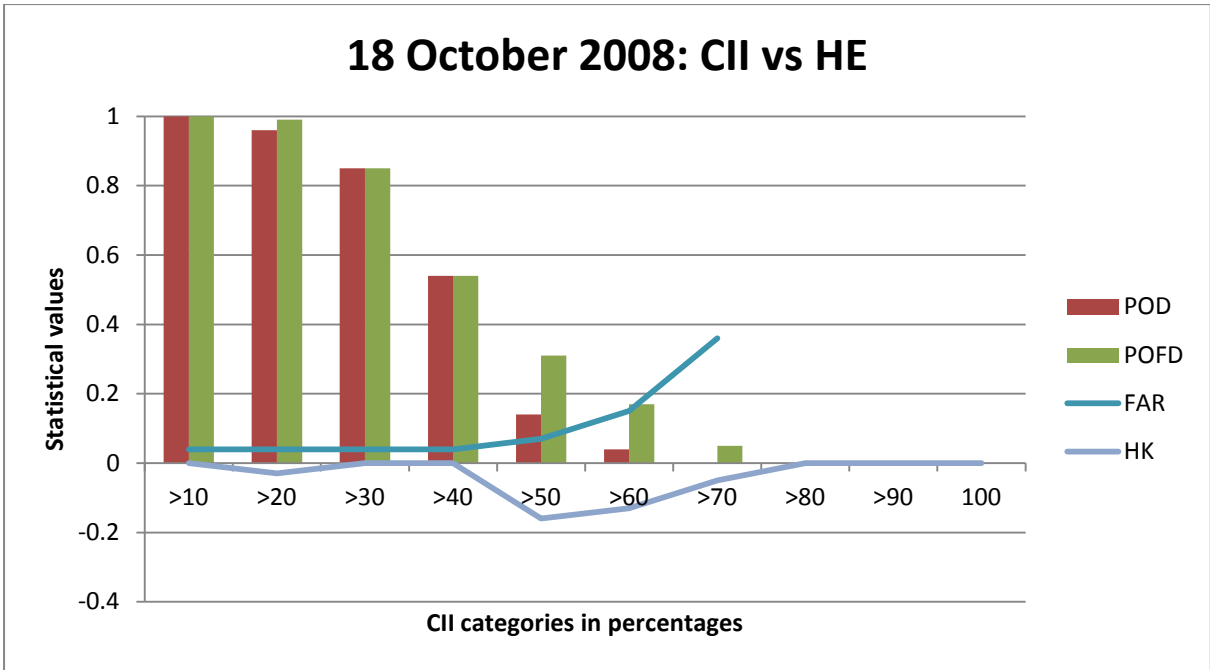


Figure 6.7 Statistical scores of CII versus HE for 18 October 2008

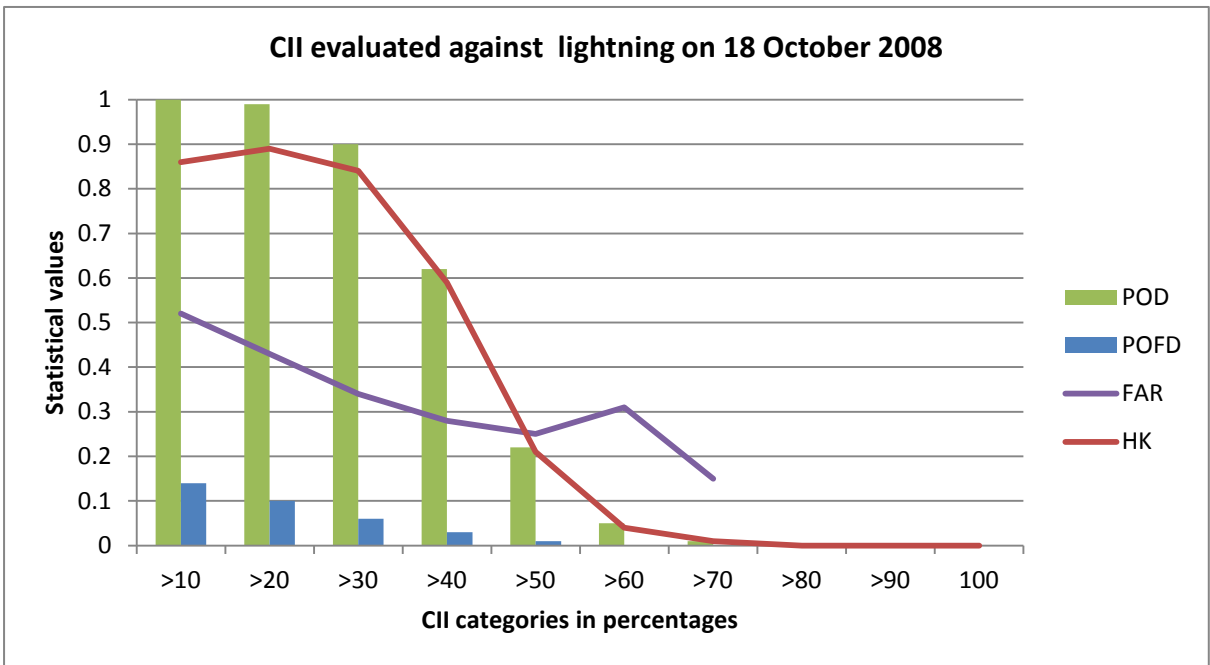


Figure 6.8 Statistical scores of CII versus lightning for 18 October 2008

EXAMPLE 2: 12 November 2008

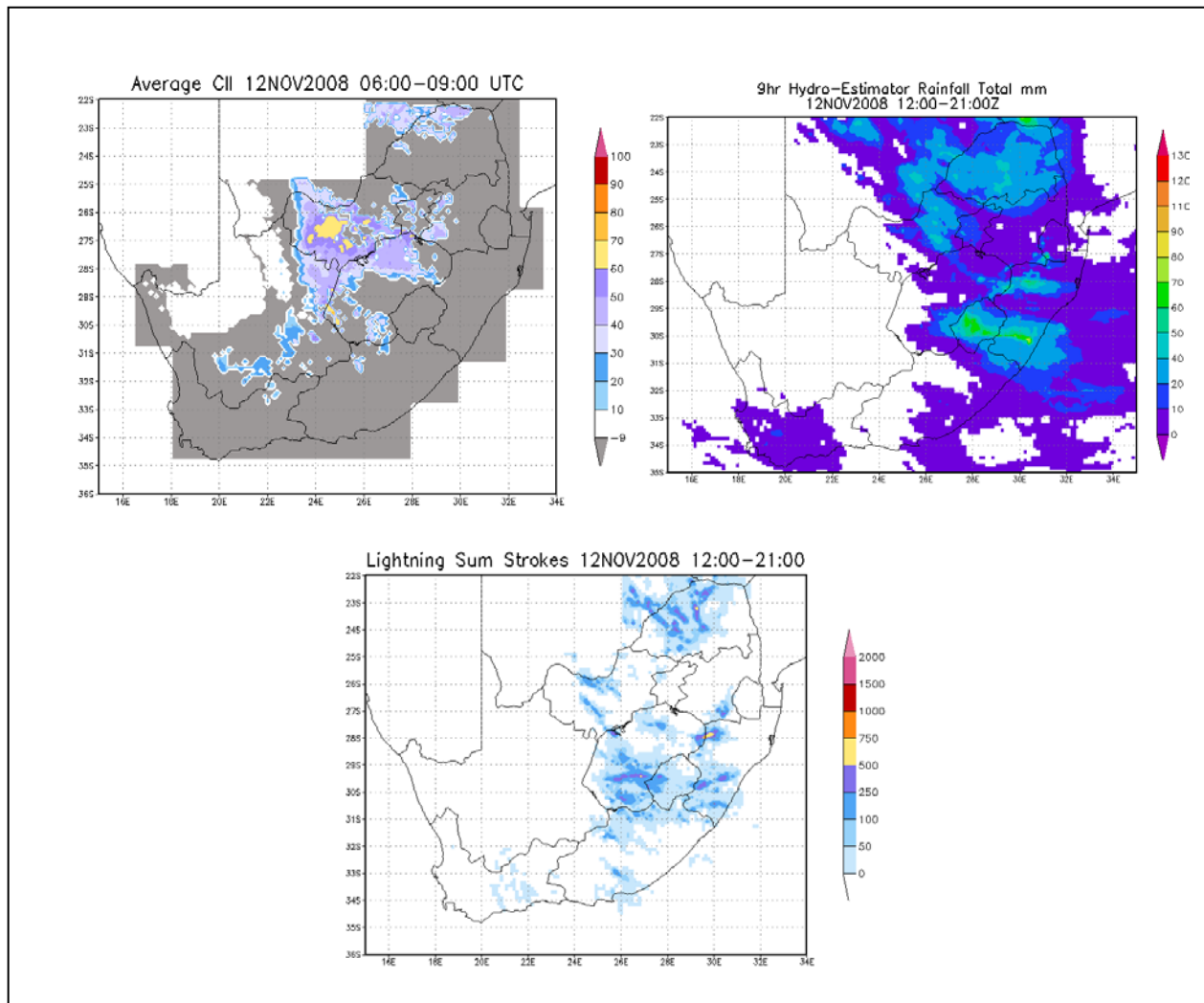


Figure 6.9 CII (top left), HE nine hour total (top right), sum of lightning strokes for nine hours (bottom) for 12 November 2008

Figure 6.9 shows that the CII gave the biggest chance (greater than 50%) for convection over the Northwest Province (Figure 6.11, top left). According to the HE (top right) some rain fell in that area, but the high amounts were further northwards, eastwards and southeastwards in the areas which were already covered by cloud early in the morning. Lightning occurred over the eastern half of the country (bottom), with high amounts over the southern Free State, KwaZulu-Natal and Limpopo Province (where CII could not be calculated due to cloud cover). The CII (top left) did not accurately predict the lightning occurrence (bottom) well, mostly due to the cloudy start of this day. Lightning did occur in the area where the CII probability was above 60%. Evaluation statistics for this day, using the contingency table approach for rainfall more than 1 mm are shown in Figure 6.10.

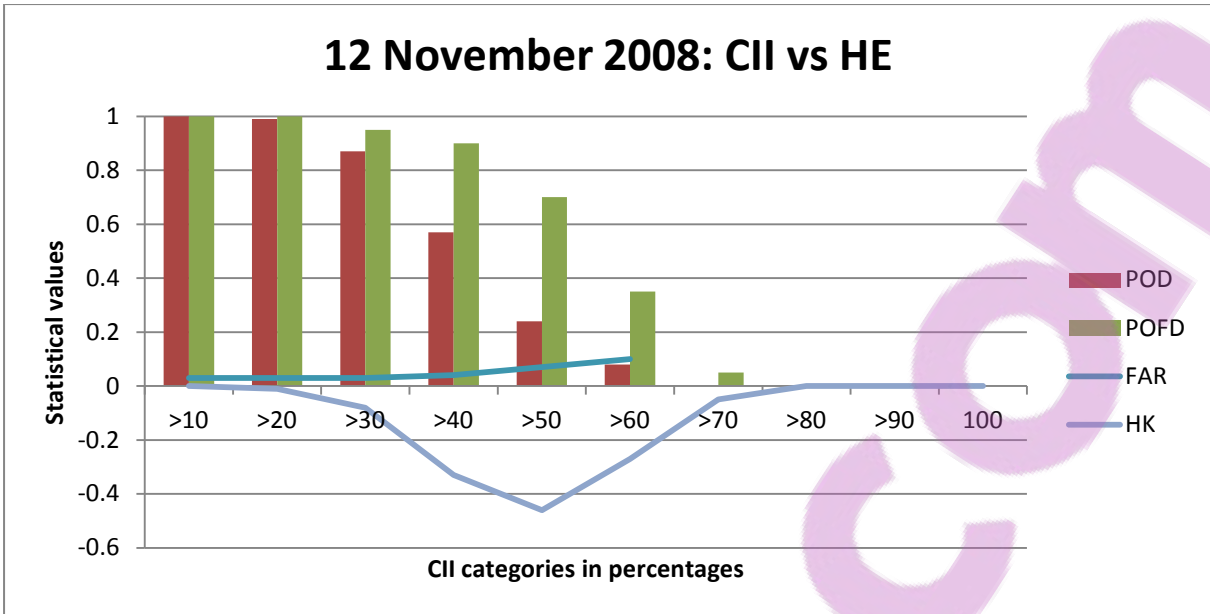


Figure 6.10 Statistical scores of CII versus HE for 12 November 2008

The same trend as in Example 1 is seen that, despite the high POD, the POFD is equally high or even higher than the POD and thus the HK is very low and even negative. The FAR remains less than 0.2 for all CII values. The evaluation statistics for CII versus occurrence of lightning are much better (Figure 6.11), although it was not a clear sky morning and thus the ability of CII was limited.

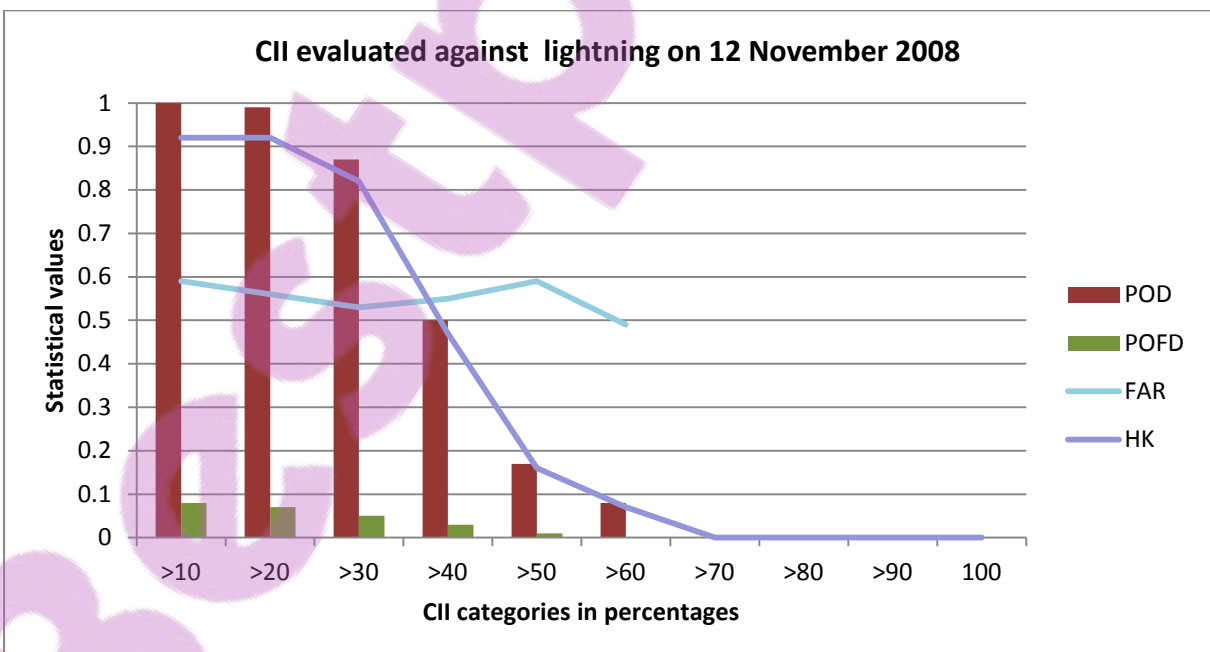


Figure 6.11 Statistical scores of CII versus lightning for 12 November 2008

## 6.5 STATISTICS FOR CII VERSUS HE FOR ALL FIFTY CASES

Comparison of the CII against the HE for all fifty cases is shown in Figure 6.12. Not surprisingly, the evaluation figures do not look nearly as good as when the CII is compared to the occurrence of lightning. The fact that the CII values do not exist in areas which already have clouds early in the morning, limits any quantitative evaluation method in such areas. To find a comprehensive or absolute way of confirming that convection occurred by evaluating the CII against the HE, rain gauges and/or the occurrence of lightning is, clearly, a daunting task and consequently the evaluation statistics using these tools should be seen in this perspective.

The HE has not yet been properly tested, refined or calibrated for South African conditions. Once better correlation is achieved between the rainfall fields from the model, the rain gauges and the HE, evaluation statistics might improve. HE is by no means perfect, but since the HE uses IR10.8 temperatures (i.e. cold cloud tops) it is a good proxy for convection. The CII should therefore have some relationship with the HE. In a continent lacking in more sophisticated tools to detect convective activity, the CII could be used outside the borders of South Africa as a nowcasting and/or very short range forecasting tool for convection, in spite of all the limitations of the various tools considered here.

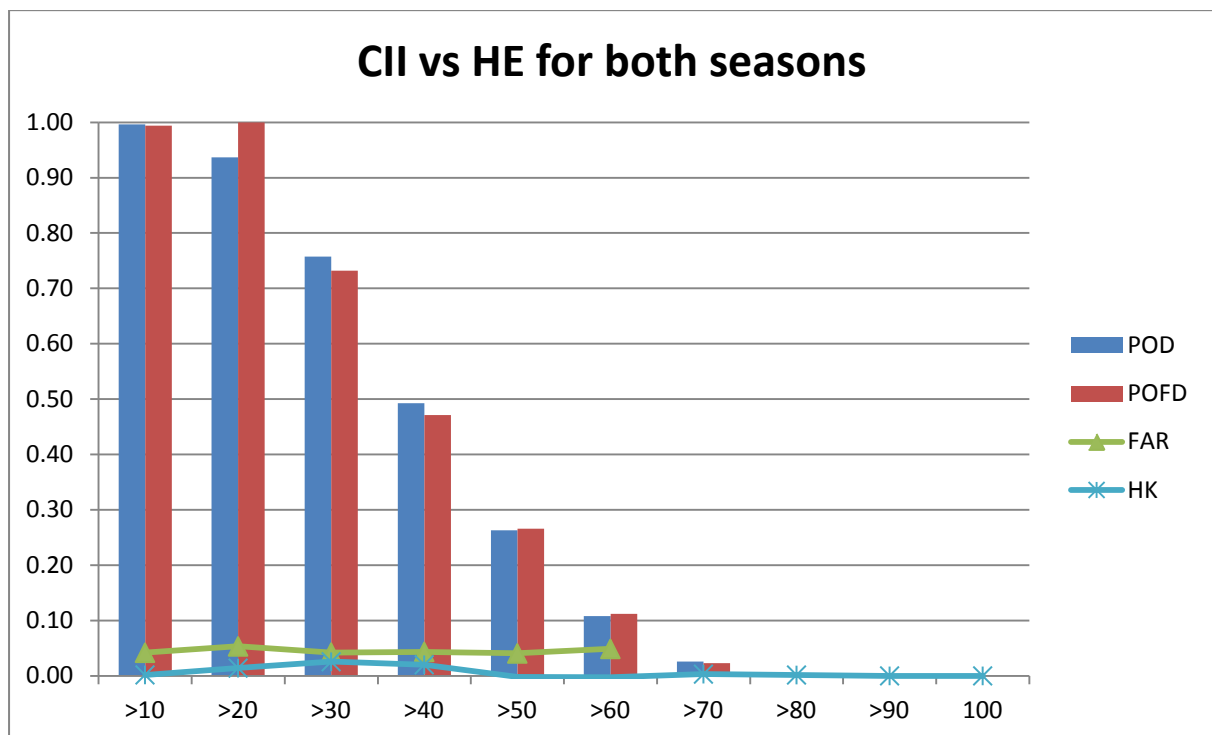


Figure 6.12 CII versus HE for all fifty cases from the two summer seasons

## 6.6 VISUAL COMPARISONS OF THE OPERATIONAL CII, LIGHTNING OCCURRENCE AND THE HE RAINFALL OVER SOUTHERN AFRICA

In this section the CII and HE for the entire area south of the equator will be considered. The proposed CII has been operational since the end of 2009. A few operational examples are shown.

From Figure 6.13 it is clear that the CII (top left) gave the best probability for convective development (greater than 60%) over central Africa and this is also where the most rain was detected by the HE both at 1600 UTC (bottom left) and in the nine hour total rainfall (top right). Greater than 30% probabilities also existed over Zimbabwe and rain was detected there by the HE. In South Africa a 30-60% area was also predicted over the Northwest Province and northern Free State. The HE detected very little any rain in that area (top right).

*EXAMPLE 1: 1 February 2010*

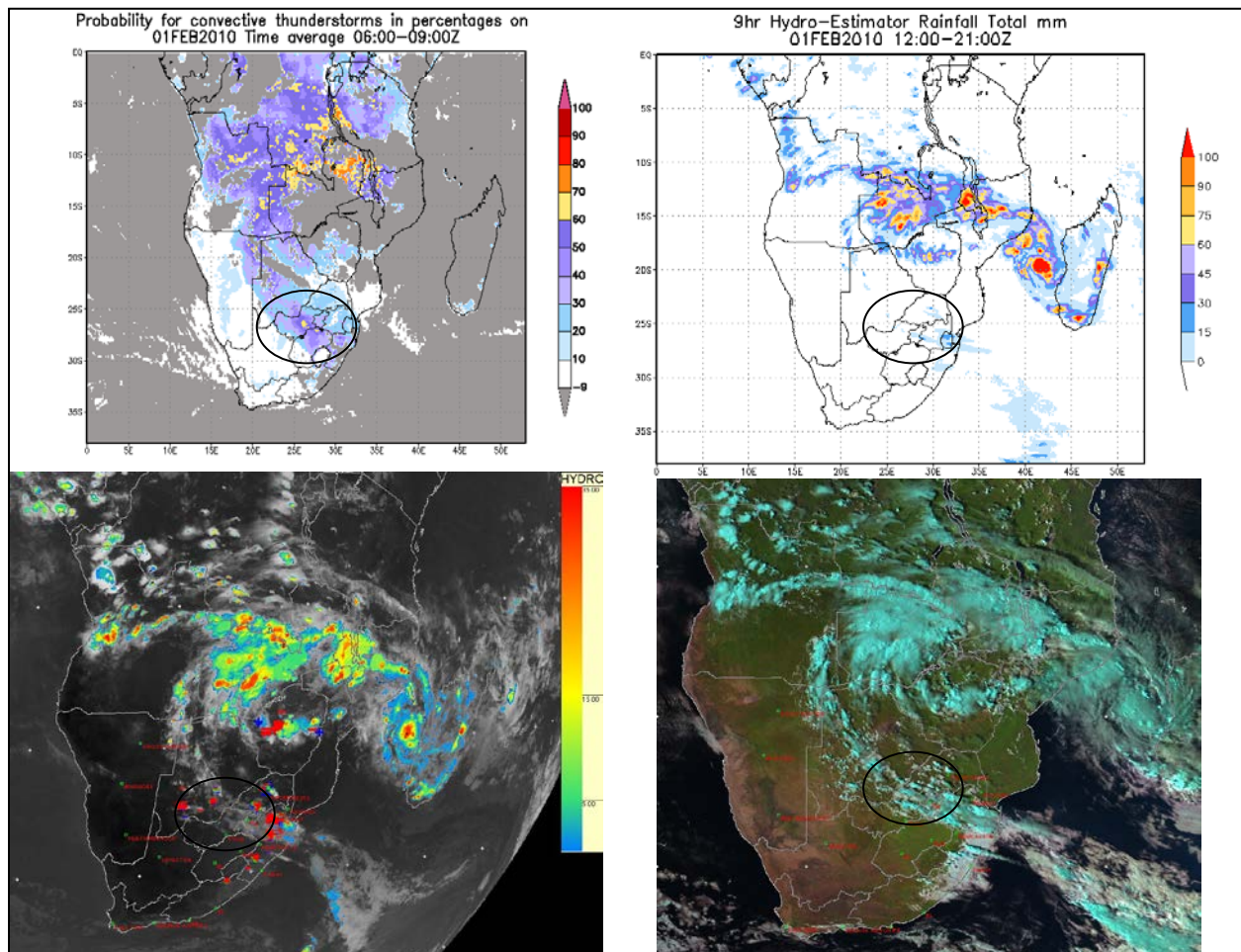


Figure 6.13 CII time average (top left), HE nine hour total (top right), HE together with IR108 and lightning occurrence (indicated by red, green and blue crosses) at 1600 UTC (bottom left) and MSG Day Natural RGB at

1500 UTC (bottom right) for 1 February 2010

Another MSG RGB combination which is very useful is the Day Natural RGB: Visible MSG channels (VIS0.8 and VIS0.6) are combined with the Near Infrared band (NIR1.6) to generate an almost “true colour” image known as the Day Natural RGB (Kerkmann, 2005). The cyan colour in such an image depicts the high level, convective clouds with ice content, while low level water clouds are pink. Vegetation is green and the ocean black. Convective development in the cyan colour is thus visible over Northwest Province and into Botswana at 1500 UTC (Figure 6.15, bottom right) even though no rain was detected by the HE in the nine hour period. Lightning is also visible at 1600 UTC (Figure 6.13, bottom left). The red symbols are all strokes reported in the last 5 min, the blue strokes are those reported 5–10 min ago, and the green strokes are those reported between 10 and 15 min ago. These colours are not important since it just indicates lightning in the last 15 minutes.

Figure 6.14 shows that the CII (top left) had the highest probabilities over the central parts of South Africa as well as further north over Zimbabwe. High rainfall totals are evident in South Africa in the nine hour HE accumulation (top right), but very little rain over Zimbabwe. Lightning was, however, detected at 1600 UTC (bottom left) in both of these regions. In the Day Natural RGB (bottom right) at 1500 UTC the convective development over central South Africa as well as over Zimbabwe is evident.

Figure 6.15 shows that the CII (top left) and the HE nine hour totals (top right) were in good agreement, i.e. the higher CII probabilities coincide with the areas of rainfall detected by the HE. Over the southwestern part of South Africa the probabilities of the CII were not matched by HE rainfall totals, but at 1500 UTC (bottom left) it is clear that lightning did occur in that area and the Day Natural image at 1500 UTC (bottom right) shows that convective development did take place there.

These three operational examples confirm that cloud-to-ground-lightning detection and precipitation estimates from the HE do not necessarily agree completely. This is not surprising since cloud-to-ground lightning is only observed in the mature phase of convection while precipitation can also occur earlier in the life stages of convection. Precipitation and lightning are usually in good agreement, but they can also occur separately.

The CII is intended as an early morning tool (with little cloud present) to give an indication of the area where convection (evidenced by lightning) is most likely to occur later in the day. Finding a data set to evaluate this quantitatively is not only a challenge in South Africa or southern Africa, but worldwide. The CII does, however, give a good indication of the preferred areas for the likelihood of convective activity if all observation tools are seen in combination. Although CII was developed with the use of South African lightning data, it also seems to effectively capture the events over southern Africa and could possibly be a useful tool in countries other than South Africa.

EXAMPLE 2: 10 February 2010

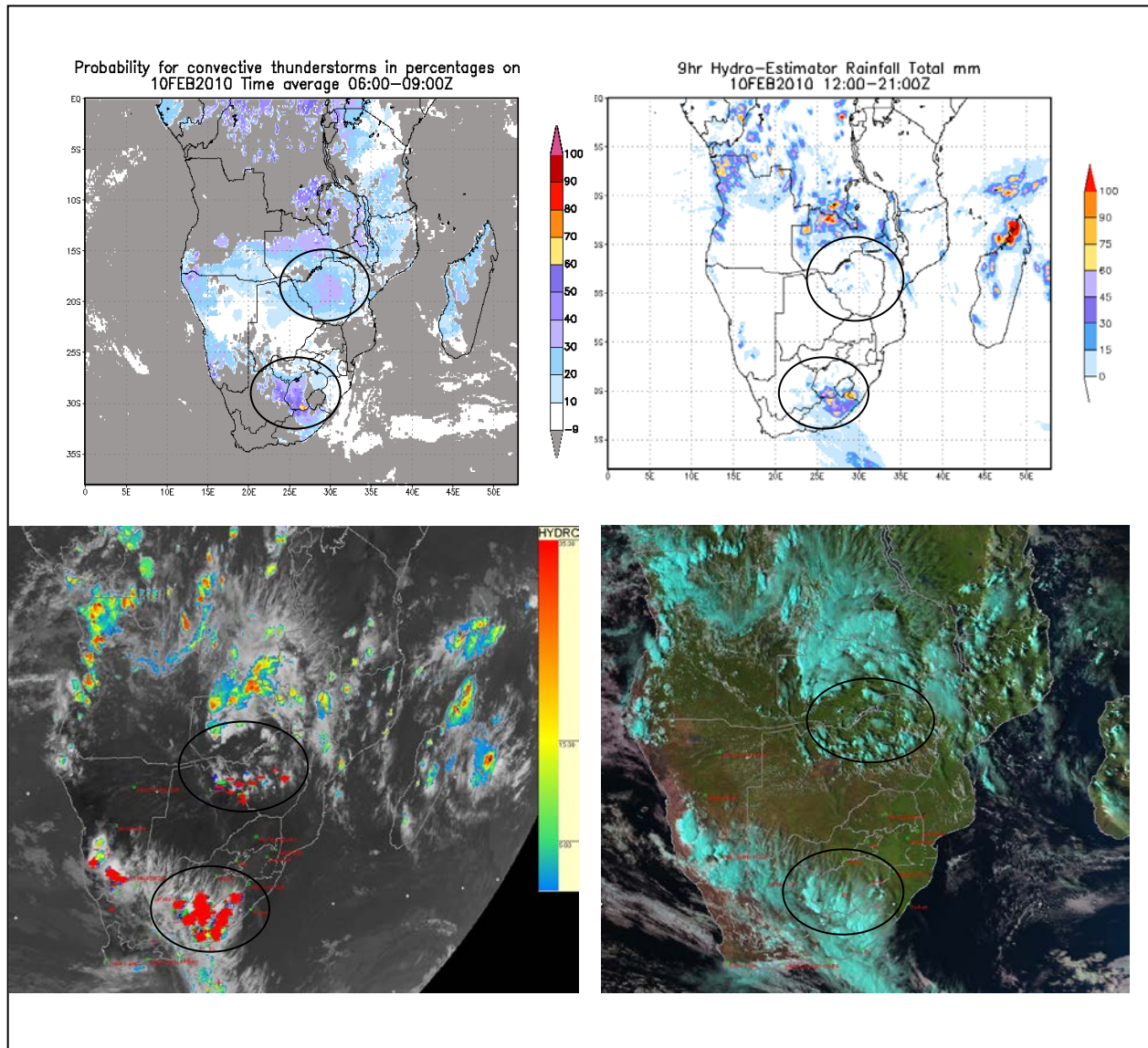


Figure 6.14 CII time average (top left), HE nine hour total (top right), HE together with IR108 and lightning occurrence (indicated by red, blue and green crosses) at 1600 UTC (bottom left) and MSG Day Natural RGB at 1500 UTC (bottom right) for 10 February 2010

EXAMPLE 3: 18 January 2010

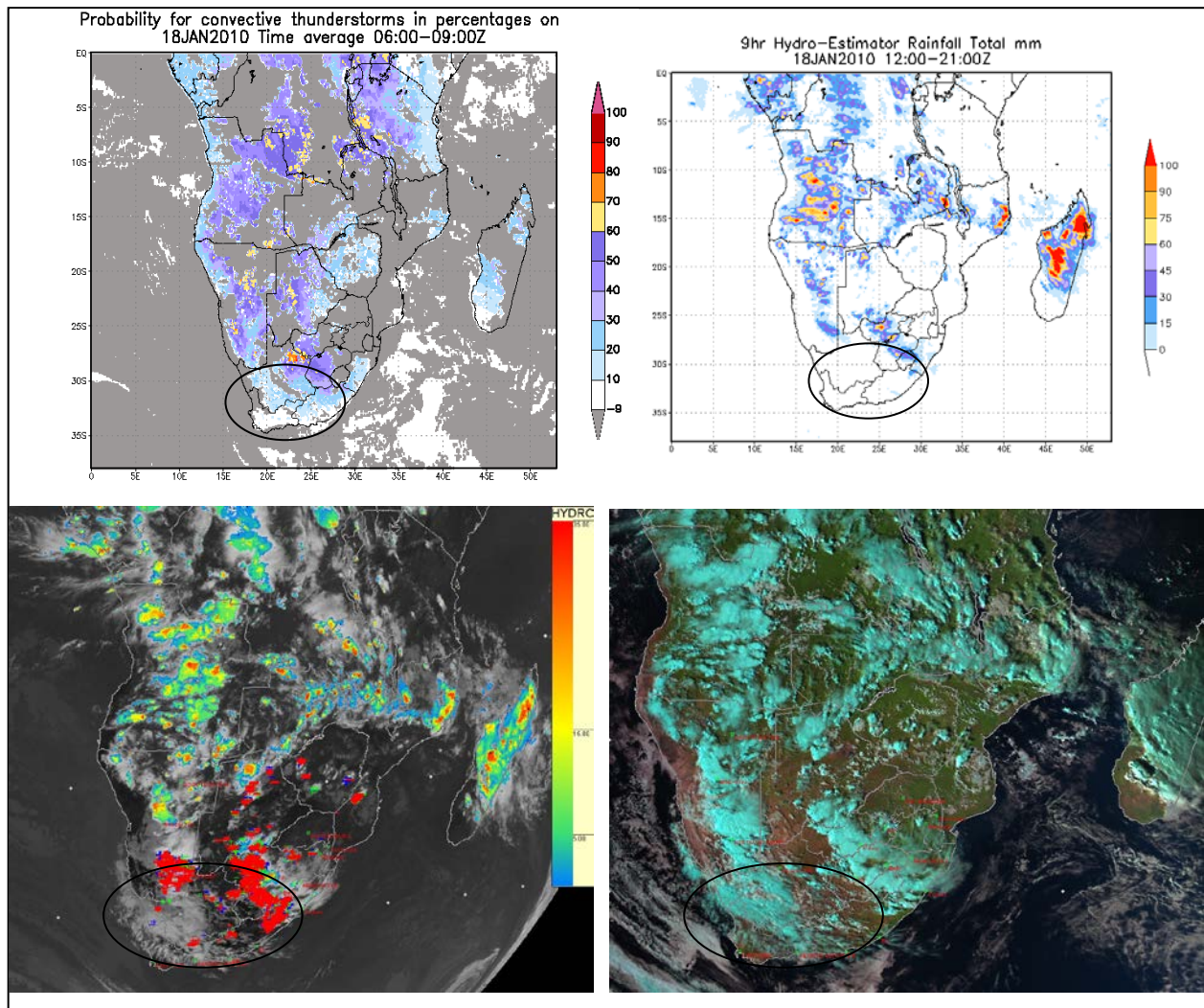


Figure 6.15 CII time average (top left), HE nine hour total (top right), HE together with IR108 and lightning occurrence (indicated by red, blue and green crosses) at 1500 UTC (bottom left) and MSG Day Natural RGB at 1500 UTC (bottom right) for 18 January 2010

## 6.7 SUMMARY

In this chapter a comparison was made between the CII and precipitation measurements and estimates. First, a visual verification was carried out between the 24 hour rain gauge totals and the 24 hour totals from the HE (Figures 6.4 and 6.5). Discrepancies were seen in areas where the HE overestimated or missed areas where rainfall did in fact occur. It is also clear that rain gauges do not necessarily capture all the precipitation and that the HE might add value in areas where gauges are not placed. The CII probabilities were also evaluated statistically against the nine hour HE totals. A comparison (Figure 6.7 vs. Figure 6.8, Figure 6.10 vs. Figure 6.11) showed that the CII versus

lightning statistics were more accurate than the CII versus HE statistics on the same days. As a consequence of the discrepancies between rain gauge observations and HE estimates, as well as the fact that the CII cannot be calculated in cloudy areas, these poor statistical values should not indicate that CII cannot be used in countries outside South Africa. In addition to this, a few operational examples (Figures 6.13-6.15) from the spring season of 2009/2010 over southern Africa showed reasonably good agreement with the HE and the lightning detection in South Africa. This indicates that the CII can be beneficial as a convection nowcasting tool in the early morning hours when it is still reasonably cloud free for the wider southern African region.

# Chapter 7

## SUMMARY, RECOMMENDATIONS AND CONCLUSION

---

### 7.1 BACKGROUND

One of the possible effects of global climate change is a higher frequency of extreme weather events. The Intergovernmental Panel on Climate Change reports that the frequency of heavy precipitation events has already increased over most land areas, consistent with warming and increases of atmospheric water vapour. It is also likely that temperature extremes, heat waves, and heavy precipitation events will continue to increase (IPCC, 2007). Findings of the Hyogo Framework for Action 2005-2010 revealed that rain was the hazard of most concern and forecasting accuracy was the primary challenge. As a consequence of these findings, the World Meteorology Organization recommended that the enhancement of the predictability of rain is the most important area of focus. They also recommended that the vulnerability of member countries should be reduced by improving the early warning of short term severe weather phenomena, especially rainstorms.

Remote sensing plays a very important role when forecasts for the time scale 0 to 12 hours need to be issued to warn the public, business and other sectors of impending bad weather. In southern Africa satellite data is the only tool available to all countries. Forecasters using the latest data from remote sensing tools such as radar and satellite, as well as conventional observational data, are able to analyze and forecast weather features at all scales for the following few hours. To use such data for very short range forecasting and nowcasting applications would thus be an important and powerful tool when issuing warnings to the general public of hazardous, high impact weather including tropical cyclones, thunderstorms and tornados which cause flash floods, lightning strikes and destructive winds.

When it is still cloud free early in the morning it is most difficult to say where convection will develop later in the day. Once clouds start to develop, it becomes easier to analyze the situation with radar and MSG RGB images. Using satellite derived products to calculate the instability indices of the atmosphere has become the international trend because upper-air soundings have become too expensive. Adding to this, upper-air soundings can only provide information twice in a day at more or less ten stations across South Africa. This is simply not enough to make a reasonable deduction of the vertical state of the atmosphere. Making use of satellite derived products (i.e. GII and RII) is the only way to get values almost everywhere (in cloud free areas) and at 15 min time intervals.

Due to the vast amount of data which have to be analyzed, it would be easier for forecasters to have various sources of information combined into one product which could focus their attention on the right areas. The ultimate goal of this research was to provide an operational probability map for the occurrence of convection and the possible related severe weather, with a three to nine hour lead time. The development of this new Combined Instability Index and its verification are described in this thesis.

## **7.2 SUMMARY AND DISCUSSION OF RESULTS**

In Chapter 2 the Meteosat Second Generation applications for nowcasting and very short range forecasting were described. A basic theoretical background was supplied for the Global Instability Indices (GII) and how they are used, displayed and evaluated in South Africa. A description was given of how the GII were adapted to South African circumstances using the local version of the Unified Model at a higher resolution than the European Centre for Medium-Range Weather Forecasts model input, creating the Regional Instability Indices (RII). The various indices used for the GII and the RII were defined, as well as the adjustments made to suit the topographical realities of the country.

In Chapter 3 the data used for this study were described, and some verification results were presented. The initial verification of the GII provided the basis of a contingency table approach for an evaluation method, which was expanded and refined when the RII came into operation. Two of the RII were compared to model fields and examples were shown. At the end of this chapter the four modified RII were evaluated by means of four statistics (Probability of Detection, Probability of False Detection, False Alarm Ratio and Hanssen-Kuipers discriminant) against the occurrence of lightning over South Africa over two summer seasons.

The fourth chapter provided a description of the data and methodology used to develop a new instability indicator. The principles of cumulative frequencies were explained and applied to the RII as well as to topography in their relation to the occurrence of lightning. Look up tables for the various contributors to the new combined index were set up and listed, and finally the formula for the Combined Instability Index was derived. Two visual verification examples were shown to demonstrate that the CII could be useful.

In Chapter 5 a more quantitative evaluation of the CII was made against the occurrence of lightning for ten individual cases, as well as overall for all fifty test cases. The same method and statistical scores were used as before, based on a contingency table approach. According to the statistics, the CII performed well, especially for thresholds less than 70% and it also outperformed the individual RII, with the exception of Mixed K Index (for some scores at some values). On those case study days, which started with a lot of cloud cover, calculation of the statistics was difficult and in these cases CII generally performed worse than on cloud free days. In the latter part of the South African summer more tropical air is in circulation causing more cloud cover. In addition, under these conditions

precipitation occurs more in the form of showers than thundershowers and consequently less lightning occurs. The newly developed index should be beneficial in helping operational forecasters to direct their attention to the right area for the development of convection and lightning, especially when clear skies are present in the early morning.

In Chapter 6 a comparison was made between the CII and precipitation measurements and estimates. A comparison was done between the rain gauge rainfall totals and the Hydroestimator precipitation totals using eyeball verification. The CII was also qualitatively evaluated against the HE. The comparison showed that the CII versus lightning statistics were much better than for CII versus HE on the same days. The discrepancies between rain gauge observations and HE estimates of rainfall makes it difficult to quantify the value of the CII as compared to the HE totals. Lightning network data is also not a complete reflection of the ground truth. Nevertheless, these are the only tools available for the verification of a convection forecasting indicator. In all southern African countries, other than South Africa the only data set for verification is the HE since there are no radar or lightning data available. Despite these shortcomings in data, the CII has been shown to be of value as a forecasting tool not only for South Africa, but also in the entire southern African region with a three to nine hour lead time.

The CII depends on Mixed K Index and Mixed Total Totals which in return depend on surface and 850 hPa temperatures and dew point temperatures. The time average products of CII will thus change with time. This accentuates the process of surface heating, relevant in heat generated thunderstorms in southern Africa. An example is shown in Figure 7.1.

### **7.2.1 Advantages of CII**

**The advantages of CII can be summarized as follows:**

1. The CII incorporates instability measures (Mixed K Index, Lifted Index and Mixed Total Totals), moisture (Precipitable Water) as well as height above sea level and thus contains the necessary ingredients for convection (excluding dynamic lift).
2. There is no need to consider four different parameters each with their own respective thresholds.
3. More than three hours lead time for convection and/or lightning activity is provided.
4. Spatial coverage is improved where the usual K Index and Total Totals could not be calculated due to elevation by using the Mixed K Index and Mixed Total Totals.

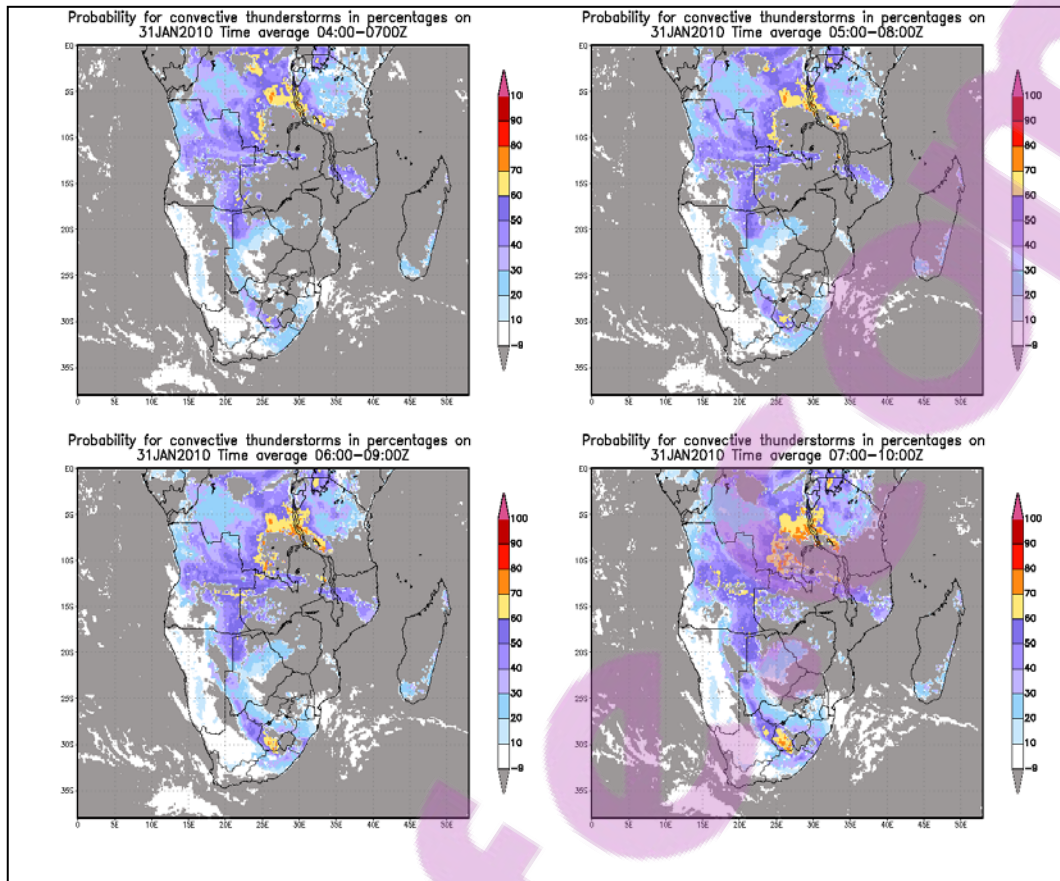


Figure 7.1 CII three hourly time averages: 0400 to 0700 UTC (top left), 0500 to 0800 UTC (top right), 0600 to 0900 UTC (bottom left) and 0700 to 1000 UTC (bottom right) for 31 January 2010

5. The statistics for the CII outperform the statistics of the individual parameters in spite the fact that lightning sometimes occurs in areas where CII could not be calculated because of cloud cover.
6. The CII can be displayed operationally every 15 minutes, like the MSG images, through free software developed in-house in the SAWS called SUMO (<http://www.weathersa.co.za/SUMO>). The CII thus vastly improves on the availability and spread of upper air sounding sites when forecasters need to make a forecast of convection while the sky is still clear.
7. In South Africa the day often starts with very little cloud and convection only develops later in the day when the surface heats up; thus CII can be utilized on many summer days. If most of the country is cloud free in the morning, the CII helps to distinguish the areas with possibilities for convection from those where it will not occur. Once clouds are present, the CII of the surrounding pixels together with satellite and radar images should be used in real time to monitor the development and decay of convection.
8. The use of time averages improves the consistency of the parameter as well as the spatial coverage. In this study a three hour time average (from 0600 to 0900 UTC) was used in the

evaluation of the CII. Three additional periods, 0400 to 0700 UTC, 0500 to 0800 UTC and 0700 to 1000 UTC, are used for the operational calculation of running averages. These four time averaged products are available at 0720, 0820, 0920 and 1020 UTC on the RSMC website (<http://www.weathersa.co.za/RSMC/login.jsp>) for forecasters to use as guidance for convective activity later in the day. This website is part of the Severe Weather Forecasting Demonstration Project (SWFDP) in southern Africa and is accessible to all southern African countries by means of a username and password.

## **7.2.2 Limitations of CII**

### **Limitations in the development of the CII would include:**

1. The CII can only be calculated in cloud free conditions. It is thus a tool suitable for use during the early morning hours when forecasters have to make a forecast for later in the day (more than nine hours ahead) and as little cloud as possible is present. Once convection starts, real time satellite and radar images should be utilized.
2. The CII is a tool developed using data from the summer months (October to March) with the aim to predict convection. It is not intended to be used for predicting stratiform rain associated with frontal systems. In very tropical conditions where a lot of clouds are present and showers occur, rather than thundershowers and lightning, CII is less useful.
3. The CII could be only be evaluated over South Africa only as a result of a lack of lightning observations over the rest of southern Africa. Lightning characteristics in other countries might be different from lightning in South Africa. Nevertheless, visual comparison of the CII with convective development in southern Africa looks promising.
4. The evaluation of the CII (or any other tool for the forecasting of convection) against precipitation remains problematic since neither rain gauges, nor radar rainfall, nor SPE offer a complete and absolute reflection of convective precipitation on the ground. In this study the occurrence of lightning was used for the evaluation of the CII over the South African domain while the local HE was used for the entire southern African domain.

## **7.3 RECOMMENDATIONS**

Apart from the obvious advantages of MSG and the visual products it provides to aid an operational forecaster to identify different cloud types and cloud microphysics, the derived products of MSG, such as the Global Instability Index and the Regional Instability Index have considerable potential to assist in the nowcasting and very short range forecasting of convection. The development of the Combined Instability Index provides the forecaster with an easy and simple guide to predict the probability of convection with a more than three hour lead time. It is therefore recommended that:

Forecasters in South Africa and the rest of southern Africa should be made aware through training opportunities of these tools that can be used for the short term forecasting of convection. These training opportunities need not happen in classrooms, but can be via internet training sessions. Whenever possible, examples showing how the tools should be used and what value they have can be presented to explain and demonstrate the advantages of the product to forecasters. The systems resulting from this research were implemented at the South African Weather Service and made available via SUMO on a 15 minute repeat cycle. Time averaged graphics of the CII are available on the RSMC website for southern African forecasters. In addition, the EUMETCast system can also be used to disseminate the information to other countries in southern Africa. The availability of the CII should be made known to the potential users. Forecasters who use the CII should be encouraged to give feedback to the developers (SAWS) in the form of case studies in their own countries.

One aspect which is not embedded in the CII is the movement of weather systems. Storm motion plays a role in very short range forecasting (up to 12 hours ahead), but this aspect is beyond the scope of the development of the CII. Although it can be argued that convective systems will move with the prevailing mid or upper level wind fields, small scale storm motion is also influenced by topography and severe storms might deviate to the left (in the southern hemisphere). Due to the complexity of the movement of convective systems, the incorporation of motion is something which is best done when the storm cells (or cloud clusters) have already started to develop. Zinner *et al.* (2008) developed a system called CbTRAM, a tracking and nowcasting algorithm which detects and tracks intense convective cells and then distinguishes whether they are in the onset, development or mature phase. The detection is based on the high resolution visible, water vapour and infrared channels from MSG. The CII can therefore be used in cloud free areas early in the morning and the CbTRAM once the convective clouds have developed. Research to use and perhaps implement such a system operationally in South Africa is ongoing and it is envisaged that this will adequately address the motion of convective cells closer to real time.

## 7.4 CONCLUSION

The very short range forecast and nowcast of convective storms is a dominant feature of the climate of southern Africa and remains a challenging task. To forecast convection in areas which are cloud free early in the morning makes this challenge even bigger. Despite the role that numerical weather prediction models play to give general guidance on where convection might be favourable, more detailed information is needed closer to time of convection. The purpose of this study was to provide guidance in the form of a probability map for convection. The CII developed and tested in this study

combines the various precursors for convection in an optimal manner to provide a probabilistic map of convection with a lead-time in excess of three hours. The CII thus fills a critical gap in the first twelve hours of forecasting providing real time information on the possibilities for convection. The fact that this new tool is based on satellite and model data that is available throughout southern Africa makes it possible to improve the very short range forecasting of convection in the entire region. The CII complements the use of more sophisticated technology, such as radar and lightning networks, where it is available. The CII also makes a direct contribution towards improved services by addressing an important gap in the nowcasting and very short range forecasting tools, which are available to forecasters. The public can benefit from more accurate and timely warnings of pending severe weather and be better prepared to avoid damage to property and loss of life.

# REFERENCES

---

Bedka, K. M. & Mecikalski, J. R. (2005). Application of Satellite-Derived Atmospheric Motion Vectors for Estimating Mesoscale Flows. *J. Appl. Meteorol.*, 44(11), 1761–1772.

Burington, R. S. & May, D. C. (1970). *Handbook of probability and statistics with tables*. 2nd edition. New York. McGraw-Hill Book Company.

Carte, A. E. & Held, G. (1978). Variability of hailstorms on the South African Plateau. *J. Appl. Meteorol.*, 17(3), 365-373.

Cecil, D. J. (2008). Seasonality of thunderstorms seen by TRMM. *Third Conference on Meteorological Applications of Lightning Data*. New Orleans, LA. 20-24 January 2008. P1.8.

Caruso, S. J., Rabin, R., Zaras, D. & LaDue, J. (2000). A new look at the McCann study of the enhanced-V signature. *10th Conference on Satellite Meteorology and Oceanography*, Long Beach, CA., 10-14 January, 2000, JP4.14.

Charba, J. P. (1977). *Operational System for predicting thunderstorms two to six hours in advance*. (Report: NOAA Technical Memorandum NWS TDL-64). National Oceanic and Atmospheric Administration, US Department of Commerce, 24pp.

Charba, J. P. (1979). Two to six hour severe local storm probabilities: An operational forecasting system. *Mon. Wea. Rev.*, 107, 268-282.

Charba, J. P. (1984). *Two-to-six hour probabilities of thunderstorms and severe local storms*. (Report: NOAA Technical Memorandum NWS TPB-342). National Oceanic and Atmospheric Administration, US Department of Commerce, 14pp.

Chevallier, F. (2002). *Sampled databases of 60-level atmospheric profiles from the ECMWF analyses*. (NWP SAF Report No. NPWSAF-EC-TR004, 27pp). EUMETSAT.

De Coning E. & Adam, B. F. (2000). The tornadic thunderstorm events during the 1998-1999 South African summer. *Water SA*, 26(3), 361-376.

De Coning E., Adam, B. F. & Banitz, L. (2000). A severe weather event on 29 December 1997: synoptic and mesoscale perspectives. *Water SA*, 26(2), 137-146.

De Coning, E. (2007). A nowcasting application study using MSG, lightning data and weather radar. *The 2007 EUMETSAT Meteorological Satellite Conference*, Amsterdam, The Netherlands. 24-28 September 2007. EUM P.50, ISBN 92-9110-079-X.

De Coning, E. & Poolman, E. R. (2010). South African Weather Service operational satellite based precipitation estimation technique: applications and improvements. *Hydrology and Earth System Sciences*. Online discussion document until 7 Jan 2011. [Retrieved on November 19, 2010, from

[http://www.hydrology-and-earth-system-sciences.net/review/review\\_process\\_and\\_interactive\\_public\\_discussion.html](http://www.hydrology-and-earth-system-sciences.net/review/review_process_and_interactive_public_discussion.html)].

Dixon, M. J. & Wiener, G. (1993). Thunderstorm Identification Tracking Analysis and Nowcasting - A radar based methodology. *J. Atmos. Ocean. Tech.*, 10(6), 785-797.

Dostalek, J. F. & Schmit, T. J. (2001). Total precipitable water measurements from GOES sounder derived product imagery. *Wea. Forecasting*, 16, 573-587.

Ebert, B., Jakob, C., Stenle, P. & Puri, K. (2006). Proposed strategy for ensemble prediction in the Bureau of Meteorology. *18th BMRC Modeling Workshop*, 28 Nov – 1 Dec 2006. [Retrieved on October 19, 2009, from: [http://www.cawcr.gov.au/bmrc/basic/wksp18/pdf\\_docs/Day\\_3\\_02\\_Ebert.pdf](http://www.cawcr.gov.au/bmrc/basic/wksp18/pdf_docs/Day_3_02_Ebert.pdf)].

Evett, R. R., Mohrle, C.R., Hall, B. L., Brown, T. J. & Stephens, S. L. (2008). The effect of monsoonal atmospheric moisture on lightning fire ignitions in southwestern North America. *Agricultural and Forest Meteorology*, 148, 1478-1487.

Eyre, J. R. (1991). *A fast radiative transfer model for satellite sounding systems*. (Report: ECMWF Research Department, Technical Memorandum No. 176, 28pp.

*Forecast Verification – Issues, methods and FAQs*. (2009). [Retrieved on April 1, 2010, from WWRP/WCRP web site: <http://www.cawcr.gov.au/projects/verification/>].

Galway, J. G. (1956). The Lifted Index as a predictor of latent instability. *Bull Amer. Meteor. Soc.*, 37, 528-529.

George, J. J. (1960). *Weather Forecasting for Aeronautics*. New York: Academic Press, p.407-415.

Gill, T. (2008a). *A lightning climatology of South Africa for the first two years of operation of the South African Weather Service Lightning Detection Network: 2006-2007*. [Retrieved on April 1, 2010, Proceedings from 2nd International Lightning Meteorology Conference, Tucson, Arizona website: [http://www.vaisala.com/files/A\\_lightning\\_climatology\\_of\\_South\\_Africa.pdf](http://www.vaisala.com/files/A_lightning_climatology_of_South_Africa.pdf)].

Gill, T. (2008b). Initial steps in the development of a comprehensive lightning climatology of South Africa. University of the Witwatersrand. Unpublished Master's thesis.

Goliger, A. M., Milford, R. V., Adam, B. F. & Edwards, M. (1997). *Inkanyamba – Tornadoes in South Africa*. Joint publication of the CSIR and the SA Weather Bureau, Department of Environmental Affairs and Tourism, Pretoria, South Africa: United Litho. ISBN 0-7988-5417-0. 77pp.

Hambridge, R. E. (1967). "*K*" chart application to thunderstorm forecasts over the western United States. (Report: Tech. Memo. WRTM-23). ESSA. 9pp.

Hayden, C. M. (1988). GOES-VAS simultaneous temperature-moisture retrieval algorithm. *J. Appl. Meteorol.*, 27, 705-733.

Held, G. (1978). The probability of hail in relation to radar echo heights on the South African Highveld. *J. Appl. Meteorol.*, 17 (6), 755-762.

Held, G. (1982). Comparison of radar observations of a devastating hailstorm and a cloud burst at Jan Smuts International Airport. In: Agee EM and Asai T (Ed.). *Cloud Dynamics*. Hamburg, Germany: D Reidel Publishing Company. 273-284.

Huang, H. L., Smith, W. L. & Woolf, H. M. (1992). Vertical resolution and accuracy of atmospheric infrared sounding spectrometers. *J. Appl. Meteorol.*, 31, 265-274.

Hurry, L. & Van Heerden, J. (1982). *South Africa's Weather patterns: a guide to the interpretation of synoptic maps*. South Africa: Via Afrika. ISBN 079940604X. 1st edition. 80pp.

*Hyogo Framework for Action 2005-2010*. (2005). [Retrieved on July 20, 2009, from World Conference on Disaster Reduction web site: <http://www.unisdr.org/wcdr/intergover/official-doc/L-docs/Hyogo-framework-for-action-english.pdf>].

*IPCC Report on global warming – Localizing a global story*. [Retrieved on July 20, 2009 from the IPCC “Climate Change 2007” web site: <http://www.ipccinfo.com/extreme.php#April6>].

Kerkmann, J. (2005). Applications of MSG – Day and night time convection – African examples. Presented at WMO Nowcasting Workshop, Pretoria, November 2005. Available at the South African Weather Service, Pretoria, South Africa.

Kitzmilller, D. H. & McGovern, W. E. (1989). VAS retrievals as a source of information for convective weather forecasts: An objective assessment and comparison with other sources of upper-air observations. *Mon. Wea. Rev.*, 117, 2095-2109.

Koenig, M. (2002). *Atmospheric Instability parameters derived from MSG SEVIRI observations*. (Report: Technical Memorandum No.9). EUMETSAT.

Koenig, M. (2007). *The Global Instability Indices Product Algorithm Theoretical Background Documents*. (Report: EUM/MET/REP/07/0164 v1). EUMETSAT.

Koenig, M. & De Coning, E. (2006). MSG for nowcasting – Experiences over Southern Africa. *The 2006 EUMETSAT Meteorological Satellite Conference*, Helsinki, Finland. 12-16 June 2006. EUM P.48, ISBN 92-9110-076-5.

Koenig, M. & De Coning, E. (2009). The MSG Global Instability Indices product and its use as a nowcasting tool. *Wea. Forecasting*, 24, 272-285.

Koenig, M., Pajek, M. & Struzik, P. (2007). MSG global instability indices for storm nowcasting – Validation studies. *Joint 2007 EUMETSAT and 15th AMS Conference*. P.50.

Koenig, M. (2007). SAWS Notes on the implementation of the Hydroestimator in South Africa. Available at the South African Weather Service, Pretoria, South Africa.

Kondragunta, C. (2007). Quantitative Precipitation Estimation in the National Weather Service. NOAA's Water Resources Information. Office of Systems Development. NOAA/NESDIS. George Washington University, DC. March 13 2007. [Retrieved on July 20, 2009 from George Washington University website: [http://www.gwu.edu/~spi/assets/docs/Chandra\\_Kondragunta-NOAA's%20Water%20Resources%20Information.pdf](http://www.gwu.edu/~spi/assets/docs/Chandra_Kondragunta-NOAA's%20Water%20Resources%20Information.pdf)].

Kotroni, V. & Lagouvardos, K. (2008). Lightning occurrence in relation with elevation, terrain slope, and vegetation cover in the Mediterranean. *J. Geophys. Res.*, 113, D21118.

Krider, E. P. (1986). Physics of lightning. In: *The earth's electrical environment*. Geophysics Study Committee, Geophysics Research Forum, Commission on Physical Sciences, Mathematics and Resources, National Research Council. 263 pp.

Kruger, A. C. (2006). Observed trend in the daily precipitation indices in South Africa: 1910-2004. *Int. J Climatol.*, 26, 2275-2285.

Kruger, A. C. (2007). *Climate of South Africa, Precipitation*. (Report No. WS47). South African Weather Service. 41pp.

Kuligowski R. J., Qiu, S., Scofield, R. A. & Gruber, A. (2001). The NESDIS QPE verification program. Preprints, *11th Conf. on Satellite Meteorology and Oceanography*, Madison, WI, Amer. Meteor. Soc., 383–384.

Kuligowski, R. J., Scofield, R. A. & Davenport, J. C. (2005). The Hydro-Nowcaster: Recent improvements and future plans. *World Weather Watch Research Programme International Symposium on Nowcasting and Very Short Range Forecasting*. Toulouse, France, 5-9 September 2005. 5.15. Available online at: [www.meteo.fr/cic/wsn05/resumes\\_long/5.15-203.pdf](http://www.meteo.fr/cic/wsn05/resumes_long/5.15-203.pdf).

Levin, Z. & Tzur, I. (1986). Models of the development of the electrical structure of clouds. In: *The earth's electrical environment*. Geophysics Study Committee, Geophysics Research Forum, Commission on Physical Sciences, Mathematics and Resources, National Research Council. 263 pp.

Lutz, H-J. (2007). *Cloud detection from MSG – algorithm theoretical basis document*. (Report: EUM/MET/REP/07/0132). EUMETSAT.

Ma, X. L., Schmit, T. J. & Smith, W. L. (1999). A nonlinear physical retrieval algorithm – its application to the GOES-8/9 sounder. *J. Appl. Meteor.*, 38, 501-513.

Mecikalski, J. R. (2007). *Satellite-based convective initiation nowcasting system Improvements expected from the MTG FCI Meteosat Third Generation capability*. (Report No. EUM/CO/07/4600000405/JKG). EUMETSAT.

Mecikalski, J. R., Bedka, K. M., Peach, S. J. & Litton, L. A. (2008). A statistical evaluation of GOES cloud top properties for nowcasting convection initiation. *Monthly Wea. Review.*, 136, (12), 4899-4919.

Mecikalski, J. R., Murray, J. J., Feltz, W. F., Johnson, D. B., Bedka, K. M., Bedka, S. T., Wimmers, A. J., Pavolonis, M., Berendes, T. A., Haggerty, J., Minnis, P., Bernstein, B. & Williams, E. (2007). Aviation applications for satellite-based observations of cloud properties, convective initiation, in-flight icing, turbulence and volcanic ash. *Bull. Amer. Meteor. Soc.*, 88, 1589-1607.

Mecikalski, J. R., MacKenzie, W. M., Koenig, M., Walker, J. R. & Muller, S. (2009). Updates on convective initiation nowcasting: Exploiting MSG infrared and visible satellite data & new initiatives. *Convection Working Group Meeting*. 8-10 October 2009, Landshut, Germany.

Menzel, W. P., Holt, F. C., Schmit, T. J., Aune, R. M., Schreiner, A. J., Wade, G. S. & Gray, D. G. (1998). Application of GOES8/9 soundings to weather forecasting and nowcasting. *Bull. Amer. Met. Soc.*, 79, 2059-2077.

Miller, R. C. (1967). *Notes on analysis and severe storm forecasting procedures of the Military Weather Warning Centre*. (Report: Tech. Report 200, AWS, USAF). Headquarters, AWS, Scott AFB, 1L 62225.

Miller, R. C. (1972). *Notes on analysis and severe storm forecasting procedures of the Military Weather Warning Centre*. (Report: Tech. Report 200 (Revised), AWS, USAF). Headquarters, AWS, Scott AFB, 1L 62225.

Miller, R. C. (1975). *Notes on analysis and severe storm forecasting procedures of the Military Weather Warning Centre*. (Report: Tech. Report 200. Revised to include CHANGE 1, AWS, USAF). Headquarters, AWS, Scott AFB, 1L 62225.

Morgan, J. (2002). *Applications of Meteosat Second Generation*. (Report No. EUM BR 11). EUMETSAT.

*MSG-2 successfully launched*. (2005). [Retrieved on July 20, 2009, from EUMETSAT Press Releases Web site: [http://www.eumetsat.int/Home/Main/News/Press\\_Releases/005023?l=en](http://www.eumetsat.int/Home/Main/News/Press_Releases/005023?l=en)].

Orville, R. E. (1994). Cloud-to-Ground Lightning Flash Characteristics in the Contiguous United States: 1989-91, *J. Geophys. Res.*, 99, 10833-10841.

Peppler, R. A. (1988). *A review of static stability indices and related thermodynamic parameters*. (Report: SWS Misc. Publ. 104, Illinois State Water Survey Division, Climate and Meteorology Section). 94 pp.

Piepgrass, M. V., Krider, E. P. & Moore, C. B. (1982). Lightning and surface rainfall during Florida thunderstorms. *J. Geophys. Res.*, 87, 11193-11201.

Poolman, E. R. (2007). *The early warning system of the South African Weather Service, Flash flood warnings*. Presented at South African Flash Flood Guidance Workshop. June 2007, Pretoria, South Africa.

Poolman, E. R. & Chikoore, H. & Lucio, F. (2008). [Retrieved on November 12, 2010, from Public benefits of the Severe Weather Forecasting Demonstration Project in south-eastern Africa. *WMO Newsletter* *MeteoWorld*, *Dec* 2008. [http://www.wmo.int/pages/publications/meteoworld/archives\\_en.html](http://www.wmo.int/pages/publications/meteoworld/archives_en.html)].

Price, C. (2008). *Lightning observations for weather and climate research*. Presented at Lightning workshop, Johannesburg, South Africa. 13 August 2008.

Rao, P. A. & Fuelberg, H. E. (1997). Diagnosing convective instability from GOES-8 radiances. *J. Appl. Meteor.*, 36, 350-364.

Reap, R. M. (1986). Evaluation of Cloud to Ground Lightning Data from the Western United States for the 1983 – 1984 Summer Seasons, *J. Climate Appl. Meteor.*, 25, 785-799.

Rodgers, C. D. (1976). Retrieval of atmospheric temperature and composition from remote measurements of thermal radiation. *Rev. Geophys. Space Phys.*, 14, 609-624.

Rosenfeld, D. & Lensky, I. (2006). The time-space exchangeability of satellite retrieved relations between cloud top temperature and particle effective radius. *Atmos. Chem. Phys. Discuss.*, 5, 11911-11926.

Saunders, R., Matricardi, M. & Brunel, P. (1999). An improved fast radiative transfer model for assimilation of satellite radiance observations. *Q. J. R. Meteorol. Soc.*, 125, 1407-1425.

Schmit, T. J., Feltz, W. F., Menzel, W. P., Jung, J., Noel, A. P., Heil, J. N., Nelson, J. P. & Wade, G. S. (2002). Validation and use of GOES sounder moisture information. *Wea. Forecasting*, 17, 139-154.

Schulz W. & G. Diendorfer. (1999). Lightning characteristics as a function of altitude evaluated from lightning location network data. *International Conference on Lightning and Static Electricity*. 22-24 June 1999, Toulouse, France. 5 pp.

Scofield, R. A. (2001). Comments on "A quantitative assessment of the NESDIS Auto-Estimator". *Wea. Forecasting*, 16, 277-278.

Scofield, R. A. & Kuligowski, R. J. (2003). Status and outlook of operational satellite precipitation algorithms for extreme-precipitation events. *Wea. Forecasting*, 18, 1037-1051.

Seemann, S. W., Borbas, E. E., Knuteson, R. O., Stephenson, G. R. & Huang, H-L. (2008). Development of a global infrared land surface emissivity database for application to clear sky sounding retrievals from multi-spectral satellite radiance measurements. *J. Appl. Meteor. Clim.*, 47(1). 108-123.

Setvák, M. & Doswell III, C. A. (1990). The AVHRR Channel 3 cloud top reflectivity of convective storms. *Monthly Wea. Review*, 119 (3), 841-847.

Setvák, M. & Rabin, R. M. (2005). MSG observations of deep convective storms. *The 2005 EUMETSAT Meteorological Satellite Conference*, Dubrovnik, Croatia. EUMETSAT P.46, ISBN 92-9110-073-0, ISSN 1011-3932, 460-466.

Setvák, M., Rabin, R. M., Doswell III, C. A. & Levizzani, V. (2003). Satellite observations of convective storm top features in the 1.6 and 3.7/3.9  $\mu\text{m}$  spectral bands. *Atmospheric Research*. 67-68, 607-627.

Setvák, M., Rabin, R. M. & Wang, P. K. (2007). Contribution of the MODIS instrument to observations of deep convective storms and stratospheric moisture detection in GOES and MSG imagery. *Atmospheric Research*, 83, 505-518.

Setvák, M., Lindsey, D. T., Rabin, R. M. & Wang, P. K. (2008). Indication of water vapour transport into the lower stratosphere above midlatitude convective storms: Meteosat Second Generation satellite observations and radiative transfer model simulations. *Atmospheric Research*, 89, 400-408.

*Severe weather indices page*. [Retrieved on July, 20, 2009 from The Weather Prediction Web site: <http://www.theweatherprediction.com/severe/indices>].

Sowetan (2005). Heavy Storms batter Villages. (8 November 2005). p4.

STAR Satellite Rainfall Estimates. [Retrieved on July 20, 2009 from Centre for Satellite Applications and Research website: <http://www.star.nesdis.noaa.gov/smcd/emb/ff/index.php>].

Struzik, P., Pajek, M. & Koenig, M. (2006). Use of MSG global instability indices (GII) for storm prediction in Poland – validation study. *The 2006 EUMETSAT Meteorological Satellite Conference*, Helsinki, Finland. 12-16 June 2006. EUM P.48, ISBN 92-9110-076-5.

Terblanche, D. E., Pegram, G. G. S. & Mittermaier, M. P. (2001). The development of weather radar as a research and operational tool for hydrology in South Africa. *J. Hydrol.*, 241, 1-2, 3-25.

Vicente, G., Scofield, R. A. & Mentzel, W. P. (1998). The operational GOES infrared rainfall estimation technique. *Bull Amer. Meteor. Soc.*, 79, 1883-1898.

Vicente, G. A., Davenport, J. C. & Scofield, R. A. (2002). The role of orographic and parallax corrections on real time high resolution satellite rainfall rate distribution. *Int. J. Remote Sensing*, 23(2), 221-230.

Wagner, T. J., Feltz, W. F. & Ackerman, S. A. (2008). The temporal evolution of convective indices in storm producing environments. *Wea. Forecasting*, 23, 786-794.

Wilks D. S. (2005). *Statistical Methods in Atmospheric Sciences*, Second Edition. Elsevier Science & Technology Books. ISBN-13: 9780127519661. 627pp.

WMO Public Weather Service (PWS) programme. [Retrieved on July 20, 2009, from the WMO web site: <http://www.wmo.int/pages/prog/amp/pwsp/Nowcasting.htm>].

Zajac, B. A. & Rutledge, S. A. (2001). Cloud to ground lightning in the contiguous United States from 1995 to 1999. *Mon Wea Rev.*, 129, 999-1019.

Zinner, T., Mannstein, H. & Tafferner, A. (2008). Cb-TRAM: Tracking and monitoring severe convection from onset over rapid development to mature phase using multi-channel Meteosat-8 SEVIRI data. *Meteorology and Atmospheric Physics*, 101, (3-4), 191-210.